The influence of chromatin structure on DNA double strand break repair pathway choice

Inaugural-Dissertation

zur

Erlangung des Doktorgrades

Dr. rer. nat.

der Fakultät für Biologie

an der

Universität Duisburg-Essen

vorgelegt von

Marilen Demond

aus Dorsten

Februar, 2016

Die der vorliegenden Arbeit zugrunde liegenden Experimente wurden am Institut für Medizinische Strahlenbiologie an der Universität Duisburg-Essen, Standort Essen, durchgeführt.

1. Gutachter: Prof. George Iliakis

2. Gutachter: Prof. Hemmo Meyer

Vorsitzender des Prüfungsausschusses: Prof. Stefan Westermann
Tag der mündlichen Prüfung: 10. Mai 2016

Table of contents

List of figures

List of tables

List of abbreviations

53BP1	p53 binding protein
Ab	Antibody
ADP	Adenosine diphosphate
alt-EJ	Alternative end joining
ATM	Ataxia telangiectasia mutated kinase
ATP	Adenosine triphosphate
ATR	ATM and Rad3 related kinase
BLM	Bloom syndrome protein
B-NHEJ	Backup non-homologous end joining
bp	base pair
BRCA1/2	Breast cancer susceptibility protein 1/2
BSA	Bovine serum albumin
Cdc25a	Cell division cycle 25a
Cdk/s	Cyclin-dependent kinase/s
Chk1/2	Checkpoint kinase 1
CLSM	Confocal laser scanning microscopy
c-NHEJ	classical non-homologous end joining
CtIP	C-terminal binding protein interacting protein
d	day
DAPI	4',6-diamidino-2-phenylindole
DDR	DNA damage response
DIC	Differential interference contrast
D-loop	Displacement loop
DMEM	Dulbecco's modified eagle's medium
DMSO	Dimethyl sulfoxide
DNA	Deoxyribonucleic acid
Dna2	DNA replication ATP-dependent helicase/nuclease DNA2
DNA-PK	DNA-dependent protein kinase
DNA-PKcs	Catalytic subunit of DNA-PK
D-NHEJ	DNA-PK dependent non-homologous end joining

DSB/s	Double strand break/s
DSBR	Double-stranded break repair
dsDNA	Double stranded DNA
EC	Euchromatin
EDTA	Ethylene diamine tetraacetic acid
e.g.	exempli gratia
et al.	et alii
Exo1	Exonuclease 1
FACS	Fluorescence activated cell sorting
FBS	Fetal bovine serum
GFP	Green fluorescent protein
Gy	Gray
h	hour
H3	Histone H3
HAT	Histone acetyl transferase
HC	Heterochromatin
HP1	Heterochromatin protein 1
HRR	Homologous recombination repair
i.e.	id est
IF	Immunofluorescence
IR	Ionizing radiation
IRIF	Ionizing radiation induced foci
K	Lysine
KAP1	KRAB-domain associated protein 1
keV	kilo electronvolt
LET	Linear energy transfer
LIF	Leica image format
m	mouse
M	Mega (10^6)
mM	millimolar
Mab	Monoclonal antibody
MDC1	Mediator of DNA damage checkpoint protein 1
MEM	Minimal essential medium

min	minute/s
MMEJ	Microhomology mediated end joining
MMSET	Multiple myeloma SET domain containing protein
Mre11	Meiotic recombination 11
MRN complex	Mre11/Rad50/Nbs1 complex
Nbs1	Nibrin
ng	nanogram
NHEJ	Non-homologous end joining
nM	nanomolar
Pab	Polyclonal antibody
pATM	phospho-ATM
PARP-1	Poly (ADP-ribose) polymerase 1
PAXX	Paralog of Xrcc4 and Xlf
PBS	Phosphate-buffered saline
PFA	Paraformaldehyde
PFGE	Pulsed-field gel electrophoresis
PI	Propidium iodide
PI3K	Phosphoinositide 3-kinase
PIKK	Phosphoinositide 3-kinase-related protein kinase
Plk1	Polo-like kinase 1
PMT	Photomultiplier tube
Pnk	Polynucleotide kinase
PTIP	PAX transactivation activation domain-interacting protein
Puro	Puromycin resistance gene
r	rabbit
RAP80	Receptor-associated protein 80
RIF1	RAP1-interacting factor 1
RNF8/168	Ring finger protein 8/168
ROS	Reactive oxygen species
RPA	Replication protein A
rpm	revolutions per minute
RT	Room temperature
SDSA	Synthesis dependent strand annealing

Ser	Serine
SMARCAD1	SWI/SNF-related matrix-associated actin-dependent regulator of chromatin, subfamily A, containing DEAD/H box 1
SSA	Single strand annealing
SSB	Single strand break
ssDNA	Single stranded DNA
SUV39H1	Suppressor of variegation 3-9 homolog 1
SWI/SNF	Switch/Sucrose non-fermentable
Tdp1	Tyrosyl-DNA phosphodiesterase 1
Wrn	Werner syndrome protein
Xlf	Xrcc4-like factor
XRCC1/2/3/4	X-ray cross-complementing protein 1/2/3/4
γH2AX	phosphorylated H2AX at Ser-139

1. Introduction

The DNA of all human cells is continuously confronted by the action of multiple endogenous or environmental factors, which can cause thousands of random alterations in the DNA molecule. Maintaining DNA integrity is essential for cell survival, and accurate elimination of DNA alterations is crucial for suppressing mutagenesis. Endogenous sources generating DNA lesions are reactive oxygen species (ROS), by-products of normal aerobic metabolism, DNA replication errors, which result in nucleotide mismatches, and spontaneous alterations of DNA bases. DNA damage can be induced by ionizing radiation (IR), generated by natural sources, or by human activities, as well as by chemical agents such as alkylating or cross-linking agents. One of the most severe lesion in the DNA molecule is the DNA double strand break (DSB), which disrupts the sugar-phosphate backbones of both DNA strands, thus hampering their accurate repair using the second DNA strand as template. Unrepaired or misrepaired DSBs are known to trigger mutagenic events, which are the basis of cancer development (Jackson and Bartek, 2009).

To counteract the detrimental effects of DSB generation, cells have evolved several mechanistically distinct repair pathways. The repair of DSBs can be carried out by two major repair processes: Non-homologous end joining (NHEJ), represented by the classical NHEJ (c-NHEJ) and homologous recombination repair (HRR). Moreover, an alternative form of end joining (alt-EJ) has been identified together with another homology based DSB repair process, the single strand annealing (SSA). Although, it has been shown that both processes share certain similarities, mechanistic and biochemical studies indicated that alt-EJ and SSA are triggered by specific events and participate in the repair of specific subsets of DSB.

The probability to mediate faithful repair strongly depends on the balance between DSB repair pathways. In this regards, HRR is the only DSB repair pathway which could faithfully restore not only the DNA integrity, but also the exact sequence at the damage site, while c-NHEJ and especially alt-EJ are known to induce sequence alterations and translocations, more pronounced when alt-EJ is activated. SSA induces large deletions of the intervening DNA sequence between two repeated DNA regions. If the cell is not able to effectively repair the DNA damage, or if a large amount of DNA damage accumulates, apoptosis, senescence or generation of mutations are the inevitable consequences.

This study is focused on DSB repair pathway choice - especially on the activation of HRR and on the question, to what extent HRR is involved in the repair of IR induced DSBs. Particular emphasis is placed on the role of chromatin structure as a parameter influencing the repair pathway choice.

1.1 Ionizing radiation and the induction of DNA damage

To investigate the repair of DSBs, ionizing radiation (IR) is commonly used as inducing agent. It can be applied at controlled doses, allowing thus the induction of a known number of DSBs per cell. As in this study IR is primarily used to induce DSBs, the next sections provide an overview about the physics and chemistry of IR action and its DNA damaging properties.

1.1.1 Physics of ionizing radiation

Ionizing radiation (IR) is radiation which possesses sufficient energy to eject electrons from an atom or molecule and could be classified as particle or electromagnetic radiation. Particle radiation includes α-particles (helium nuclei), β-particles (electrons or positrons), neutrons, protons and heavy ions. X-rays and γ-rays consist of energetic photons and belong to electromagnetic radiation. As in this study only electromagnetic ionizing radiation in the form of X-rays was used to induce DNA damage, the next paragraph focuses on X-rays.

X-rays occupy the part of the electromagnetic spectrum between ultraviolet and γ-rays and have a wavelength ranging from 0.01 to 10 nm. X-rays consists of high energy photons with low wavelengths and high frequencies, which carry enough energy to ionize atoms or to disrupt molecular bonds.

The interaction of X-rays with material depends on the energy of the X-rays and on the chemical composition of the absorbing matter. At low photon energies the photoelectric process is most important. Thereby, the photon gives up its entire energy to an orbital electron in the absorbing matter, which becomes ejected and the vacancy is filled by an electron from an outer orbit or by a free electron. Compton scattering is the dominating process when high energy X-rays such as those used in radiotherapy, interact with soft tissue: The incident photon interacts with a loosely bound outer shell electron of an atom of the absorbing tissue. Thereby, part of the photon energy is given to the electron as kinetic energy and the photon proceeds with reduced energy and deflected from its original path as a scattered photon. The

electron proceeds as a fast electron, able to ionize other atoms or break chemical bonds and leaves an ionized atom (Hall and Giaccia, 2006).

The production of a large number of fast electrons, also called secondary electrons, determines the biological effect of IR. The DNA is the critical target of IR and can be damaged directly or indirectly by secondary electrons. In direct action, the secondary electron interacts with the DNA itself to generate an effect. The indirect action involves the production of a hydroxyl radical (OH^-) which in turn causes damage to the DNA. In particular, X-rays interact frequently with water molecules, because 90% of a cell is composed of water. Ionization of a water molecule results in the formation of highly reactive OH^-:

$$H_2O \rightarrow H_2O^+ + e^-$$
$$H_2O^+ + H_2O \rightarrow H_3O^+ + OH^-$$

It is estimated that two thirds of the biological damage is caused by hydroxyl radicals (Hall and Giaccia, 2006).

In biological materials, X-rays generate an ionization pattern with a relatively sparse distribution of ionization events, which are considered to have a low linear energy transfer (LET). In contrast, particle ionizing radiations like α-particles and neutrons, produce dense ionization tracks and are considered to be densely ionizing with high LETs (Fig. 1). The LET describes how much energy an ionizing particle transfers to the material per unit length. LET is expressed in keV/µm. Considering the DNA as the critical target, the probability to induce multiple or clustered DNA damages with low LET radiation is lower than with high LET radiation. As a result, high LET radiation has an increased biological effectiveness as it induces more clustered DNA damage that is more effective in killing cells or in inducing mutations. However, X-rays are also able to induce clustered DNA damage, which is described in more detail in the next section.

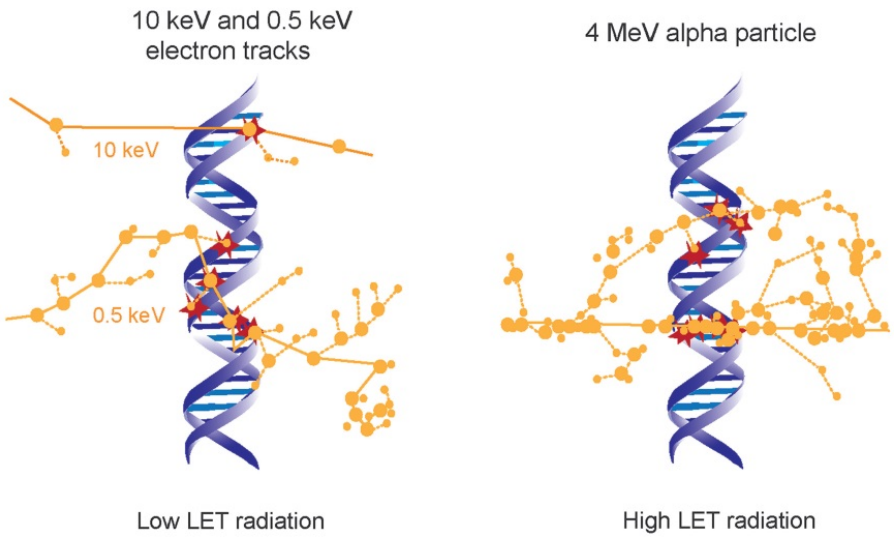

Figure 1: Distribution of ionization events after exposure to low and high LET radiation. Large dots indicate ionizations and small dots represent excitations along the electron tracks. With increasing LET the induction of clustered damage increases (modified from Schipler and Iliakis, 2013).

1.1.2 Induction of DNA damage by ionizing radiation

An important characteristic for IR is that the DNA damage inducing ionization events are not evenly distributed in space, rather they occur along particle tracks and can therefore induce clustered damage (Hall and Giaccia, 2006). The DNA is considered as the primary target of IR for several of the biological effects observed, as IR-induced DNA damage formation correlates with cell survival. Ionization events can either directly damage the DNA molecule, or generate free radicals in the vicinity of the DNA, which then damage the DNA. Along those lines, low LET radiation (X-rays or γ-rays) induces around 1000 base damages, 1000 single-strand breaks (SSBs) and 20-40 DSBs in mammalian cells per Gray and DNA damage induction increases linearly with increasing radiation dose. However, it is still not clear how the cells respond to different doses of radiation and whether these responses are the same at low and high radiation doses.

To counteract the detrimental effects of DNA damage induction, mammalian cells have evolved several repair mechanisms, e.g. base excision repair, nucleotide excision repair and mismatch repair to remove such DNA lesions, when they affect only one DNA strand. The double stranded nature of the DNA facilitates such repair mechanisms, in that the second DNA strand serves as a template to restore the original DNA sequence. Therefore, the repair

of SSBs and base damages is very efficient with a low probability to generate error-prone repair events.

In contrast to the repair of DNA lesions affecting only one DNA strand, the induction of DSBs, either by direct interruption of both DNA strands or due to occurrence of two SSBs in close proximity (not more than ~ 4-5 bp apart), represent a severe challenge to the cellular repair mechanisms, as information is also missing from the second DNA strand. Therefore, DSBs are considered to exhibit a highest probability of inducing biologically dangerous DNA intermediates, including deletions and insertions or mutated DNA regions, which are the basis of cell death or carcinogenesis.

The induction of DSBs by IR is frequently associated with the generation of complex clustered DNA lesions, characterized with presence of additional bases or sugar lesions in the vicinity. The nature and number of these additional lesions define the complexity of DSBs and can affect the repair pathway choice. Moreover, the increasing complexity could increase the probability of generating errors during the repair process (Schipler and Iliakis, 2013). In general, IR induced DSBs frequently comprise 3'-phosphoglycolate and a 5'-OH at the DNA ends, which according to our classification represents the T2-type of DSBs (Fig. 2 B) (Henner et al., 1982, Henner et al., 1983). These specific DNA end modifications require DNA end-processing steps during the repair and prevent an immediate religation of the break site (Weinfeld et al., 2011). Increased complexity of DSBs could evolve further, if base damages or the loss of bases arise in the vicinity of the DSBs (Fig. 2 C) (Datta et al., 2006, Datta et al., 2005). This can delay and complicate repair, as different repair processes have to operate on the same site at the same time. The induction of one repair process could prevent or impede the other repair processes, as it was shown for base excision repair (Bellon et al., 2009, Eccles et al., 2011, Dobbs et al., 2008). Furthermore, during indirect induction of a DSB through two base lesions that are processed simultaneously, indirect induction of a DSB can follow, which would further complicate the repair process (Fig. 2 D) (Georgakilas et al., 2012). Moreover, another form of indirect DSBs was shown to form within the first post irradiation hour by temperature-dependent chemical processing of radiation-induced labile sites at the sugar moiety (Fig. 2 E) (Jones et al., 1994, Singh et al., 2011, Singh et al., 2009, Singh et al., 2013). The recognition and repair of indirectly forming DSBs may be impaired, as repair proteins involved in the repair of base damages, sugar lesions or SSBs are most probably already present at the damage sites and could suppress the recruitment of repair factors engaged in

DSB repair. Moreover, if DSB clusters (several DSBs induced in close proximity) are formed, they have the potential to destabilize chromatin structure from nucleosome loss or even the loss of larger chromatin segments (Fig. 2 F) (Schipler and Iliakis, 2013). This form of DSB has been indicated as T6 and has been considered as the most deleterious one, with a higher probability to generate repair accidents.

The increase of lesion complexity naturally influences repair fidelity and enhances the probability of interrupted or error-prone repair. However, as the nature of DSBs can be so diverse it is not surprising that mammalian cells have evolved several mechanistically distinct repair pathways, with diametrically different repair efficiencies, to process DSBs. The DNA damage response and the mechanistic aspects of DSB repair pathways will be presented in the next section.

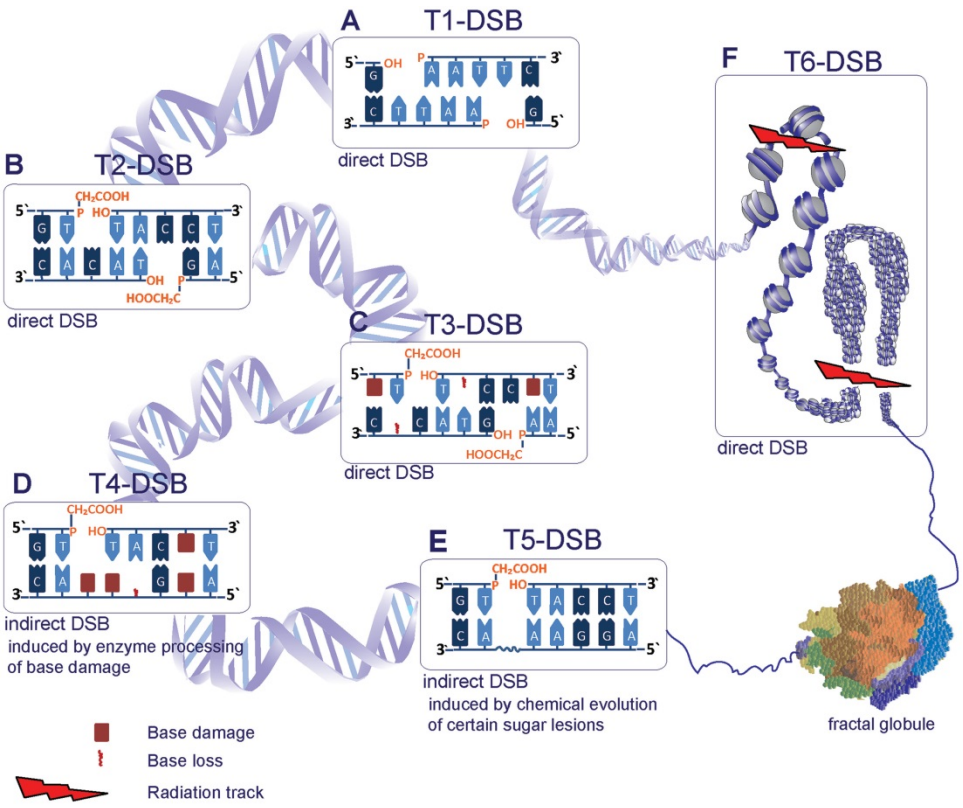

Figure 2: Illustration of DSBs with different complexity levels. The different types of DSBs are described in the text. With increasing complexity of the DSB, the probability of errors during processing increases (Schipler and Iliakis, 2013).

1.2 Cellular responses to DSBs: The eukaryotic DNA damage response

Eukaryotic cells have developed a complex protein network, the so called DNA damage response (DDR) network, which becomes activated upon DNA damage induction to preserve genome integrity and to prevent the accumulation of DNA alterations. DDR involves the coordinated sensing (detection), signaling (transduction), activation of DNA repair processes and the coordination of DNA repair with cell cycle progression through initiation of the checkpoint response (Bekker-Jensen and Mailand, 2010). Therefore, proteins involved in DDR are categorized into sensors, transducers, mediators and effectors. DNA sensors are proteins which recognize the DNA lesion and initiate the signaling response, whereas transducer proteins, together with mediator enzymes, amplify the signal generated by the DNA damage. The signal is relayed to several downstream pathways by the effector proteins, whose targets are cell cycle regulators, transcription factors, DNA repair factors and the apoptotic machinery (Bekker-Jensen and Mailand, 2010, Polo and Jackson, 2011).

1.2.1 Activation of DNA damage induced cell cycle checkpoints

The main function of DDR is the regulation of cell cycle progression under conditions of DNA damage to maintain genome stability. This is achieved by the activation of cell cycle checkpoints, whose main targets are cyclins and cyclin-dependent kinases (Cdks) forming cyclin/Cdk complexes (Deckbar et al., 2011). The cell cycle arrest, initiated by the cell cycle checkpoints, provides time for DNA repair mechanisms and prevents entry into S phase or mitosis in the presence of unrepaired damage. The main event in the initiation of DDR is the activation of ATM (ataxia telangiectasia mutated) and ATR (ATM and Rad3 related) in response to DSBs and ssDNA, respectively. However, recent findings from our laboratory revealed an absolute requirement of ATR for G_2 checkpoint activation if DSBs are induced in S and G_2 phase, demonstrating that ATR plays a hitherto unknown central role in checkpoint activation after DSB induction (Fan et al. unpublished). ATM and ATR directly target the checkpoint kinases Chk1 and Chk2 (Bartek and Lukas, 2003).

The entry into S phase is regulated by the cyclin D/Cdk4/6 and cyclin E/Cdk2 complexes. Upon DNA damage induction in G_1 phase cells, a signal cascade gets activated which inactivates the above complexes. Two different mechanisms have been described (Iliakis et al., 2003): The rapidly initiated pathway via Chk2, which leads to degradation of the phosphatase Cdc25a and prevents the removal of inhibitory phosphorylation of Cdk2, leaving

the cyclin E/Cdk2 complexes inactive. The second mechanism is a slowly activated pathway, which requires p53 initiated transcription of p21 and takes several hours to become activated (Deckbar et al., 2011, Falck et al., 2001, Mailand et al., 2000). Up-regulated p21 inhibits the complex cyclin E/Cdk2, whose activity correlates with cell transition from G_1 to S phase.

The G_2/M transition is driven by an increase in cyclin B/Cdk1 activity. The mechanisms which prevent mitotic entry following DNA damage induction in G_2 phase cells are similar to those triggered during the G_1/S checkpoint activation. The G_2/M checkpoint is also established by the phosphorylation of ATM and the effector kinases Chk2 and Chk1, which results in phosphorylation of Cdc25a and its subsequent degradation, which inhibits the interaction with cyclin B/Cdk1. Moreover an increase of Wee1, mediated by negative regulation of Plk1 (polo-like kinase 1) by ATM and ATR, reduces Cdk1 activity to establish a strong G_2 arrest, which prevents entry to mitosis.

1.2.2 Detection of DSB and signaling activation

Several molecules are known to be able to bind to DNA ends after DSB induction and are therefore categorized as DSB sensor molecules: The MRN (Mre11/Rad50/Nbs1) complex, the Ku70/Ku80 heterodimer and PARP-1 (poly(ADP-ribose) polymerase 1) are one of the first molecules to be recruited to damaged chromatin (Mladenov and Iliakis, 2011). Any of these putative damage sensors are associated with specific repair pathways. MRN recruitment is connected to initiation of DNA end resection, a key step in HRR, while the binding of Ku70/Ku80 heterodimer initiates the repair of DSBs by c-NHEJ. The binding of PARP-1 to the damaged chromatin directs the repair reaction towards alt-EJ.

The binding of the MRN complex to DSBs facilitates the activation of the PI3K related kinase ATM (Uziel et al., 2003). Autophosphorylated, active ATM monomers mediate the phosphorylation of H2AX, an H2A histone variant that comprises 10-15% of total H2A in higher eukaryotes, generating the so called γH2AX (Rogakou et al., 1998, Fernandez-Capetillo et al., 2004). The phosphorylation of H2AX at Ser139 is a major marker for DDR activation and is directly recognized by MDC1 (mediator of DNA damage checkpoint protein 1) which serves as a central recruitment platform for multiple DDR members (Stucki et al., 2005). MDC1 amplifies the DDR signal through the activation of a positive feedback loop by recruiting more MRN molecules, involved in recruitment and activation of more ATM monomers to the DSB (Panier and Boulton, 2014). The phosphorylation of MDC1 by ATM

leads to the recruitment of the E3 ubiquitin ligase RNF8 (RING finger 8), which is an important DDR transducer via ubiquitylation of the histones H2AX and H2A (Huen et al., 2007). In addition, RNF168, another key E3 ubiquitin ligase, is recruited to the DSB and promotes the ubiquitylation of the damaged chromatin, which provides another platform for further recruitment of repair proteins (Doil et al., 2009). These involve 53BP1 (p53 binding protein) and BRCA1 (breast cancer protein 1), which get attracted by the ubiquitin mark, generated either by RNF8 or RNF168 (Fradet-Turcotte et al., 2013, Wang et al., 2007).

It has been shown that the assembly of DDR proteins occurs in a temporal sequential and coordinated manner, which can be branched into two different recruitment kinetics (Fig. 3) (Lukas et al., 2004, Bekker-Jensen et al., 2005). Within the first minutes, MRN binds to the break and initiates the formation of γH2AX and MDC1 recruitment (Bekker-Jensen and Mailand, 2010). The second wave of repair proteins recruited to the damage site include the mediator proteins 53BP1 and BRCA1 (Bekker-Jensen and Mailand, 2010).

After induction of DSBs the activation of DDR leads to the sensing of the lesion within seconds. The signal transducers like ATM and ATR amplify the damage signal together with the mediators so effectively that several repair proteins of the DDR can be visualized as repair foci by immunofluorescence microscopy, as they cover a huge chromatin region around the break site (1.4).

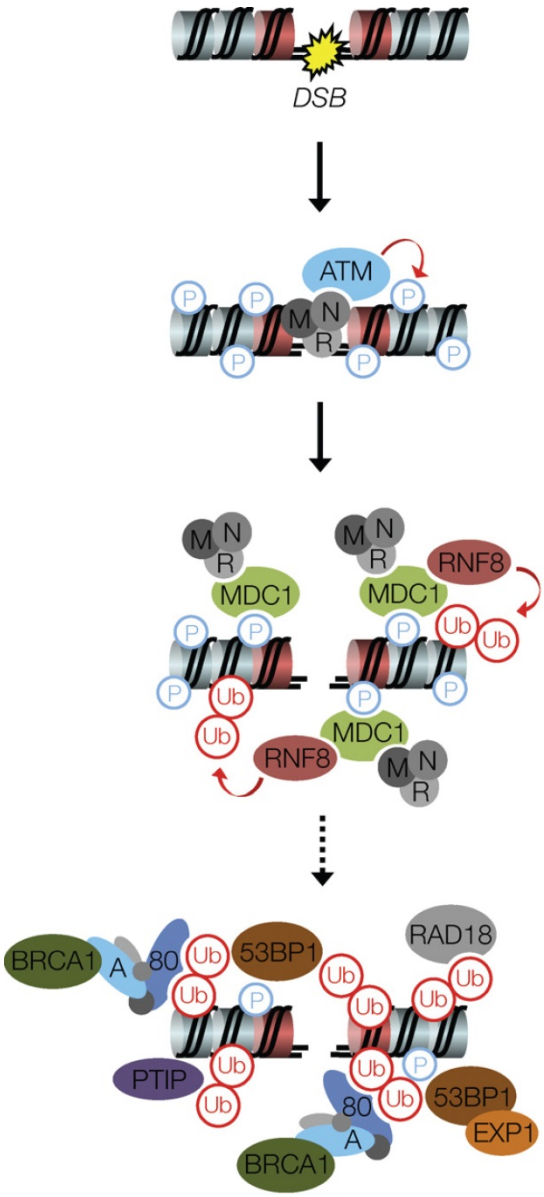

Figure 3: Hierarchical order of protein recruitment to DSBs. The assembly of the DDR proteins occurs in a temporally organized way. The early recruited proteins get attracted by phosphorylation of chromatin in the DSB vicinity and the second wave of repair proteins requires ubiquitylation signals. P: Phosphate, Ub: Ubiquitin, M: MRE11, R: RAD50, N: NBS1, A: Abraxas, 80: RAP80, EXP1: EXPAND1 (modified from Bekker-Jensen and Mailand 2010).

1.2.3 Binding of 53BP1 and BRCA1 influences repair pathway choice

It was shown that the recruitment of 53BP1 and BRCA1 coordinates the repair of DSBs with the cell cycle and conduct the initiation of c-NHEJ and HRR, respectively. 53BP1 suppresses DNA end resection, which has been considered as a distinctive trait of HRR, during the G_1 phase of the cell cycle. On the other side, it was reported that during the S and G_2 phase of the

cell cycle, BRCA1 antagonizes the action of 53BP1 by promoting its removal from the damaged sites, thus allowing DNA end resection and initiation of HRR (Bothmer et al., 2010, Bunting et al., 2010). Clear evidence, supporting the opposing roles of 53BP1 and BRCA1 in DSB repair coordination, emerged from experiments with mice deficient for BRCA1. It was shown that the negative effects of BRCA1 deficiency could be rescued by a concomitant loss of 53BP1 (Cao et al., 2009, Bouwman et al., 2010). These findings unequivocally support the assumption that BRCA1 antagonizes the activity of 53BP1 at damaged chromatin.

In 2013 two effector proteins of 53BP1 were identified and implicated in the repair pathway selection coordinated by BRCA1 and 53BP1. It was shown that 53BP1 undergoes phosphorylation at its N-terminus. However, this phosphorylation is not required for 53BP1 recruitment to DSBs, rather this post-translational modification acts as a recruitment signal for the newly identified 53BP1 effector protein RIF1 (RAP1-interacting factor 1) (Escribano-Diaz et al., 2013, Zimmermann et al., 2013, Feng et al., 2013, Chapman et al., 2013). RIF1 restricts BRCA1 accumulation at the break site, which results in negative regulation of DNA end resection. In addition, an interaction of RIF1 with the BLM helicase was identified. This suggests an inhibition of BLM (Bloom helicase) activity by RIF1 to suppress DNA unwinding, which is also essential for DNA end resection (Xu et al., 2010). The second effector protein of 53BP1, which mediates the inhibitory effect of 53BP1 on HRR is PTIP (PAX transactivation activation domain-interacting protein) (Fig. 4) (Callen et al., 2013). PTIP was shown to directly interact with the phosphorylated N-terminus of 53BP1 and to suppress resection, similar to 53BP1 and RIF1 (Munoz et al., 2007, Callen et al., 2013).

To ensure the correct pathway selection, 53BP1 and BRCA1 have to actively block each other in the respective cell cycle phase. However, it was demonstrated that 53BP1 can be recruited to DSBs in G_2 cells if BRCA1 is depleted and that depletion of 53BP1 is associated with the formation of BRCA1 foci during the G_1 phase of the cell cycle (Escribano-Diaz et al., 2013).

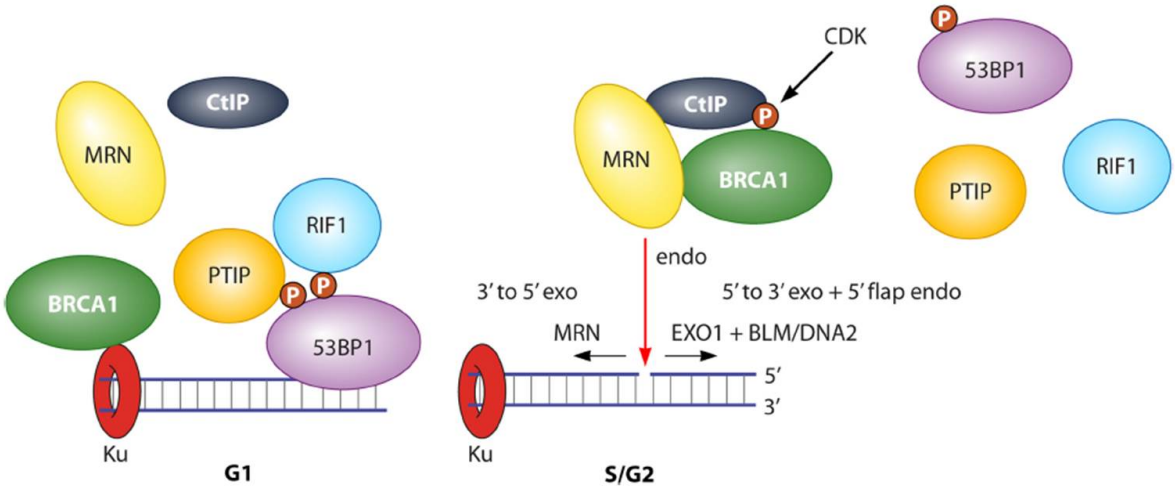

Figure 4: The cell cycle regulated choice between 53BP1 and BRCA1 influences DSB repair pathways. In G_1 phase cells the phosphorylation of 53BP1 attracts its two effector proteins PTIP and RIF1 to suppress resection. In late S and G_2 phase, the phosphorylation of CtIP by Cdks induces the formation of the CtIP/BRCA1/MRN complex, which blocks 53BP1 accumulation and initiates end resection to direct repair towards homologous recombination (Daley and Sung, 2014).

1.2.4 DSB repair by homologous recombination

Homologous recombination repair is the only mechanism by which the damaged DNA sequence after DSB induction can be restored in an error-free manner. HRR can faithfully repair DSBs, as it utilizes the sequence information from a homologous DNA molecule. Although, the homologous chromosome is available in G_1 phase of the cell cycle, the predominant homologous DNA template is the sister chromatid, which becomes gradually available during the DNA replication phase and is entirely available in G_2 phase. This dependency restricts HRR to S and G_2 phase of the cell cycle - in contrast to the other repair pathways, which can effectively operate throughout the cell cycle.

The key initiation step of HRR, which has been considered to determine the efficiency of HRR, is DNA end resection, taking place at the break sites during late S and G_2 phase of the cell cycle. As already described (1.2.3), the initiation of resection is regulated by the antagonistic interplay between BRCA1 and 53BP1. To ensure HRR activity exclusively in S and G_2 phase, the cell cycle dependent phosphorylation of CtIP initiates its recruitment to the DSB (Sartori et al., 2007). CtIP contains two well conserved Cdk phosphorylation sites. Upon S phase entry, Ser327 of CtIP gets phosphorylated and is essential for the interaction with BRCA1 (Yu and Chen, 2004, Yun and Hiom, 2009). The second Cdk target, Thr847, was also shown to play an important role in resection activation (Huertas and Jackson, 2009).

Moreover, Mre11, a member of the MRN complex, was described to directly interact with Cdk2, thereby promoting CtIP phosphorylation (Buis et al., 2012). The phosphorylated CtIP in cooperation with MRN and BRCA1 forms a G_2-specific complex, which triggers the removal of 53BP1 in S and G_2 phase (Fig. 4) (Chen et al., 2008). Furthermore, the CtIP/BRCA1/MRN complex suppresses RIF1 accumulation in G_2 phase, restricting 53BP1-mediated NHEJ to G_1 phase (Escribano-Diaz et al., 2013). CtIP and MRN facilitate short-range resection, whereas long-range resection is facilitated by BLM, Exo1 (Exonuclease 1) and Dna2 helicase/nuclease generating 3' ssDNA overhangs (Nimonkar et al., 2008, Nimonkar et al., 2011). The ssDNA is rapidly coated with the heterotrimer RPA (replication protein A) to prevent the formation of secondary structures and to protect from nucleolytic cleavage.

RPA is displaced by the Rad51 recombinase, generating a Rad51 nucleoprotein filament. The assembly of Rad51 onto ssDNA is promoted by BRCA2 (Jensen et al., 2010, Liu et al., 2010) and additionally supported by the five Rad51 paralogs (Rad51B, Rad51C, Rad51D, Xrcc2 and Xrcc3). The Rad51 nucleoprotein filament searches for and invades the homologous DNA strand, creating a D-loop (displacement loop) structure, which is necessary for finding homology and for generating the Holliday junction. The motor protein Rad54 that translocates along dsDNA, was shown to stimulate DNA strand exchange activity of Rad51 and to promote chromatin remodeling and protein displacement from dsDNA (Petukhova et al., 1999, Alexiadis and Kadonaga, 2002, Alexeev et al., 2003, Mazin et al., 2010). After D-loop formation and DNA synthesis, two major pathways can be used to finalize the repair process by HRR: Synthesis dependent strand annealing (SDSA) and double-stranded break repair (DSBR). During SDSA the newly synthesized 3' end anneals to the other 3' overhang in the damaged chromatid and the gaps are filled up by polymerases. This form of repair results in non-crossover recombinant products. The DSBR involves the formation of a second Holliday junction and their resolution can result in either crossover or non-crossover products. In the end, completion of HRR results in an error-free restoration of the DNA sequence around the DSB.

However, next to HRR, resected DSBs can be repaired by the mutagenic single strand annealing (SSA) repair. SSA is another homology-directed repair that mediates repair if long homologous sequences are exposed after resection. Repair is facilitated by annealing these complementary sequences, resulting in large deletions as the sequence between the complementary sequences as well as one copy of the repeat gets lost during repair.

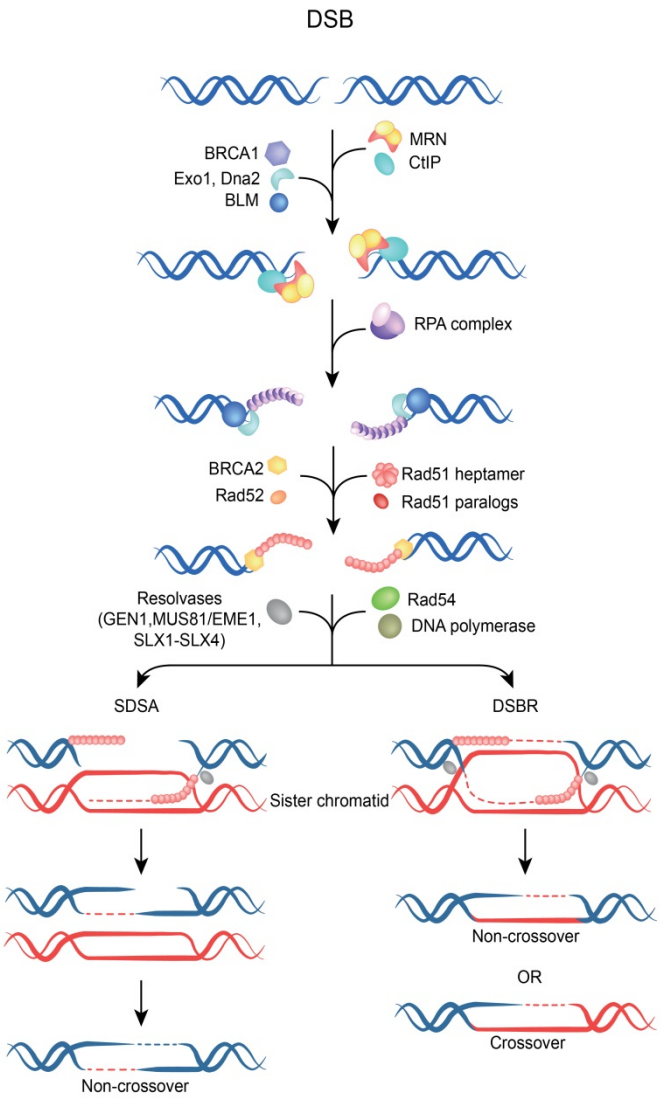

Figure 5: DSB processing by homologous recombination repair. A large repertoire of repair proteins is required for HRR. The recognition of the DSB involves the binding of the MRN complex. The key step of HRR is end resection and is initiated through the recruitment of CtIP and BRCA1 and requires Exo1, Dna2 and BLM. The resulting ssDNA is protected by RPA molecules, which get displaced by Rad51 with the help of BRCA2, Rad52 and the Rad51 paralogs. The completion of HRR with the homologous sister chromatid can be mediated by synthesis-dependent strand annealing (SDSA) and double-stranded break repair (DSBR) which leads to DNA sequence restoration with non-crossovers or with crossovers (Dueva and Iliakis, 2013).

1.2.5 DSB repair by simple end joining mechanisms

In higher eukaryotes the major repair pathways involved in the elimination of DSBs rely on a simple rejoining reaction between the two ends of the broken DNA molecule. It has been shown that NHEJ, which can occur independently of the cell cycle phase as no homologous template is required, is the predominant DSB repair pathway at all cell cycle stages. NHEJ

includes two mechanistically different repair pathways: the classical or DNA-PKcs-dependent NHEJ (c-NHEJ) and the alternative end joining pathway (alt-EJ) which is also known to function as a back-up pathway.

1.2.5.1 c-NHEJ

The c-NHEJ repair pathway is a fast process with half times of about 10-30 min, which restores molecular integrity of the DNA by a simple rejoining reaction between the DNA ends, without the capacity to restore the original DNA sequence (Dueva and Iliakis, 2013). The process of c-NHEJ is initiated by the binding of the Ku70/Ku80 heterodimer, which is known to have a high affinity for DNA ends and its high abundance in human cells ensures a binding to the damage sites within seconds (Mladenov and Iliakis, 2011). It has been speculated that Ku70/Ku80 protects DNA ends from nuclease processing. However, recent papers have shown that Ku70/Ku80 acts as a AP-lyase, capable to process the DNA ends before further c-NHEJ activation (Roberts et al., 2010). Nevertheless, the major role of Ku heterodimer is to recruit DNA-PKcs to damaged DNA, which results in a dramatic increase of DNA-PKcs kinase activity and the formation of an active DNA-PK holoenzyme complex.

The subsequent rejoining reaction between the broken DNA ends is catalyzed by activity of the Ligase 4/Xrcc4/Xlf complex (Fig. 6, left pathway). The Ligase 4/Xrcc4/Xlf complex tolerates imperfectly matched DNA ends and can execute ligation in the presence of small overhangs, mismatched bases or missing nucleotides and chemical modifications at the ends (Povirk, 2012). If minimal DNA end processing is required, for example addition of 5'-phosphate by Pnk (polynucleotide kinase), removal of 3'-phosphoglycolates by Tdp1 (tyrosyl-DNA phosphodiesterase 1) or end processing by Artemis, it takes place before the final ligation reaction (Schipler and Iliakis, 2013). Moreover, missing nucleotides can be filled-in by the action of DNA polymerase λ and μ. Recent publications reveal that Xrcc4 and Xlf form long helical protein filaments that provide DNA end protection and commit repair to c-NHEJ (Mahaney et al., 2013). Moreover, a new component of the NHEJ machinery was identified and named PAXX (paralog of Xrcc4 and Xlf) (Ochi et al., 2015, Xing et al., 2015). PAXX interacts with Ku and promotes DSB repair.

The outstanding advantage of c-NHEJ is the speed of repair. However, it includes the probability for inducing errors, as no build-in mechanism is present to ensure the restoration of

the original DNA sequence. Therefore, additions or deletions of several base pairs leading to sequence alterations at the junction are known to result from c-NHEJ.

1.2.5.2 alt-EJ

Evidence for an additional repair pathway arose from experiments with mutant cell lines deficient for c-NHEJ and HRR factors, which efficiently repair DSBs (Kabotyanski et al., 1998, Wang et al., 2001b, Wang et al., 2001a). This repair pathway was shown to be an alternative form of c-NHEJ, hence named alternative end joining. Other terms like back-up pathway, point out the back-up function of this repair pathway. One of the outstanding characteristics of alt-EJ is, that it can involve the utilization of microhomologies, hence this pathway is frequently referred as microhomology-mediated end joining (MMEJ).

The basic mechanism of alt-EJ is comparable to c-NHEJ and is based on a simple rejoining of DNA ends. However, the process is slower than c-NHEJ with repair half times between 2 and 20 h and is associated with significantly more and extensive DNA end processing as compared to c-NHEJ (Dueva and Iliakis, 2013). Several proteins have been implicated in alt-EJ. Deficiency for Ligase 1 and Ligase 3, Xrcc1 and PARP-1 results in a decrease or even elimination of alt-EJ (Fig. 6, right pathway) (Audebert et al., 2004, Wang et al., 2005, Paul et al., 2013). Also the MRN complex, CtIP and Wrn were implicated in alt-EJ, which strongly supports the finding that alt-EJ frequently requires extended DNA end processing (Della-Maria et al., 2011). The DNA end processing steps involved in alt-EJ also suggest that a form of alt-EJ is initiated to back-up failures during HRR.

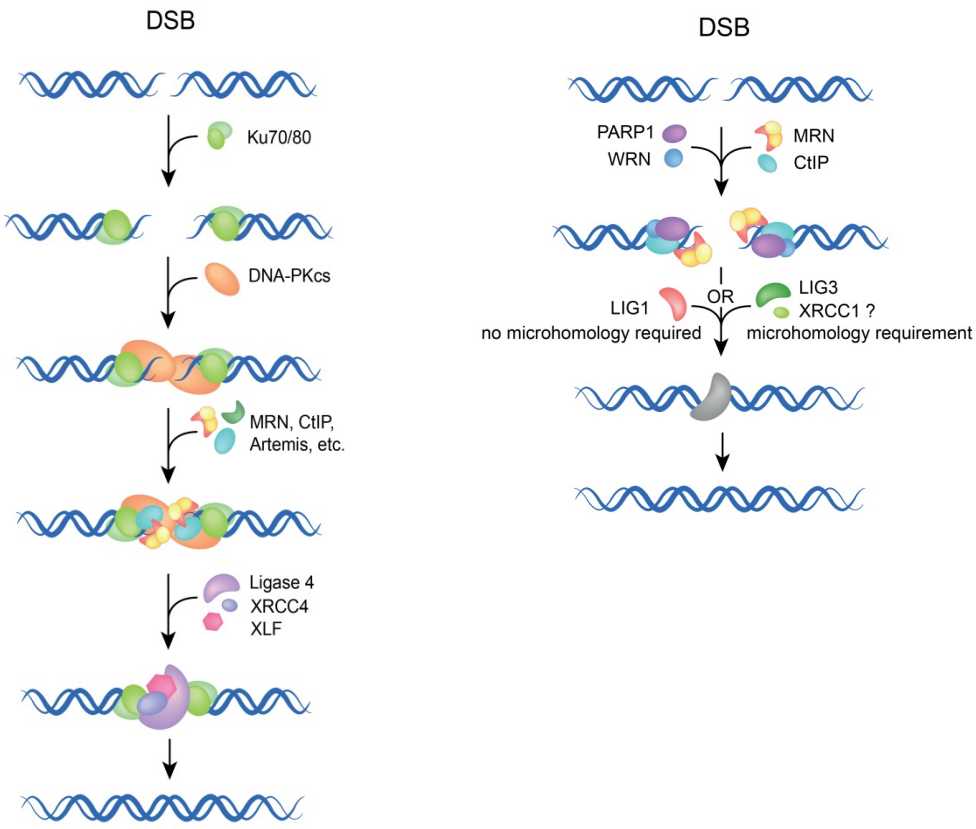

Figure 6: DSB repair by c-NHEJ or alt-EJ. The sequential progression of c-NHEJ is illustrated on the left side and the molecular interplay during alt-EJ is shown on the right side. C-NHEJ involves the binding of the heterodimer Ku70/Ku80, which together with DNA-PKcs forms the DNA-PK holoenzyme. Minimal end processing can occur before the break is rejoined by the Ligase 4/Xrcc4/Xlf complex. Proteins which are associated with the alt-EJ pathway include PARP-1, Ligase 1, Ligase 3 and Xrcc1 (Dueva and Iliakis, 2013).

1.2.6 Characteristics of DSB repair pathways

As already indicated, the different DSB repair pathways have distinct characteristics and properties with regards to repair half times, cell cycle dependencies and most remarkably, their propensity to induce errors. The majority of DSBs is known to be repaired by c-NHEJ, whose main advantage is its impressive speed. The proteins involved in this repair pathway operate together as one complex to facilitate the fast processing of the break. The binding of Ku and the recruitment of DNA-PKcs keeps both ends in close proximity to ensure the ligation of the correct ends and to prevent the ligation of distant, non-related ends which would lead to chromosomal aberrations and genomic instability. Indeed, c-NHEJ is known to suppress chromosomal translocations, although no mechanism during this repair process can actually prevent the joining of unrelated ends (Iliakis et al., 2004, Lieber, 2010). However,

there are evidences that c-NHEJ is involved in the formation of chromosomal translocations, which suggests that there are multiple mechanisms ensuring the rejoining of proper DNA ends (Ghezraoui et al., 2014). DSBs induced by IR have modified ends at the break sites, which will require end processing during c-NHEJ and will increase the probability of induction of sequence alterations through nucleotide addition or deletion (Fig. 7). The function of c-NHEJ is not dependent on the cell cycle and c-NHEJ occurs in every cell cycle phase.

Most hazardous for the cell fate is the engagement of alt-EJ in DSB processing. This pathway has a higher probability to induce sequence alterations and is considered as the main source of chromosomal translocations and genomic instability (Fig. 7) (Iliakis et al., 2007, Lieber, 2010). Although it is also based on simple religation of the break sites, the repair of DSBs by alt-EJ is slower, compared to c-NHEJ. The alt-EJ is known to work as a back-up repair pathway when the main DSB repair processes are chemically or genetically inactivated, or when local failures of c-NHEJ and HRR occur at the break sites. Therefore, the activity of alt-EJ is functionally suppressed when the two other pathways operate physiologically (Dueva and Iliakis, 2013). Alt-EJ activity is independent of the cell cycle, but in contrast to c-NHEJ it shows cell cycle fluctuations, characterized by increased activity in G_2, reduced activity in G_1 and almost lack of activity in plateau phase cells (Windhofer et al., 2007, Wu et al., 2008, Iliakis, 2009).

HRR utilizes the sister chromatid as a template during the repair process and is noted for being the only error-free repair pathway enabling the correct restoration of the DNA sequence. The complex repair machinery of HRR implies a slow repair time and the requirement of the sister chromatid restricts HRR to late S and G_2 phase of the cell cycle. The phosphorylation of repair proteins by Cdks assures the precise regulation of HRR activity in S/ G_2 phase.

Considering the specific properties of all these repair pathways, it is plausible that repair pathway choice may not be regulated by simple competition; rather it should be a well-regulated decision. The parameters influencing the appropriate pathway selection are at present not completely understood and determined. However, the currently known main determinants of the repair pathway selection will be discussed in the next section.

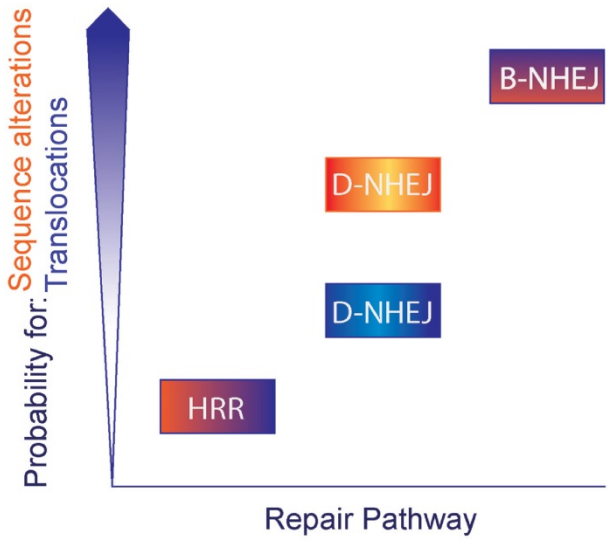

Figure 7: Error probabilities of the three DSB repair pathways. The probability of inducing sequence alterations is indicated with orange shading and the probability for translocations is indicated in blue. HRR is the only known error-free repair pathway and has the lowest probability to induce sequence alterations or translocations. C-NHEJ (here D-NHEJ) has a relatively high probability to induce sequence alterations, whereas the formation of translocations is an occasional event during c-NHEJ. The highest probability of error induction has the alt-EJ (here B-NHEJ), as it is known to frequently induce sequence alterations and translocations (Schipler and Iliakis, 2013).

1.2.7 Repair pathway choice

One of the main factors influencing repair pathway selection is the damage complexity, as it was shown that high LET irradiation specifically inhibits c-NHEJ (Wang et al., 2008). Heavy ion beams release their energy at high density along their tracks and induce complex DSBs comprising multiply damaged sites (Terato et al., 2008, Hada and Georgakilas, 2008, Tokuyama et al., 2015). It was demonstrated that complex damage induction by carbon-ions slows down DSB repair and strongly enhances end resection and HRR, as demonstrated by RPA and Rad51 foci analysis (Shibata et al., 2011). Accordingly, a massive phosphorylation of CtIP was observed after heavy ion radiation and immunofluorescence experiments revealed that 85% of heavy ion induced DSBs undergo resection in G_2 phase. Additionally, an increase of resection signal in G_1 cells was also observed (Yajima et al., 2013), suggesting most probably an increase of alt-EJ.

Unpublished results from our laboratory reveal a dose dependent component of the DSB repair pathway choice in G_2 phase cells. The formation of γH2AX foci, representing the overall amount of DSBs generated at a given IR dose and the numbers of Rad51 foci, indicating DSBs

processed by HRR, were analyzed specifically in G_2 phase cells after X-ray irradiation. The calculation of the ratio between γH2AX foci and Rad51 foci demonstrated that the percentage of DSBs undergoing HRR is remarkably high (60%) at low doses (0.2 Gy) and decreases with increasing radiation dose. After irradiation with 2 Gy, the percentage of DSBs processed by HRR is reduced to about 20% and doses equal to or greater than 4 Gy limit HRR to less than 20% of the induced DSBs (Fig. 8 A). As a result of such correlations the number of Rad51 foci does not increase with increasing IR dose. Rather, it saturates at doses above 2 Gy (Fig. 8 B) and it was shown that this was not due to limited Rad51 protein level in the nucleus. These findings suggest that the initial load of DSBs, introduced by different doses of radiation, could affect repair pathway choice. Low DSB induction seems to promote the error-free repair by homologous recombination, while at high DSB burden, the preferred DSB repair process is c-NHEJ. However, up to now the cellular mechanisms underlying such correlation remain unknown.

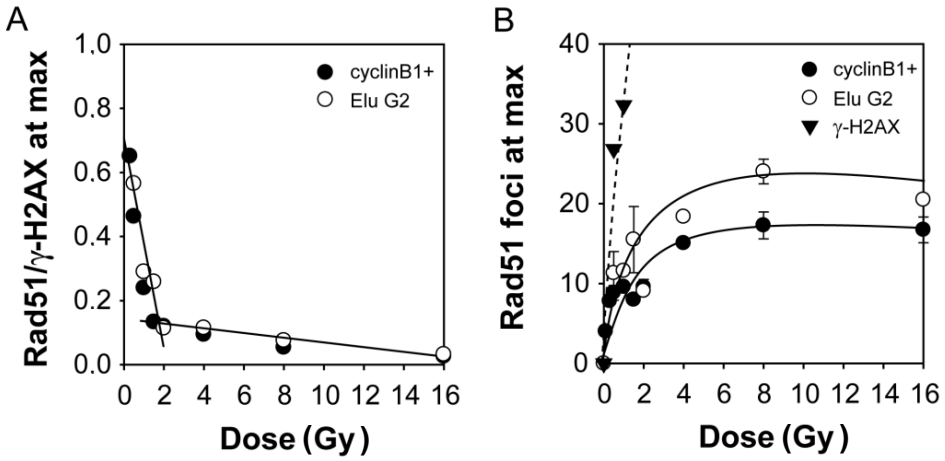

Figure 8: The contribution of HRR decreases with increasing radiation dose. The amount of γH2AX and Rad51 foci was determined in A549 cells after different doses of IR. To discriminate late S and G_2 phase cells, either the cell cycle marker cyclin B1 or centrifugal elutriation of G_2 cells was used. (**A**) The calculation of Rad51 foci/γH2AX foci revealed a high contribution of HRR after low doses of IR, whereas with increasing DSB amount the percentage of HRR declines. (**B**) The analysis of Rad51 foci also reveals a saturation of HRR at higher doses as the numbers of Rad51 foci do not further increase with increasing damage induction.

In addition to this new parameter in DSB repair pathway selection, it was reported that the localization of DSBs could also have a considerable influence on repair pathway choice. The induction and repair of DSBs in actively transcribing gene regions or in highly repetitive sequences in compacted chromatin regions could be conducted in a completely different manner. Depending on chromatin structure in the vicinity of the break site, varying chromatin remodeling processes are initiated to secure and promote the subsequent DSB repair reaction.

Thus chromatin structure and chromatin remodeling machines could serve as an additional level of regulation of repair pathway choice. In the next section a short overview of chromatin organization and its role in DSB repair is given.

1.3 Chromatin structure and its influence on DSB repair pathway choice

1.3.1 Chromatin organization

To accommodate about 3 billion base pairs of DNA in the nucleus, the DNA of higher eukaryotes is tightly packed into chromosomes in a complex series of folding and coiling processes.

The basic unit of chromatin is the nucleosome, containing a histone octamer, which binds and wraps 146 base pairs of double stranded helical DNA in approximately 1.7 DNA turns. The histone octamer is built up of four different histones H2A, H2B, H3 and H4, each of which dimerize in the context of the histone octamer. The nucleosomes appear as a "beads on a string" filament, which was first visualized by electron microscopy (Olins and Olins, 1974). The addition of the linker histone H1 wraps 20 additional base pairs around the histone octamer, completing 2 turns of DNA around the histone complex. The nucleosomes are additionally folded to produce a 30 nm fiber. However, the elucidation of the detailed fiber architecture is yet incomplete and remains a controversial issue (Grigoryev and Woodcock, 2012). The 30 nm fiber can undergo extensive folding into loops, compression and tightly coiling until a 250 nm fiber is reached, which marks the chromatid of the chromosomes. Chromosomes occupy defined regions within the nucleus, and are organized into discrete chromosome territories (Cremer and Cremer, 2001).

To allow transcription or replication, chromatin has to be transiently modified and open up to allow enzymes to access the DNA molecule. Post-translational modifications like acetylation or methylation influence the chromatin compaction or relaxation and could be read from the chromatin remodeling complexes, which could temporally displace the entire nucleosome.

The induction of a DSB is associated with dramatic chromatin changes. DSB processing also requires remodeling of chromatin structure to allow access of repair proteins to the damaged sites. From all DSB repair mechanisms, HRR has the greatest benefit from the extensive chromatin remodeling and nucleosome repositioning. These events are expected to facilitate DNA end resection and to allow strand invasion (Jeggo and Downs, 2014). Chromatin

structure is not only a barrier during DSB repair; it is known to provide binding interfaces and to support the accumulation of repair proteins. The chromatin remodeling processes and chromatin modification mechanisms are described in the following sections along the ways through which they facilitate DSB repair.

1.3.2 Chromatin modifications in response to DSB induction and the recruitment of repair proteins

It has been suggested that the initial DSB detection is first triggered by an alteration in chromatin structure (Thompson, 2012) and that dynamic modifications in chromatin regions at the break sites regulate the accumulation of repair proteins and have a decisive influence on repair pathway choice. It was shown that immediately after DNA damage induction, chromatin sustaining DSBs undergoes an energy-dependent local expansion, corresponding to a 30-40% reduction in the density of the chromatin fibers in the vicinity of the break (Kruhlak et al., 2006). ATP-dependent chromatin remodeling complexes like SWI/SNF complexes and SMARCAD1 are recruited to DSBs to mediate alterations of nucleosome structures. SWI/SNF was shown to be involved in DSB repair by promoting the phosphorylation of H2AX (Park et al., 2006), whereas SMARCAD1 promotes HRR as its loss results in impaired DNA end resection and decreased HRR efficiency (Costelloe et al., 2012). Another chromatin-remodeling complex, associated with the initial steps of DSB end processing is INO80, which is demonstrated to mediate 5'-3' resection during HRR (Gospodinov et al., 2011).

Post-translational modifications of histones are also regulating chromatin accessibility during DSB repair. Acetylation of N-terminal histone tails is known to weaken the interaction between histones and DNA, resulting in chromatin relaxation. It is therefore not surprising that histone acetyltransferases (HAT) are essential for DSB repair. Tip60 is associated with DNA repair, which was demonstrated in cells lacking histone acetylase activity. These cells lost their apoptotic competence upon DNA damage induction, suggesting a defect in the cells' ability to signal the presence of DNA damage (Ikura et al., 2000). Tip60 is associated with histone H4 hyperacetylation, promoting chromatin relaxation and accumulation of repair proteins at DSBs (Murr et al., 2006). Another important role of Tip60 is the acetylation of ATM, stimulating its autophosphorylation and activation after IR (Sun et al., 2005).

The most important and well characterized post-translational modification in response to DSB induction is the phosphorylation of histone H2AX at serine 139, which spread along a

megabase-sized chromatin region around the generated DSB (Rogakou et al., 1999). The following recruitment of E3 ubiquitin ligase RNF8, initiates ubiquitylation events at H2A and H2AX (Mailand et al., 2007). Together with the second ubiquitin ligase RNF168, the ubiquitin signal gets amplified, which is required for the recruitment and retention of the two major DSB repair mediating factors, 53BP1 and BRCA1 (Doil et al., 2009). RNF8 plays also a critical role in checkpoint induction, as depletion of RNF8 leads to a defective G_2/M arrest and increased IR sensitivity (Huen et al., 2007, Kolas et al., 2007). Another ubiquitin-dependent signaling pathway via RAP80 facilitates the recruitment of BRCA1. RAP80 contains a tandem ubiquitin-interacting motif domain, which facilitates the binding of RAP80 to ubiquitylated histones. RAP80 targets a protein complex containing BRCA1 (Kim et al., 2007, Sobhian et al., 2007). Moreover, histone methylation around DSBs by methyltransferase MMSET was described to facilitate DSB repair by increasing methylation of H4 at lysine 20 (K20), a recruitment signal for 53BP1 (Pei et al., 2011). Another histone methylation signal, which is known to be a mark for 53BP1 recruitment, is methylation of H3 at lysine 79 (K79), indicated as H3K79me. As methylation of histone H3K79 is unaltered in response to DNA damage, it is proposed that 53BP1 senses DSBs indirectly through changes in the chromatin structure that expose the 53BP1 binding signal (Huyen et al., 2004).

1.3.3 Repair of DSBs in heterochromatin

Heterochromatin (HC), as opposed to euchromatin (EC), illustrates the highly compacted form of chromatin, which comprises transcriptionally inactive and highly repetitive DNA sequences. In contrast to HC, EC is characterized by open chromatin structures, which are transcriptionally active and contain gene-rich DNA sequences. The post-translational modifications on histones have a high impact on defining chromatin state, and specific histone marks are distinctively distributed and enriched among hetero- and euchromatin regions. In this regard, methylated histones are common in HC regions, which are associated with depletion of acetylated histones, while such histone modifications are common and more abundant in EC regions. A specific marker of highly condensed and repetitive DNA sequences is the trimethylation of histone H3 on lysine 9 (H3K9me3). H3K9me3 directly interacts with heterochromatin protein 1 (HP1), which is necessary for the maintenance of heterochromatic structures (Maison and Almouzni, 2004). HP1 also interacts with KAP1 (KRAB-domain associated protein 1), which is involved in regulating the HC state (Iyengar and Farnham,

2011). The high compaction of HC regions is assumed to constitute a barrier for DNA repair, and it was demonstrated that DSBs induced in HC regions are processed slower, than those formed in EC (Goodarzi et al., 2008, Lemaître and Soutoglou, 2014). However, recent findings reveal that HC-associated proteins play a positive role in DNA repair, which suggests that DSB repair is activated in HC as well (Soria et al., 2012, Lemaitre et al., 2012).

In insect cells it was shown that heterochromatic DSBs can be mobilized to move outside the compacted regions, in order to complete processing and escape the compacted environment of HC, which limits accessibility to repair proteins (Chiolo et al., 2011). However, in human cells it was demonstrated that the formation of γH2AX foci after IR preferentially occurs in EC, implying different processing for heterochromatic and euchromatic DSBs (Cowell et al., 2007).

Independent of the cell cycle phase, heterochromatic DSBs are reported to be repaired with slower kinetics and with a strong requirement for ATM and Artemis proteins (Kühne et al., 2004, Riballo et al., 2004, Goodarzi et al., 2008, Beucher et al., 2009). Genetic studies showed that in G_1 phase cells the fast and slow repair component require NHEJ factors, while the slow component in G_2 phase cells requires HRR factors (Beucher et al., 2009, Jeggo et al., 2011). The results of these findings lead to the formulation of the following cell cycle dependent model: In G_1 and G_2 phase cells, the majority of IR-induced DSBs are repaired with fast repair kinetics (~ 80%) and a minor fraction (~ 20%), which represents a sub-fraction of DSBs located within or close to HC regions, are repaired with slow kinetics. Moreover, in G_1 phase cells, DSB repair depends on NHEJ factors such as DNA ligase 4 and Xlf, as well as on ATM and Artemis if the break is induced in HC regions. In G_2 phase cells, the majority of breaks are also repaired with fast kinetics by c-NHEJ. However, in G_2 phase cells, the slow repair of HC breaks (~ 20%) is executed through HRR (Goodarzi et al., 2010). Nevertheless, the validity and the generality of this model are debated.

The requirement for ATM activity to facilitate the repair of HC breaks is due to its capacity to phosphorylate KAP1 on serine 824, which triggers global chromatin relaxation to promote DSB repair and was shown to enhance cell survival after IR exposure (Goodarzi et al., 2008, Ziv et al., 2006). Besides the initiation of chromatin remodeling, ATM is also involved in re-directing repair towards HRR in G_2 phase by phosphorylating CtIP at serine 664/745 (Li et al., 2000). Artemis was shown to function as an endonuclease during DSB repair and was characterized as a promoting factor for c-NHEJ (Ma et al., 2002, Riballo et al., 2004). In G_2

phase cells, depletion of Artemis reduced the formation of Rad51 foci, suggesting a role for Artemis in the efficient end resection required during HRR. Additionally to the involvement of Artemis in c-NHEJ and HRR, recent findings from our laboratory revealed a role of Artemis in alt-EJ (Moscariello et al., 2015). These findings indicate that ATM and Artemis promote different repair pathways to repair HC breaks, NHEJ in G_1 and HRR in G_2 phase cells (Goodarzi et al., 2010).

HP1 proteins are also implicated in the DNA damage response of heterochromatic DSBs as it was shown that HP1 isoforms are recruited to DSBs and promote RPA loading. However, the precise mechanism of HP1 contribution to DSB repair remains to be elucidated. It is proposed that HP1 facilitates DNA repair by reorganizing chromatin structures (Dinant and Luijsterburg, 2009, Ayoub et al., 2009, Soria and Almouzni, 2013).

1.3.4 Modifications of chromatin structure to investigate DSB repair

In order to investigate the influence of chromatin structure on the initiation and repair of DSBs, we have evaluated the induction and repair of DSBs in the context of chromatin by following the formation of IR induced foci in hetero- and euchromatic regions. Additionally, we have utilized treatments, which result in global modification of chromatin structure, for example incubation in hypertonic or hypotonic solutions. Moreover, the methylation status of the histone proteins was selectively modified by inhibiting histone methyltransferases.

Hypertonic treatment of cells is a method to reversibly modify chromatin structure by inducing chromatin condensation (Reitsema et al., 2005, Albiez et al., 2006). In 1972 Dettor et al. reported, that hypertonic treatment of Chinese hamster cells increased radiosensitization through higher cell killing and increased chromosomal aberrations (Dettor et al., 1972). Similar results were obtained from Raaphorst and his colleagues as well (Raaphorst et al., 1977). Investigation of DSB rejoining ability of cells under hypertonic medium (300 mM NaCl) showed a decrease in the fast rejoining component. However, slow rejoining was evident at hypertonic treated cells, with a half-time similar to those observed in control cells, investigated under isotonic conditions (Iliakis et al., 1993). It was shown that hypertonic treatment (500 mM NaCl) inhibited the nuclear translocation of Ku80 and Ku70 after IR and resulted in an increase in the size of γH2AX foci, suggesting reduced ability to repair DSBs (Endoh et al., 2001, Reitsema et al., 2004).

The incubation of cells in hypotonic medium leads to decondensation of chromatin (Delpire et al., 1985). In a recent study, hypotonic treatment was used to reveal a link between alt-EJ and chromatin condensation status, as it was shown that chromatin decondensation generated by hypotonic treatment promotes alt-EJ in plateau phase cells (Moscariello and Iliakis, 2013). However, the influence of hypertonic and hypotonic treatment, and the resulting chromatin changes in DSB repair efficiency are incompletely understood and are therefore one focus of this thesis.

Inhibition of histone methyltransferases can be used to modify chromatin structure by targeting specific post-translational chromatin modifications. In this study we have used the fungal mycotoxin chaetocin, isolated from *Chaetomium minutum*, which was identified as a specific inhibitor of histone methyltransferase SUV39H1 by a high-throughput screening (Greiner et al., 2005). Inhibition of SUV39H1 leads to a decrease of di- and trimethylated histone H3 at lysine 9. SUV39H1 plays a vital role in heterochromatin organization as it methylates H3K9 and its loss impairs heterochromatin structures and genome stability (Peters et al., 2001). In this study we have used chaetocin to inhibit SUV39H1 in order to investigate the effect of chromatin structure on DSB signaling and repair.

1.4 Ionizing radiation induced foci (IRIF) formation

To study the repair of DSBs we have used analysis of ionizing radiation induced foci (IRIF) as a powerful tool to indirectly visualize DSB induction and repair. Several DDR proteins and downstream repair molecules are known to be recruited in large numbers to DSBs and neighboring chromatin regions in response to IR. Such recruitment is illustrated by the formation of distinct sub-nuclear structures, called foci, which can be visualized by immunofluorescence microscopy. The formation of γH2AX foci upon DSB induction was described first by the group of Rogakou et al. and revolutionized the study of DSB induction and repair (Rogakou et al., 1998, Rogakou et al., 1999). It was shown, that within seconds after DSB induction the histone variant H2AX gets phosphorylated at its C-terminal serine 139, forming γH2AX and that this signal spreads over thousands of base pairs (Rogakou et al., 1998, Rogakou et al., 1999).

The number of γH2AX foci increases linearly with increasing radiation dose. Before the discovery of IRIF formation, induction and repair of DSBs was directly quantified by pulsed-field gel electrophoresis (PFGE). To measure repair kinetics with PFGE, cells have to be

irradiated with relatively high doses of IR in order to induce measurable signals in this assay. Moreover, PFGE requires protein-free DNA which is achieved by high temperature lysis, which has the potential to induce additional DSBs by the transformation of heat-labile sites into DSB, resulting in overestimation of initial damage load (Kinner et al., 2008, Singh et al., 2009). In comparison, the analysis of IRIF comprises several advantages, as they are formed already after low doses of IR, which are therapeutically more relevant and by using fluorescent fusion proteins, the formation and disappearance of foci can be even monitored during live cell measurements.

Besides the formation of γH2AX foci, autophosphorylated ATM at Serine 1981 (pATM) and 53BP1 are known to form IRIF (Bakkenist and Kastan, 2003, Anderson et al., 2001). Changes in chromatin structure induce rapid autophosphorylation of ATM, which leads to dimer dissociation and consequent increase in the ATM kinase activity (Bakkenist and Kastan, 2003). As this response becomes highly amplified, pATM appear as nuclear foci after DSB induction. The amount and kinetics of pATM foci were shown to be comparable to γH2AX foci (Suzuki et al., 2006, Rothkamm et al., 2015). The formation of 53BP1 foci is a readout of intact chromatin-based DSB signaling, including histone phosphorylation, ubiquitylation and acetylation (Panier and Boulton, 2014). The accumulation and decay of 53BP1 foci is also generally accepted as an indicator of DSB induction and repair and is often equated with γH2AX foci. Nevertheless, it has to be considered that 53BP1 is involved in DSB repair pathway choice as a suppressor of end resection and promoter of NHEJ. However, it was demonstrated that 53BP1 is also required for the repair of heterochromatic DSBs in G_2 phase cells by HRR, as it is retained at the break site during HRR. This observation rules out 53BP1 as an explicit marker of NHEJ (Kakarougkas et al., 2013).

The only repair pathway, which can be definitely visualized by foci formation is HRR, as the assembly of RPA and Rad51 at ssDNA leads to the formation of nuclear foci (Haaf et al., 1995, Raderschall et al., 1999). However, the formation of RPA foci cannot always be associated with HRR activation, as it is known that RPA heterotrimers are accumulating at chromatin during DNA replication. Therefore, the investigation of IRIF should be combined with detailed cell cycle analysis. In order to investigate the repair of DSBs by HRR in late S and G_2 phase of the cell cycle, we have utilized cyclin B1 immunostaining.

2. Aim of the work

The purpose of this study is to examine the influence of the chromatin structure on repair pathway choice with a focus on HRR activity. Recent findings from our laboratory revealed a relative contribution of HRR to the overall DSB repair, ranging from over 50% at low radiation doses to less than 5% at radiation doses above 8 Gy. In order to reconcile these findings with the published data, stating that NHEJ is the major DSB repair pathway even in G_2 phase cells and demonstrating that HRR is involved in the repair of just 20% of the total DSBs mainly induced in HC areas, we designed systematic studies to evaluate DSB repair in HC and EC areas. Additionally, we analyzed the influence of altered chromatin condensation on DSB repair efficiency.

To achieve the main goals of this study we have designed the following experiments:

1. We utilized immunofluorescence staining and confocal laser scanning microscopy (CLSM) to investigate the formation of different IRIF in HC and EC areas in late S and G_2 phase cells. In particular, we analyzed γH2AX foci as a well-established marker of DSBs, RPA foci as an indicator of end resection and Rad51 foci as a marker of ongoing HRR. We have included analysis of 53BP1 foci, as a repair mediator suggested to promote NHEJ. In order to consider dose dependent variations of HRR-contributions to DSB repair, we applied a wide range of IR doses.
2. We have investigated the influence of altered chromatin condensation on DSB repair efficiency by monitoring the accumulation of IRIF at different osmotic conditions. According to these studies, we have established hypertonic and hypotonic treatment conditions to modulate chromatin condensation status.
3. We have specifically modulated chromatin condensation by inhibition of the histone methyltransferase SUV39H1 using chaetocin. The effects of these chromatin modifications on DSB repair processes were examined by analyzing the formation of different types of repair foci after IR.
4. Furthermore, we have utilized GFP based DSB repair reporter assays to study the impact of chromatin structure alterations on specific DSB repair pathways used to process I-*Sce*I endonuclease induced DSBs.

3. Material and Methods

3.1 Material

Table 1: Laboratory apparatuses

Apparatus	Provider
Centrifuge, Biofuge Fresco	Heraeus, Germany
Centrifuge, Multifuge 3S-R	Heraeus, Germany
Centrifuge, Rotanta 460R	Hettich, Germany
Confocal laser scanning microscope TCS SP5	Leica Microsystems, Germany
Coulter counter, Multisizer 4e	Beckman Coulter, Germany
Flow cytometer Gallios	Beckman Coulter, Germany
Heating unit	Oehmen, Germany
Inverted microscope LH50A	Olympus, Germany
Laminar flow hood, HeraSafe	Heraeus, Germany
Magnetic stirrer, MR Hei-Standard	Heidolph, Germany
MCO-18 O2/CO2 incubators	Sanyo, Germany
Micro Centrifuge, IR	Carl Roth, Germany
Minishaker MS1	IKA, Germany
Nucleofector	Lonza, Germany
O_2/CO_2 Incubator, MCO-18AIC/MCO-18M	Sanyo, Japan
pH-Mater, InoLab	WTW GmbH, Germany
Pipetboy	Falcon, Germany
Pipettes, Rainin Pipet-Lite	Mettler Toledo, Germany
Rocky shaker	Oehmen, Germany
Slide drying bench	Electrothermal, Germany
Vacuum gas pump	VWR, Germany
Vortexer, IKA MS 3 basic	IKA, Germany
Water bath, GFL 1092	Oehmen, Germany
X-ray control unit, Xrad320	PXi, USA
X-ray generator, ISOVOLT Titan	General Electrics, USA
X-ray tube, MXR320	Comet, Switzerland

Table 2: Disposable products

Disposable Product	Provider
Culture dishes (35 mm)	Thermo Scientific, Germany
Culture dishes (60 and 100 mm)	Greiner, Germany
Falcon tubes (15 and 50 ml)	Greiner, Germany
Flasks and beakers	Schott Duran, Germany
Glass cover slips (Ø 20 mm)	VWR, Germany
Imaging chamber	Zell-Kontakt GmbH, Germany
Microscope slides, cut color frosted white	VWR, Germany
Parafilm	Bremis, USA
Pipette tips	Starlab, Germany
Reaction tubes (1.5 and 2 ml)	Greiner, Germany
Serological pipettes (2, 5, 10, 25 ml)	Sarstedt, Germany

Table 3: Chemicals

Chemicals	Provider
4',6-diamidino-2-phenylindole (DAPI)	Serva, Germany
B02 (Rad51 inhibitor)	Merck Millipore, Germany
Bovine serum albumin (fraction V) (BSA)	Sigma Aldrich, Germany
Chaetocin	Sigma Aldrich, Germany
Dimethyl sulfoxide (DMSO)	Sigma Aldrich, Germany
Ethanol	Sigma Aldrich, Germany
Ethylenediaminetetraacetic acid (EDTA)	Roth, Germany
Fetal bovine serum (FBS)	Gibco Life Sciences
Gelatin	Sigma Aldrich, Germany
Non-essential amino acids (NEAA)	Biochrom, Germany
NU7441	Tocris Bioscience, USA
Paraformaldehyde (PFA)	Roth, Germany
Penicillin	Sigma Aldrich, Germany
PromoFluor Antifade	PromoKine, Germany
Propidium iodide (PI)	Sigma Aldrich, Germany
Sodium azide	Roth, Germany
Sodium chloride (NaCl)	Roth, Germany
Streptomycin	Sigma Aldrich, Germany
Tris(hydroxymethyl)aminomethane (Tris)	Roth, Germany

Triton X-100	Roth, Germany
Trypsin	Biochrom, Germany

Table 4: Solutions

Solution	Compounds
Fixation solution	3% PFA 2% Sucrose 1x PBS
PBG (Blocking buffer)	0.2% Gelatin 0.5% BSA (fraction V) PBS pH 7.4
PBS (1x)	137 mM NaCl 10 mM Na_2HPO_4 2.7 mM KCl 1.76 mM KH_2PO_4 pH 7.4
PFA	2% Paraformaldehyde in sterile water
P-solution (Permeabilization solution) Flow cytometry	0.2% Triton X-100 1x PBS
P-solution (Permeabilization solution) Immunofluorescence	100 mM Tris, pH 7.4 50 mM EDTA 0.5% Triton X-100

Table 5: Cell culture growth medium

Growth medium	Provider
Dulbecco's Modified Eagle Medium (DMEM)	Sigma-Aldrich
Leibovitz's L-15 Medium	Sigma-Aldrich
McCoy's 5A Medium	Sigma-Aldrich
Minimum Essential Medium (MEM)	Sigma-Aldrich

Table 6: Human cell lines and growth medium

Cell line	Cell type	Growth medium	Serum
82-6 hTert	Immortalized fibroblasts	MEM + 1% NEAA	15%
A549	Lung adenocarcinoma	McCoy's 5A	10%
U2OS	Osteosarcoma	McCoy's 5A	10%
U2OS 279A EJ2-GFP	Osteosarcoma	McCoy's 5A	10%
U2OS 280A EJ5-GFP	Osteosarcoma	McCoy's 5A	10%
U2OS 282C DR-GFP	Osteosarcoma	McCoy's 5A	10%

Table 7: Antibodies and dilutions. The conditions in different methods are indicated (FC: Flow cytometry and IF: Immunofluorescence)

Antibody	Host species	Type	Dilution	Incubation time	Provider
53BP1 (H300)	rabbit	polyclonal	1:300 (IF)	1.5 h (IF)	Santa Cruz Biotechnology
53BP1	mouse	monoclonal	1:20 (IF)	1.5 h (IF)	IFMSB, UK-Essen
Alexa Fluor 488 Anti-mouse	goat	polyclonal	1:400 (IF)	1 h (IF)	Invitrogen
Alexa Fluor 488 Anti-rabbit	goat	polyclonal	1:400 (IF)	1 h (IF)	Invitrogen
Alexa Fluor 568 Anti-mouse	goat	polyclonal	1:400 (IF)	1 h (IF)	Invitrogen
Alexa Fluor 568 Anti-rabbit	goat	polyclonal	1:400 (IF)	1 h (IF)	Invitrogen
Alexa Fluor 647 Anti-rabbit	goat	polyclonal	1:200 (FC) 1:400 (IF)	2 h (FC) 1 h (IF)	Invitrogen
CyclinB1-TRITC	rabbit	polyclonal	1:50 (IF)	1.5 h (IF)	Santa Cruz Biotechnology
H3K9ac	mouse	monoclonal	1:1000 (IF)	1.5 h (IF)	Abcam
H3K9me3	rabbit	polyclonal	1:500 (IF)	1.5 h (IF)	Abcam
pATM	rabbit	polyclonal	1:500 (IF)	1.5 h (IF)	Abcam
Rad51 (14B4)	mouse	monoclonal	1:500 (IF)	1.5 h (IF)	Genetex
Rad51 (Ab-1)	rabbit	polyclonal	1:400 (IF)	1.5 h (IF)	Merck Millipore
RPA	mouse	monoclonal	1:200 (IF)	1.5 h (IF)	IFMSB, UK-Essen
γH2AX	rabbit	polyclonal	1:200 (FC)	2 h (FC)	Abcam
γH2AX [3F2]	mouse	monoclonal	1:300 (IF)	1.5 h (IF)	Abcam

Table 8: Plasmids

Plasmid	Description
53BP1-mCherry	expresses 53BP1-mCherry fusion protein
pCMV3xnlsl*Sce*I	I-*Sce*I expressing plasmid
pmaxGFP	GFP expressing plasmid

Table 9: Software

Software	Provider
Adobe Creative Suite 6	Adobe Systems Inc., USA
EndNote X7	Thomson Reuters, USA
Fiji (ImageJ)	Open source
ImarisXT 8.0	Bitplane AG, Switzerland
Kaluza 1.2	Beckman Coulter, USA
LasAF	Leica Microsystems, Germany
Microsoft Office 2010	Microsoft, USA
SigmaPlot 11	Systat Software Inc. USA

3.2 Methods

3.2.1 X-ray irradiation

Cells were exposed to X-rays using an X-ray machine (X-ray tube: MXR320 (Comet), X-ray generator: ISOVOLT Titan (General Electrics), control unit: Xrad320 (PXi)) operating at 320kV and 12.5 mA. A 1.65 mm aluminum filter was used to selectively attenuate low-energy rays. Cells were exposed to X-rays in standard tissue cell culture dishes at a distance of 50 cm from the source and a dose rate of 2.65 Gy/min. Homogeneous irradiation was ensured by rotation of the radiation table. Immediately after irradiation, cells were placed back in the O_2/CO_2 incubator until the collection of time points, according to the experiment protocol. Un-irradiated control cells were treated equally.

3.2.2 Cell culture

Cells were cultured at 37°C and 5% CO_2 atmosphere in a humidified incubator. All growth media were supplemented with 100 µg/ml penicillin and 100 µg/ml streptomycin. Additionally, 10-15% fetal bovine serum (FBS) was added to the growth medium. 82-6hTert cells required supplementation with 1% non-essential amino acids (NEA). The cell lines and media used are summarized in Tab. 6.

All cells were regularly passaged and full confluence was avoided. In order to passage or collect cells, cells were washed with PBS and incubated for 5 min at 37°C with a 0.05% trypsin solution to detach. Thereafter, cells were collected and resuspended in 5 ml growth medium. Cell numbers were determined with a Beckman Coulter cell counter (Multisizer 4e). For cell cultivation, 100 mm tissue culture dishes with 15 ml medium were used, whereas for most experiments cells were plated in 35 mm tissue culture dishes with 2 ml medium. All cells used for experiments were in the exponential growth phase.

3.2.3 Hypertonic and hypotonic cell treatment

To apply hypertonic and hypotonic treatment, the osmotic concentration of the standard growth medium was increased or decreased by a factor of two. Osmotic concentration was

increased by adding NaCl to reach an end concentration of 300 mM NaCl. Hypotonic medium was prepared by diluting standard growth medium with an equal amount of sterile water.

For immunofluorescence experiments (3.2.8), cells were plated in standard growth medium for two or three days. After irradiation, the standard growth medium was removed and substituted with the hypertonic or hypotonic medium to establish hypertonic or hypotonic conditions during DSB repair. Cells were kept in these conditions until collection.

To measure the repair of I-*Sce*I induced DSBs with cell lines containing reporter constructs (3.2.6), the standard growth medium was substituted with hypertonic and hypotonic medium 2 h after transfection and these conditions were kept for 22 h until flow cytometry analysis.

Control cells were treated equally with normal growth medium (isotonic medium).

3.2.4 Drug treatments

In order to inhibit the histone methyltransferase SUV39H1, cells were treated with chaetocin (0.01 and 0.1 μM). If not otherwise specified, cells were pretreated 6 h with chaetocin before irradiation.

Inhibitors used in the experiments to study the repair of I-*Sce*I induced DSBs in cell lines containing reporter constructs were added 2 h after transfection and kept in the medium until analysis.

All inhibitors were dissolved in DMSO and accordingly, DMSO was added to control cells.

3.2.5 Cell transfection by nucleofection

Nucleofection is an electroporation-based transfection method and was used to transfer plasmids into cells. Exponentially growing cells were collected by cell detachment with trypsin and spun down for 7 min at 970 rpm. Depending on the required cell amount, $1x10^6$-$4x10^6$ cells were used per transfection reaction. Growth medium was carefully aspirated and cells were resuspended in the 100 μl HP transfection buffer. Plasmids were added (1μg plasmid/$1x10^6$ cells) and cells were transferred to an electroporation cuvette. Nucleofection program X-01 was chosen. Immediately after transfection, cells were collected in pre-warmed (37°C) growth medium, plated and returned to the incubator.

3.2.6 Measuring repair of I-*Sce*I induced DSBs with integrated reporter constructs

To monitor repair activities of a specific DSB repair pathway, three different U2OS cell lines were used with stable chromosome-integrated repair reporter constructs. These constructs were designed to indicate repair by a specific repair pathway via restoration of a GFP expression cassette, which can be scored using flow cytometry analysis (Bennardo et al., 2008).

To induce DSBs the reporter cell lines were transiently transfected (3.2.5) with the I-*Sce*I expression vector pCMV-3xNLS-I*Sce*I. Hypertonic, hypotonic medium or inhibitors were applied 2 h after transfection. Twenty-four hours after transfection flow cytometry analysis was used to quantify repair.

3.2.6.1 DR-GFP reporter construct

With the U2OS 282C cell line, which bears a stable integration of the repair reporter construct DR-GFP, HRR activity can be measured. The integrated construct consists of two modified GFP gene sequences, oriented as direct repeats and was hence named DR-GFP (Fig. 9). The *Sce*GFP gene contains the complete GFP sequence but is interrupted by an I-*Sce*I cutting site and a premature stop-codon. The iGFP gene is an inactive copy of the GFP gene as its sequence is 5' and 3' truncated. The expression of the endonuclease I-*Sce*I leads to the induction of a DSB in the *Sce*GFP gene. If DSB repair occurs via HRR by using the iGFP gene sequence as homologous sequence, a functional GFP sequence is rebuilt. Flow cytometry analysis was used to detect GFP fluorescence signal.

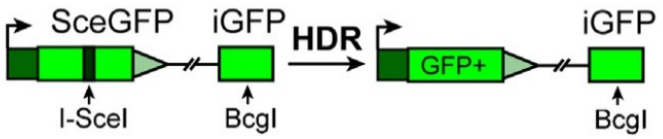

Figure 9: Schematic drawing of the DR-GFP construct (Moscariello et al., 2015).

3.2.6.2 EJ5-GFP reporter construct

The U2OS EJ5-GFP reporter cell line contains a stably integrated reporter construct to measure NHEJ events which are accompanied by extensive deletions. In the EJ5-GFP reporter construct the full length GFP open reading frame is separated from its promotor by a

puromycin (puro) gene (Fig. 10). Two I-*Sce*I cutting sites flank the puro gene region. Upon I-*Sce*I expression two DSBs are introduced. If the puro sequence is lost and the two distal ends are rejoined, the GFP signal can be detected.

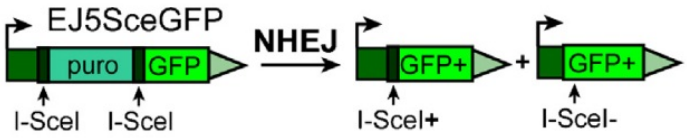

Figure 10: Schematic drawing of the EJ5-GFP construct (Moscariello et al., 2015).

3.2.6.3 EJ2-GFP reporter construct

With the U2OS EJ2-GFP reporter cell line, microhomology dependent alt-EJ events can be detected. The reporter construct (Fig. 11) contains a GFP sequence fused to an N-terminal tag sequence. The tag and GFP sequence are interrupted by an I-*Sce*I cutting site and a stop codon which are flanked by 8 nucleotides of microhomology. The repair of cut I-*Sce*I site by microhomology dependent alt-EJ restores the GFP coding frame and GFP positive cells can be directly analyzed by flow cytometry.

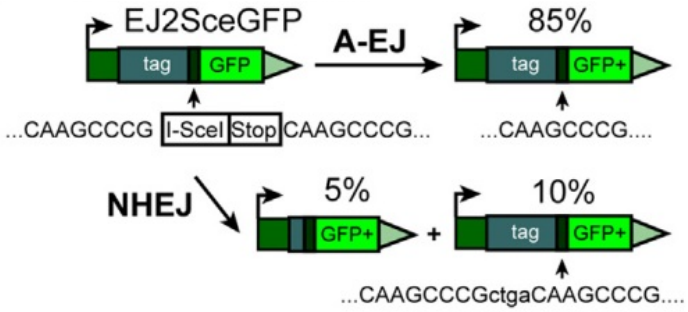

Figure 11: Schematic drawing of the EJ2-GFP construct (Moscariello et al., 2015).

3.2.7 Flow cytometry

Flow cytometry was performed with a Beckman Coulter Gallios flow cytometer and was used to analyze cell cycle distribution, to quantify the outcome of the repair reporter assays and to measure H2AX phosphorylation. The cell cycle distribution was evaluated by detecting the fluorescence intensity of the intercalating agent propidium iodide (PI) bound to nucleic acids and indicating the DNA content. PI is cell membrane impermeable. Therefore, cells have to be

permeabilized before PI staining. A maximum of $1x10^6$ cells were trypsinized, spun down and resuspended in 1 ml ethanol (70%, 4°C) for fixation and permeabilization. Cells were stored at least over night or for longer at 4°C. Before flow cytometry analysis, cells were spun down, ethanol was aspirated and cells were resuspended in PI staining solution (PBS, 40 µg/ml PI, 62 µg/ml RNAse) and incubated for 15 min at 37°C. Routinely, $1x10^4$ cells were measured by flow cytometry to determine the cell cycle distribution.

To quantify the outcome of the repair reporter assays, cells were collected 24 h after transfection for flow cytometry analysis. The emission of GFP was measured in up to $3x10^4$ cells.

Additionally, flow cytometry was used to analyze the phosphorylation of H2AX in response to irradiation at hypertonic treatment condition. Exponentially growing A549 cells were irradiated with different IR doses (2.5-20 Gy) and the standard growth medium was immediately replaced with hypertonic medium after exposure to IR. One hour after irradiation, cells were collected and 500 µl ice-cold P-solution (Tab. 4) was added and cells were incubated 2 min on ice. After centrifugation (1500 rpm, 5 min, 4°C) the P-solution was aspirated and 500 µl Fixation solution (Tab. 4) was added. Cells were incubated 15 min at RT before they were spun down (1500 rpm, 5 min). Fixation solution was aspirated and 500 µl PBG (Tab. 4) was added and cells were incubated over night at 4°C. For antibody staining, PBG was aspirated and the cells were incubated with the primary antibody (Tab. 7) 2 h at RT while gently shaking. Cells were washed with PBS before the second antibody was added for 2 h at RT while gently shaking in darkness. Finally, cells were washed once again with PBS and $3x10^4$ cells per treatment condition were analyzed.

3.2.8 Immunofluorescence staining

For immunofluorescence experiments approximately 10^5 cells were plated in 35 mm dishes, each containing an Ø 20 mm glass coverslip. After two days, cells were irradiated with the appropriate doses (0.5-16 Gy) and incubated at 37°C, 5% CO_2 until the time points at which the formation of IRIF had to be examined (30 min-18 h). To fix cells, the medium was removed and cells were briefly washed with PBS. The coverslip was transferred to a new dish containing 2 ml of 2% PFA (Tab. 4) and incubated for 15 min at RT. PFA was removed and fixed cells were washed again with PBS. For permeabilization 2 ml P-solution (Tab. 4) with

0.5% Triton X-100 was added for 7 min at RT. After removal of P-solution and washing with PBS, 2 ml PBG (Tab. 4) were added at least for 1 h at RT or over night at 4°C.

After blocking, primary antibodies were diluted in PBG and cells were incubated for 90 min at RT with primary antibodies (Tab. 7). The coverslips were washed three times for 5 min with PBS. Secondary antibodies with conjugated Alexa Fluor dyes were diluted 1:400 in PBG and cells were incubated 60 min at RT in the dark with secondary antibodies (Tab. 7). To identify late S and G_2 phase cells, cells were additionally incubated with a cyclin B1 antibody conjugated to rhodamine for 90 min at RT. Cells were washed once with PBS and incubated 10 min with 4',6-diamidino-2-phenylindole (DAPI) (25 ng/ml) to stain the DNA. Finally, coverslips were embedded on microscopic slides with PromoFluor. Slides were stored over night in the dark before scanning with confocal laser scanning microcopy.

3.2.9 Confocal laser scanning microscopy (CLSM)

In order to obtain high resolution optical images to quantify foci formation, CLSM was performed with a LEICA TCS-SP5 confocal microscope. In confocal microscopy sharper images, than those from conventional fluorescence microscopy are achieved by suppressing the detection of out-of-focus light. This is attained by the detection pinhole, through which the emitted/reflected light has to pass before it is detected and transformed into electrical signals by a photomultiplier tube (PMT). The sample is scanned line-by-line with a focused laser beam that moves over the specimen in X and Y directions, only illuminating a small focal volume of the sample at a time. In order to allow three-dimensional reconstitution of the samples, optical sectioning in steps of 0.5 µM along the z-axis was used.

3.2.9.1 Scanning of fixed cells

To detect the formation of IRIF, A549 cells were prepared and treated as described in section 3.2.8. At least five fields, well distributed all over the coverslip, were scanned for each sample. The parameters and settings used for CLSM are summarized in Tab. 10. The digital image analysis of the generated LIF files was performed with the Imaris software (3.2.9.3).

Table 10: Parameters and settings for CLSM to scan fixed cells

Hardware	**Setting**
Microscope	Leica TCS-SP5
Objective	HCX PL APO lambda blue; 63.0 x 1.4 Oil UV
Acquisition parameter	**Setting**
Scan direction	Bidirectional
Zoom	1.2
Speed	400 Hz
Resolution	1024 x 1024
Excitation laser	**Intensity setting**
405 nm	40%
488 nm	25%
561 nm	30%
633 nm	30%
Detector range	**PMT voltage / offset**
415 nm – 490 nm	800V/-4%
505 nm – 547 nm	730V/-4%
587 nm – 621 nm	850V/-4%
657 nm – 684 nm	630V/-4%

3.2.9.2 Live cell imaging

To monitor the formation and disappearance of 53BP1 foci in living cells, live cell imaging experiments were performed. Three days prior to transfection $0.2x10^6$ U2OS were plated. Cells were transiently transfected with a 53BP1-mCherry plasmid and $0.3x10^6$ transfected cells were plated in each well of an eight well live cell imaging chamber. Twenty-four hours after transfection, cells were washed with pre-warmed PBS and pre-warmed Leibovitz's L-15 medium was added to support cell growth in environments without CO_2 equilibration. Cells were irradiated and to enable exposure to different doses a customized lead cover was used to cover the other chambers. The chamber was placed in a custom-made holder and a 63x Leica water objective, which was connected to a water immersion micro dispenser was used to enable constant focusing during the long (17 h) experiment. The water dispenser was set to pump approximately 150 µl every 60 min. Live cell imaging was performed with a Leica TCS SP5 confocal microscope using next to the scanning along x-, y- and z-axis a t-dimension to record every 30 or 15 min. To ensure optimal cell growth conditions the microscope stage was

covered by an environmental chamber, providing 37°C. The parameters and settings used for CLSM are summarized in Tab. 11. In each well, two fields were tracked and nuclei with well distinguishable and countable foci were counted separately for each recorded time point.

Table 11: Parameters and settings for live cell imaging

Hardware	**Setting**
Microscope	Leica TCS-SP5
Objective	63.0x Leica water objective
Acquisition parameter	**Setting**
Scan direction	Bidirectional
Zoom	1.2
Speed	400 Hz
Resolution	1024 x 1024
Excitation laser	**Intensity setting**
561 nm	30%
Detector range	**PMT voltage / offset**
590 nm – 676 nm	800V/-1.2%

3.2.9.3 Digital image analysis with Imaris

After immunofluorescence staining and scanning, the generated LIF files were analyzed with the Imaris software (Imaris 8, Bitplane). The cell detection mode was used to determine the nucleus, the heterochromatic regions as well as foci as surface objects (Fig. 12 A). The gray value threshold for the separation of signal and background were kept constant for all objects within experiments, to ensure comparability of different samples. Moreover, foci were defined as objects with a minimum diameter of 0.5 µm. For every dose and time point at least 5 images were quantified. To discriminate late S and G_2 phase cells, only cells with a visible cyclin B1 staining in the cytoplasm were selected for analysis (Fig. 12 B).

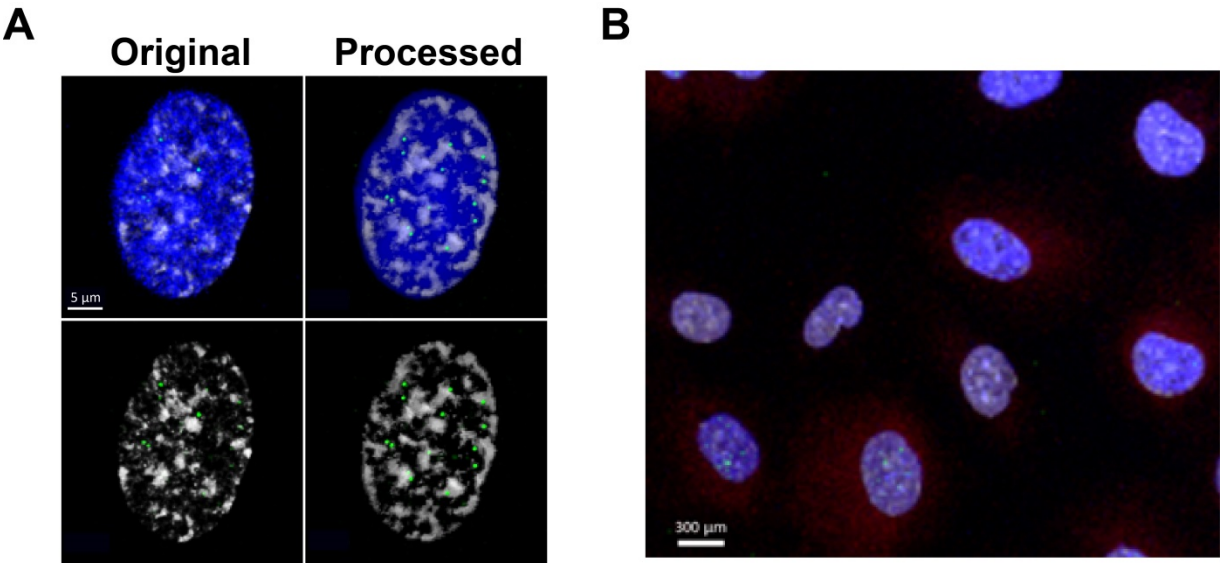

Figure 12: Image analysis of CLSM files. (**A**) Example of a nucleus showing DAPI staining (blue), the heterochromatin marker (grey) and foci (green) before (left side) and after (right side) image processing. (**B**) Cytoplasmic cyclin B1 staining (red) was used to discriminate late S and G_2 phase cells from the other cell population.

4. Results

4.1 Formation of IRIF in heterochromatin and euchromatin

The analysis of IRIF by immunofluorescence microscopy is a well-established technique to investigate the induction, processing and repair of DSBs (Rogakou et al., 1998, Kinner et al., 2008). In order to examine the influence of the chromatin structure on DSB repair pathway choice we used immunofluorescence microscopy to analyze the occurrence of IRIF in HC and EC regions. Moreover, these data were generated to reconcile our findings of dose dependent variation of HRR activity (1.2.7 and Fig. 8) with the published data suggesting a role for HRR only in the repair of heterochromatic DSBs (1.3.3). Formation of γH2AX foci was used to monitor total DSB induction and repair. To specifically measure the occurrence of HRR, we analyzed formation and decay of RPA and Rad51 foci. In order to focus our analysis on late S and G_2 phase cells, in which all three repair pathways can operate to repair DSBs, we have utilized cyclin B1 as a cell cycle marker, which is specifically expressed in S and G_2 phase cells. To examine the appearance of foci in HC and EC regions, two distinct chromatin markers were employed: H3K9me3 and H3K9ac identify heterochromatic and euchromatic nuclear regions, respectively. The formation of IRIF was examined in exponentially growing, A549 human lung adenocarcinoma cells. To generate DSBs, cells were exposed to increasing doses of X-rays.

4.1.1 Validation of chromatin markers

The post-translational modifications of the N-terminal histone tails are important regulators of chromatin organization and are crucial for epigenetic control of gene expression. H3K9me3, a marker of constitutive heterochromatin, is associated with highly condensed, repetitive DNA sequences and transcriptional repression.

We first tested the affinity of the H3K9me3 antibody in mouse embryonic fibroblasts (MEF). In mouse cells, constitutive heterochromatin regions are clustered into structures known as chromocentres. These chromocentres can be easily identified by DAPI staining and occur as DAPI-intense regions (Fig. 13 A). The staining with the utilized heterochromatin marker

H3K9me3 overlaps exactly with the position of chromocentres, proving the specificity of this antibody for heterochromatic regions (Fig. 13 B).

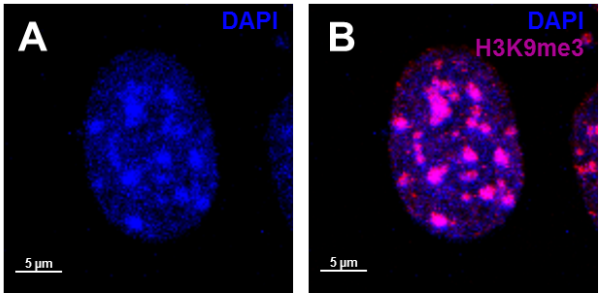

Figure 13: Heterochromatin marker H3K9me3 staining overlaps with mouse chromocentres. (**A**) In mouse nuclei, constitutive heterochromatin is organized in chromocentres which can be visualized by DAPI staining. (**B**) The H3K9me3 staining overlaps precisely with chromocentres in MEF nuclei.

In human cells, heterochromatic regions are more evenly distributed in the nuclei and cannot be visualized by DAPI staining (compare Fig. 13 A and Fig. 14 A). To discriminate heterochromatic regions in human A549 cells, the H3K9me3 antibody was applied. H3K9me3 stains several irregular areas throughout the nucleus and smaller areas adjacent to the nuclear envelope, according to the repressive chromatin regions interacting with the nuclear lamina (Fig. 14 B) (Bank and Gruenbaum, 2011).

To define euchromatic regions, an antibody against H3K9ac was used. H3K9ac is associated with transcriptional activity and appears in promoter regions. Staining of A549 cells with the euchromatin marker H3K9ac shows an even distribution of the euchromatin marker H3K9ac in the nucleus with some irregular non-stained areas (Fig. 14 C). The co-immunostaining with H3K9me3 reveals that these gaps display positive signals for the heterochromatic staining (Fig. 14 D).

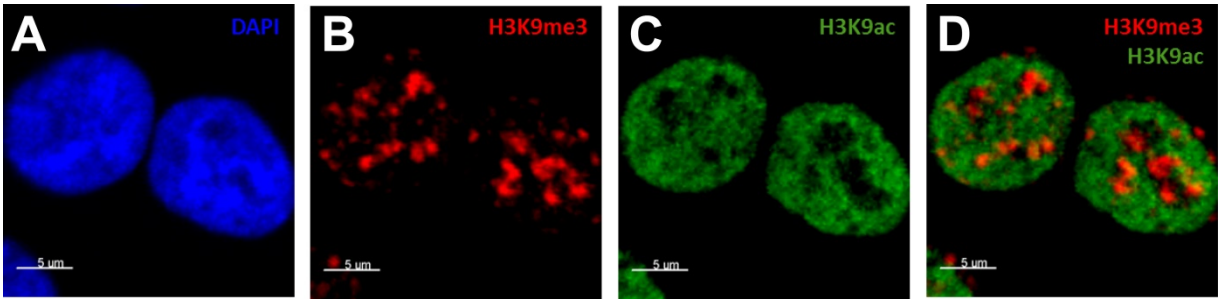

Figure 14: Immunofluorescence staining of the heterochromatin marker H3K9me3 and euchromatin marker H3K9ac in human A549 nuclei. (**A**) DAPI staining of human A549 nuclei. (**B-D**) Co-immunostaining with heterochromatin marker H3K9me3 (**B**) and euchromatin marker H3K9ac (**C**) in A549 cells.

In the majority of the following experiments we used the HC marker H3K9me3 to examine the formation of IRIF in condensed chromatin. To simplify terminology hereafter, H3K9me3 positive stained areas are referred to as HC and EC is defined as DAPI positive but H3K9me3 negative areas in the nucleus. In experiments with the EC marker H3K9ac, the H3K9ac positive areas are termed EC and H3K9ac negative areas HC. To estimate the formation of IRIF in HC and EC regions we made serious effort to adhere closely and consistently to our protocols in the different experiments, in order to keep the conditions constant during antibody staining, microscopy scanning and image analysis. Despite these efforts, we observed variations of chromatin marker staining, which can be explained by dynamic modification and remodeling processes, influencing the cellular chromatin architecture. Since we observed variations in the amount of HC also in non-irradiated cells, we concluded that in our studies irradiation had no detectable effect on HC variations (suppl. 8.1).

4.1.2 The formation of γH2AX foci in hetero- and euchromatic regions

The phosphorylation of histone H2AX on serine 139, commonly known as γH2AX, is one of the earliest events after induction of DSBs and depends on members of the PIKK family, including ATM, ATR and DNA-PK. Upon DSB induction, the phosphorylation of H2AX spreads over a chromatin region, covering several Mbp around the break site. This response is exploited for the detection of DNA double strand breaks by immunofluorescence, as antibodies against γH2AX stain visible and discrete nuclear foci, which serve as a marker of total DSBs present in a cell.

In order to investigate the induction and repair of total DSBs in HC and EC regions, the heterochromatin marker H3K9me3 was used to define condensed regions. DNA was counterstained with DAPI to detect the cell nucleus and only cyclin B1-positive cells were taken into account.

Fig. 15 shows representative pictures of A549 nuclei fixed 1 h post irradiation, showing the appearance of γH2AX foci in H3K9me3 positive and H3K9me3 negative regions.

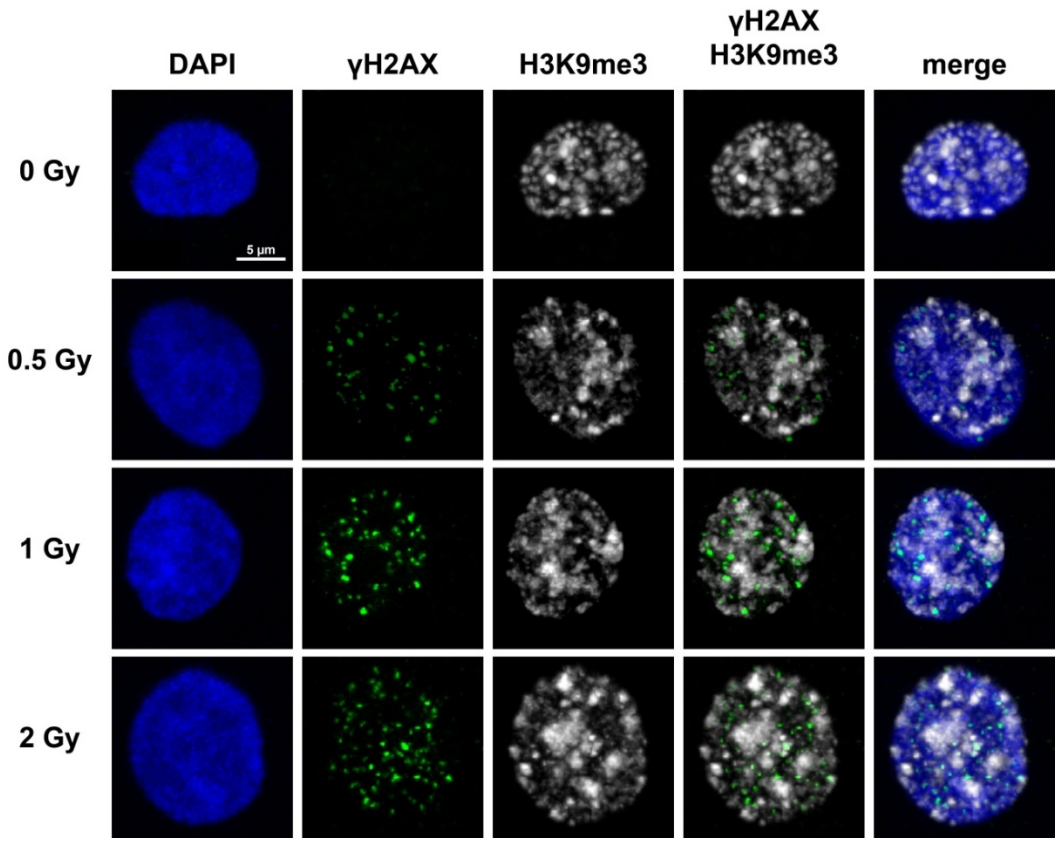

Figure 15: Approach to measure the formation of γH2AX foci in heterochromatic regions in human A549 cells. Representative pictures of A549 nuclei fixed 1 h after irradiation with increasing dose were selected. The DNA was stained with DAPI to visualize the cell nucleus. Co-immunostaining of γH2AX foci, together with the HC marker H3K9me3 was applied, to discriminate foci appearing in H3K9me3 positive HC regions and H3K9me3 negative EC regions.

For each radiation dose (0.5, 1 and 2 Gy), we scored the number of γH2AX foci in the entire nucleus (all foci), as well as the number of foci found in EC or HC areas at several time points after IR (Fig. 16 A-C). The majority of γH2AX foci were detected in EC areas. For example, one hour after exposure to 1 Gy, on average 50 foci were scored per nucleus. Thereof, 40 foci occurred in EC and 10 foci were detected in HC. Taken all data points into account, on average 83% of γH2AX foci occurred in EC areas and 17% of γH2AX foci co-localized with HC areas. In comparison, the proportion of HC and EC areas was 12% and 88%, respectively (suppl. Tab. 12). This quantification demonstrates similar formation of γH2AX foci in EC and HC areas, suggesting similar induction of DSBs in EC and HC areas.

The maximum amount of γH2AX foci in EC as well as HC areas was found between 30 min and 1 h after IR, revealing a similar time frame for the phosphorylation of H2AX in decondensed and condensed chromatin regions. Moreover, the repair kinetics of γH2AX foci

in EC and HC are comparable, indicating similar repair rates of DSBs localized in EC and HC, respectively (Fig. 16 A-C).

To obtain dose response curves, the maximum numbers of γH2AX foci were plotted against the applied radiation dose (Fig. 16 D). The maximum amount of γH2AX foci increased linearly with rising IR dose and reflects the linear increase of DSBs with rising radiation dose. This dose response of γH2AX foci was independent of the chromatin condensation status, pointing to similar DSB induction and recognition in condensed and decondensed chromatin regions.

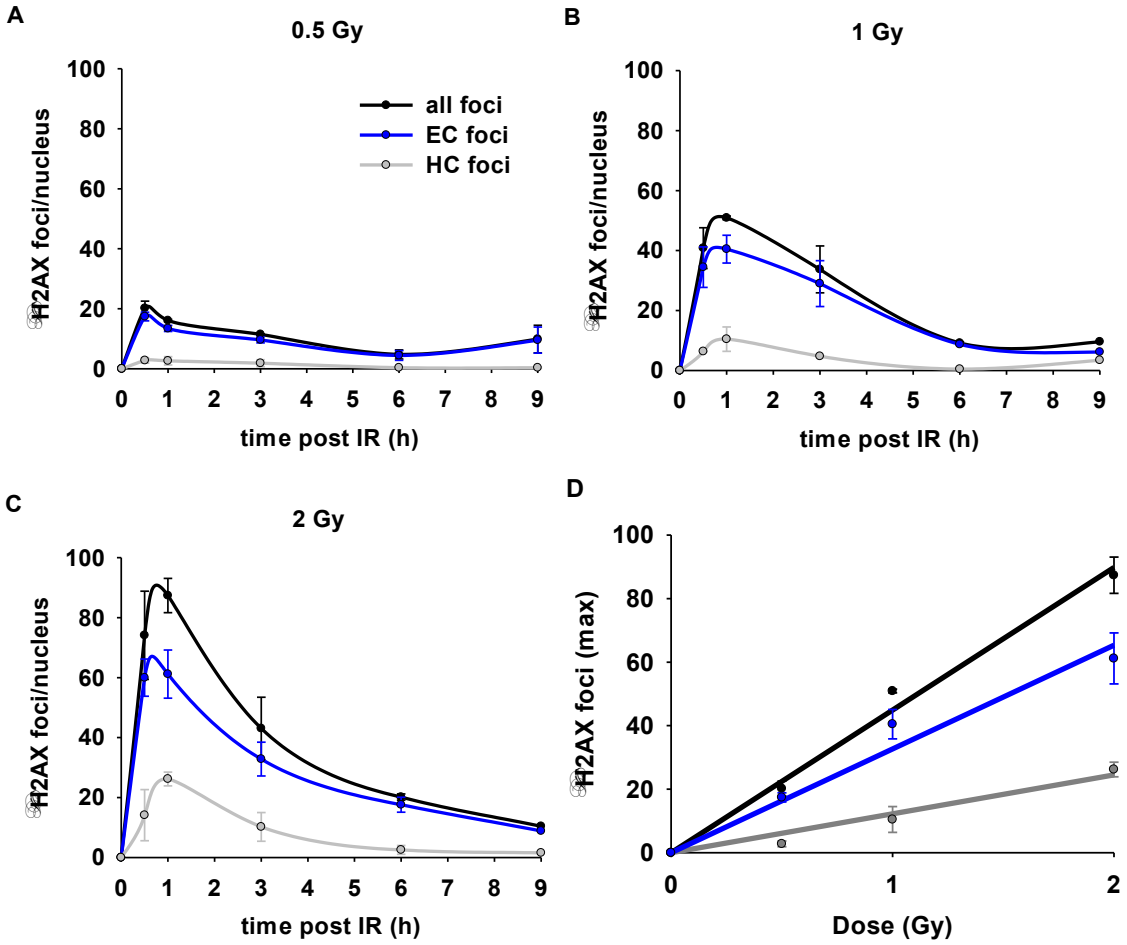

Figure 16: γH2AX foci form in heterochromatic and euchromatic regions with similar kinetics. Exponentially growing A549 cells were exposed to increasing radiation doses and fixed at different times after irradiation. H3K9me3 and cyclinB1 antibodies allowed the identification of HC and G_2 cells, respectively, and thus also the categorization of γH2AX foci in these compartments. (**A-C**) Total γH2AX foci (all foci) as well as γH2AX foci occurring in EC and HC regions were counted and the average number of foci per nucleus calculated. (**D**) The dose response curves depict the maximum numbers of γH2AX foci for each radiation dose. Data points represent the mean from two independent experiments and error bars indicate the standard error of the mean values. On average, γH2AX foci were counted in 19 (+/- 5) nuclei per time point and experiment.

4.1.3 The formation of HRR associated repair foci in hetero- and euchromatic regions

The obvious advantage of HRR, in contrast to the homology-independent pathways c-NHEJ and alt-EJ, is the error-free repair that allows the faithful restoration of the original DNA sequence. The decisive step shunting a DSB repair to HRR is DNA end resection, leading to ssDNA overhangs. RPA molecules are immediately loaded onto the ssDNA and are subsequently replaced by Rad51, generating the Rad51 nucleoprotein filament, which facilitates homology search and strand invasion to form the Holliday junction. The accumulation of RPA and Rad51 molecules at the break sites can be visualized by immunofluorescence staining as they are known to form nuclear foci.

Here we used the analysis of Rad51 and RPA to examine, whether the choice of HRR is dependent upon chromatin structure. Moreover, we used these data to compare our observation that after low doses of IR HRR processes more than half of all DSBs with previous studies, demonstrating that HRR is utilized to repair only ~ 20% of total DSBs, namely DSBs occurring in heterochromatic regions.

To take into account the dose-dependent utilization of HRR, formation of Rad51 and RPA foci were measured after low doses (0.5-2 Gy), mid-range doses (4 Gy) and high doses (8 Gy-16 Gy) of IR in human A549 cells. Cells were fixed at several times after irradiation (30 min, 1, 3, 6, 9, 18 h) and stained with antibodies against Rad51 and RPA. The HC marker H3K9me3 and the cell cycle marker cyclin B1 were used to identify foci forming in HC as well as in late S and G_2 phase cells. DNA was counterstained with DAPI to detect the cell nucleus.

The immunofluorescence staining revealed that Rad51 foci occurred in HC and EC regions (Fig. 17). Foci were evenly distributed in the cell nucleus and several foci co-localized with H3K9me3 positive HC regions, although the majority of Rad51 foci appeared in EC areas.

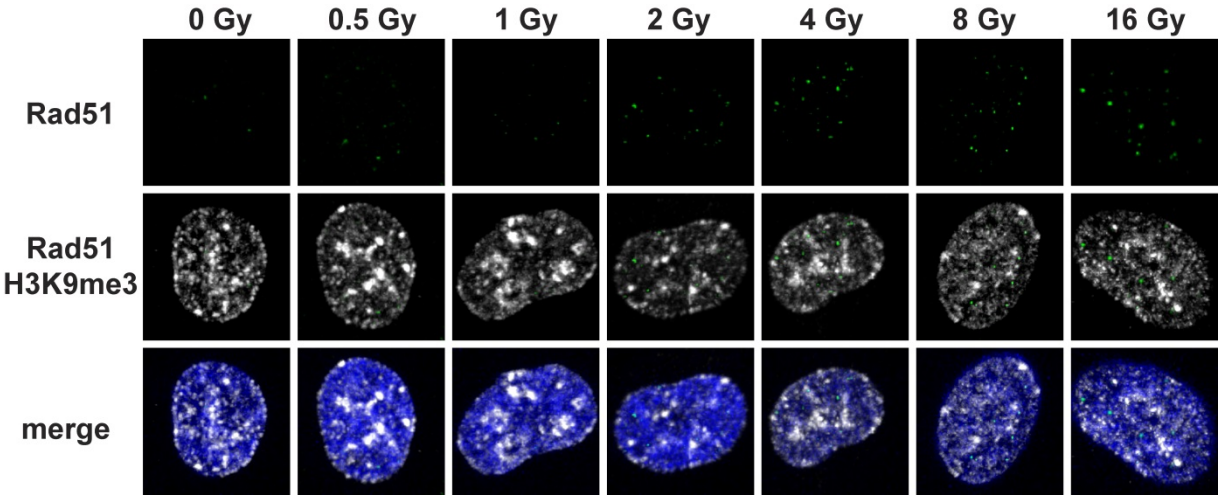

Figure 17: Formation of Rad51 foci in heterochromatic areas in human A549 cell nuclei. Representative images of A549 nuclei fixed 1 h after irradiation with increasing radiation doses were selected. The DNA was stained with DAPI to visualize the cell nucleus. Co-immunostaining of Rad51 foci together with the HC marker H3K9me3 was applied to discriminate foci appearing in HC and EC regions.

The accurate quantification of Rad51 foci numbers in HC and EC confirmed the observation of increased occurrence of Rad51 in EC areas: On average, 80% of Rad51 foci were detected in EC and only the minority, on average 20%, of Rad51 foci appeared in HC regions (Fig. 18). These data strongly suggest that HRR is active in HC, as well as in EC regions, without detectable preference of HRR taking place at DSBs induced in HC regions. Indeed, considering the distribution of EC and HC staining, which was on average 87% and 13% (suppl. Tab. 13), an equal distribution of Rad51 foci in EC and HC can be deduced. We concluded that HRR can be equally active in HC and EC regions, which supports our previous findings that HRR gains prevalence after low radiation doses.

Moreover, the results are in accordance to the aforementioned findings from our laboratory demonstrating HRR saturation at high doses, since we detected no clear increase in Rad51 foci numbers after irradiation at doses higher than 2 Gy (Fig. 18). A maximum of 22 Rad51 foci per nucleus was detected after 2 Gy, which was not significantly exceeded at 4 Gy (24 Rad51 foci), 8 Gy (26 Rad51 foci) or 16 Gy (17 Rad51 foci). Moreover, with increasing radiation dose, the maximum formation of Rad51 foci is reached at later time points. For example, after irradiation with 0.5-4 Gy the maximum numbers of Rad51 foci occurred 1 h post IR, whereas after 8 Gy the time point of maximum Rad51 foci formation is shifted to 6 h post IR.

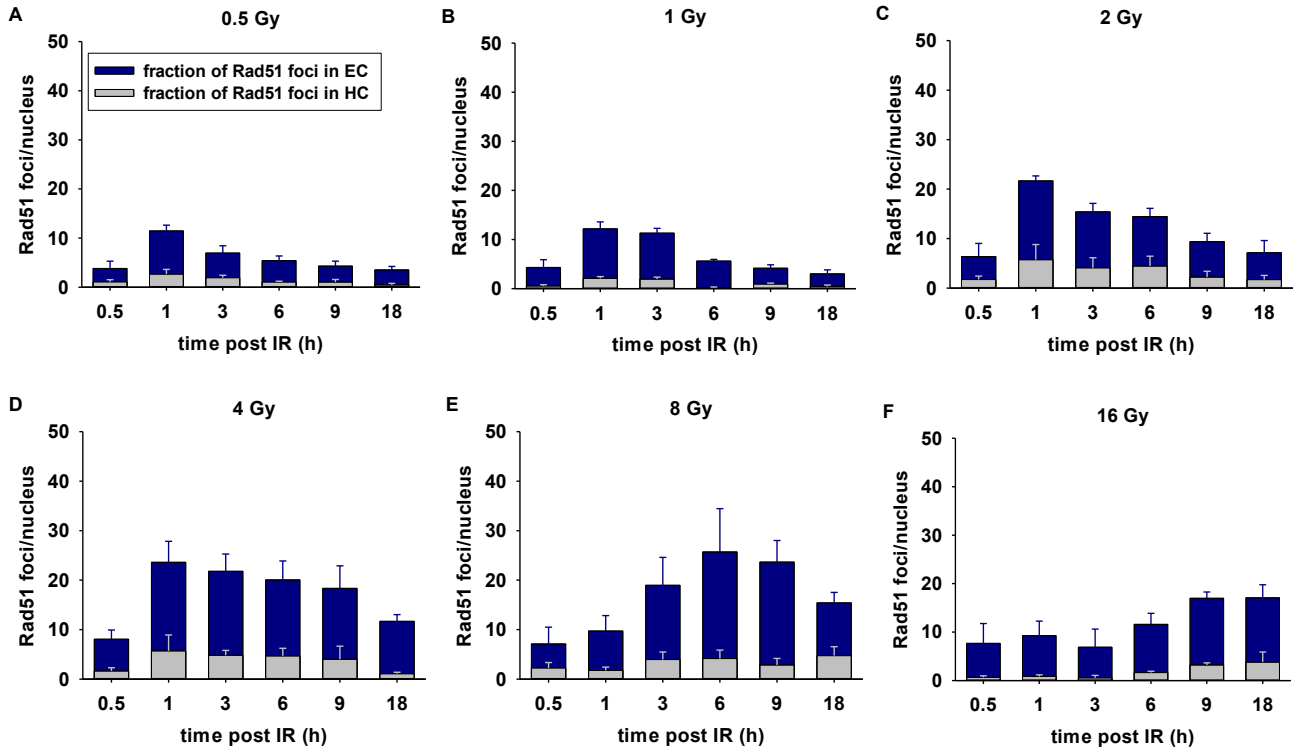

Figure 18: Numbers of Rad51 foci in heterochromatic and euchromatic regions in A549 nuclei. Proliferating A549 cells were irradiated with increasing doses of IR (0.5, 1, 2, 4, 8 and 16 Gy) and collected at different times thereafter (30 min, 1, 3, 6, 9 and 18 h) for immunofluorescence staining. Rad51 foci were counted in H3K9me3 positive HC and H3K9me3 negative EC regions. The grey bar reflects the amount of Rad51 foci scored in H3K9me3 positive regions and the blue bars the fraction of Rad51 foci detected in H3K9me3 negative regions. Bars represent the mean from at least three independent experiments (n = 3-5) and error bars indicate the standard error of the mean values. On average, Rad51 foci were counted in 20 (+/- 6) nuclei per time point and experiment.

In order to verify these results, the euchromatin marker H3K9ac was used to determine the formation of Rad51 foci in EC regions. H3K9ac is associated with transcriptional activation and its presence in promoter regions is associated with a low nucleosome density in the neighborhood of transcription start sites. Co-staining of H3K9ac and Rad51 clearly revealed that the majority of Rad51 foci appeared in EC areas, which is in concordance with the previous findings using the HC marker and verifies the observation that HRR is not solely used for the repair of heterochromatic DSBs (Fig. 19).

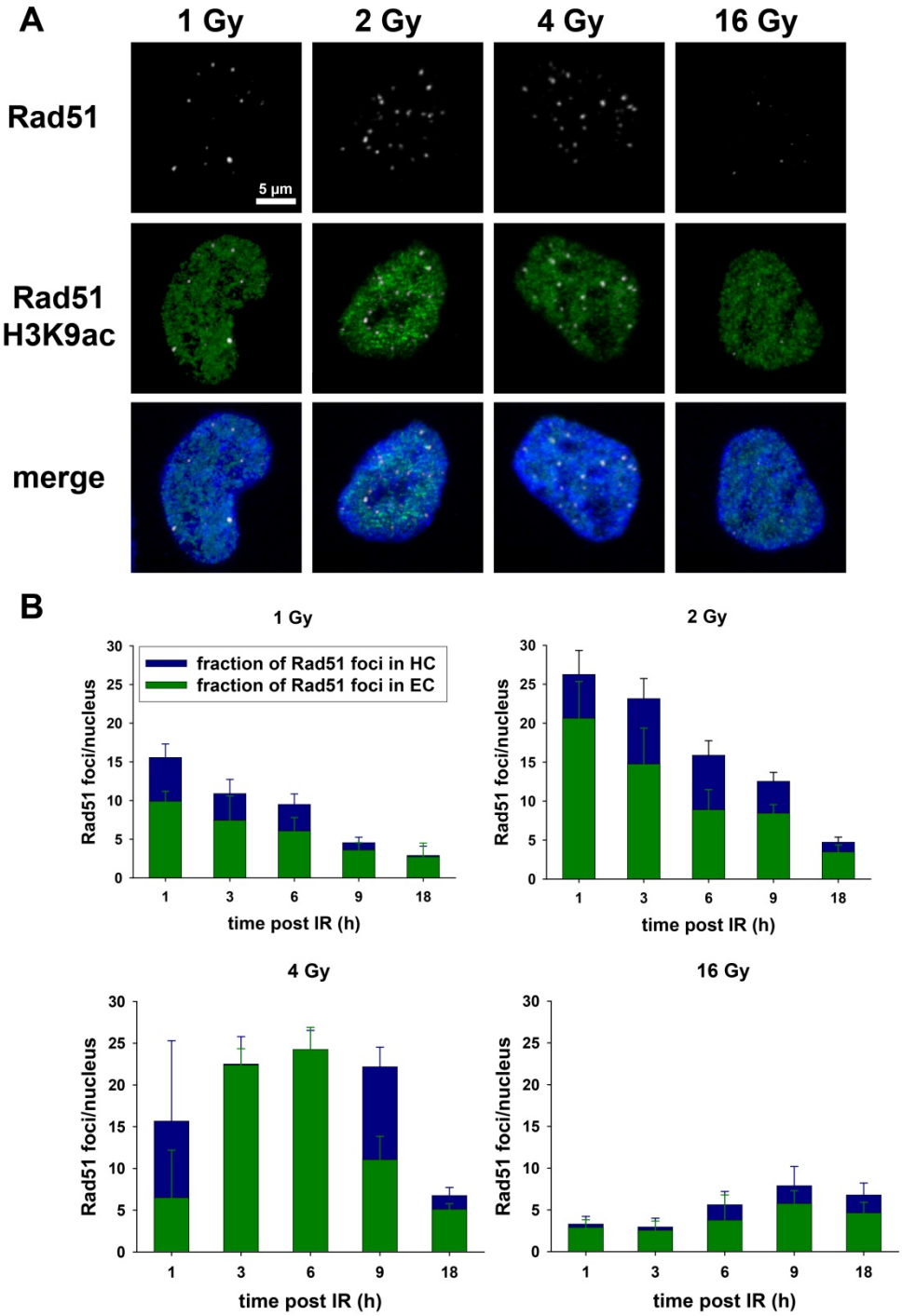

Figure 19: Formation of Rad51 foci in euchromatic regions in human A549 nuclei. (**A**) Representative pictures of A549 nuclei fixed 3 h after irradiation with increasing doses. DNA was stained with DAPI to visualize the cell nucleus. Co-immunostaining of Rad51 foci together with the EC marker H3K9ac was applied to discriminate foci appearing in H3K9ac positive EC regions and H3K9ac negative HC regions. (**B**) Rad51 foci were counted in EC and HC regions at several time points after increasing IR exposure. The green bars reflect the amount of Rad51 foci scored in H3K9ac positive regions and the blue bars show the fraction of Rad51 foci detected in H3K9ac negative regions. Error bars indicate the standard error of Rad51 foci per nucleus in all cells analyzed in one experiment (in average 39 (+/- 24) cells per time point).

In addition to Rad51 foci, the formation of RPA foci was analyzed as a second HRR indicator to investigate if HRR occurs with a preference in heterochromatic or euchromatic areas. As in the experiments analyzing Rad51 foci, RPA foci were detected in HC as well as EC areas, supporting the previous findings that there is no preference for HRR occurring in heterochromatic DSBs (Fig. 20).

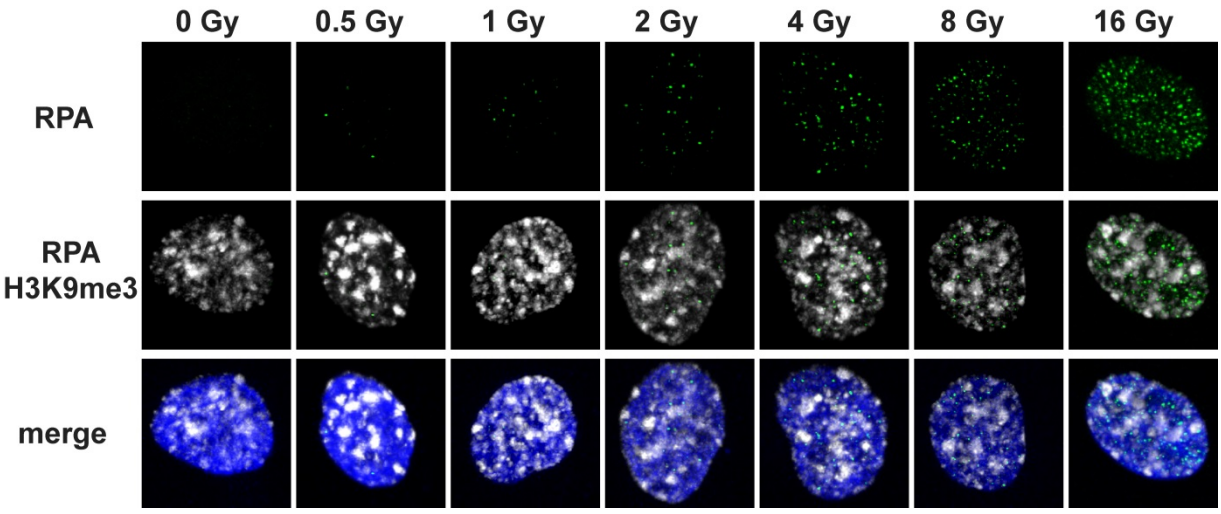

Figure 20: Formation of RPA foci in heterochromatic areas in human A549 nuclei. Representative pictures of A549 nuclei fixed 3 h after irradiation with varying doses. DNA was stained with DAPI to visualize the cell nucleus. Co-immunostaining of RPA foci together with the HC marker H3K9me3 was applied to discriminate foci appearing in H3K9me3 positive HC regions and H3K9me3 negative EC regions.

The average RPA foci number per cell nucleus scored in HC and EC regions for each IR dose and time is shown in Fig. 21. Independently of the applied radiation dose, the majority of RPA foci occurs in EC regions (on average 66 %). However, also in H3K9me3 positive regions, several RPA foci form (on average 34 %). The distribution of RPA foci in HC and EC seems to be independent of the applied radiation dose, as after low, mid-range and high doses of IR the same distribution of HC and EC foci is observed. Moreover, the time interval between IR exposure and cell fixation had no influence on the distribution of HC and EC foci (Fig. 21). In comparison to the distribution of HC and EC staining, being in average 26% and 74%, respectively (suppl. Tab. 14), the detection of 34% HC RPA foci and 66% EC RPA foci once again reveals a similar distribution of HRR activity in EC and HC.

In Fig. 21 G-I the repair kinetics of RPA foci in EC (Fig. 21 H) and HC (Fig. 21 I) are depicted. The repair kinetics of total RPA foci (Fig. 21 G) indicate a rapid accumulation of RPA foci after irradiation, with a maximum reached between 1 and 6 h post irradiation. The

repair kinetics of EC and HC RPA foci exhibit no obvious differences when compared with the repair kinetics of total RPA foci. In both chromatin compartments the formation and decay of RPA foci take place with comparable kinetics.

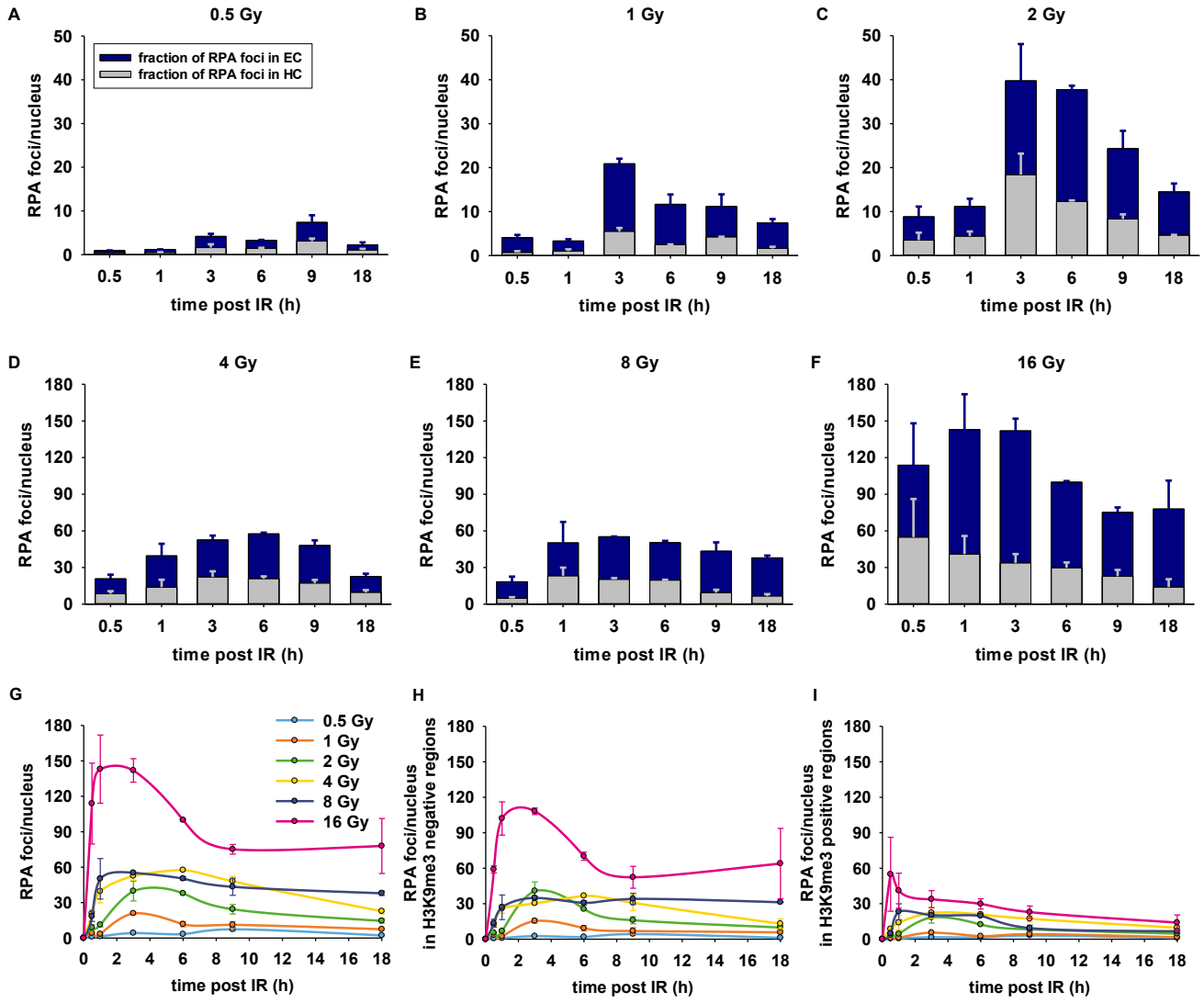

Figure 21: Number of RPA foci in heterochromatic and euchromatic regions in A549 nuclei. Proliferating A549 cells were irradiated with increasing doses of IR and collected at different times (30 min, 1, 3, 6, 9 and 18 h) for immunofluorescence staining. (**A-F**) RPA foci were counted in HC and EC regions. The grey bars reflects the amount of RPA foci scored in H3K9me3 positive regions and the blue bars the fraction of RPA foci detected in H3K9me3 negative regions. (**G-I**) Repair kinetics of RPA foci scored in the entire nucleus (**G**), in EC (**H**) and HC regions (**I**). Data points represent the mean from two independent experiments and error bars indicate the standard error of the mean values. On average, RPA foci were counted in 15 (+/- 4) nuclei per time point and experiment.

In summary, the results for Rad51 and RPA foci strongly suggest that HRR is equally active at DSBs generated in heterochromatic or euchromatic regions. The proportion of HRR associated foci in HC regions is similar to the proportion of H3K9me3 staining in the nucleus: On average, 20% of Rad51 and 34% of RPA foci occurred in HC regions, which is similar to the fraction of H3K9me3 chromatin staining of 13% and 26% in the respective experiments. This suggests that the distribution of RPA and Rad51 foci does not follow specific HC or EC patterns. Therefore, we conclude that the repair pathway decision towards HRR is not influenced by the condensation state of chromatin in the vicinity of the DSB. At least with the here used confocal laser scanning microscopy technique and the markers H3K9me3 and H3K9ac we could not detect an impact on DSB repair pathway choice towards HRR by the condensation state of chromatin.

4.1.4 Saturation of HRR is independent of chromatin condensation

As unpublished data from our laboratory revealed a saturation of HRR with increasing radiation doses, we examined if this saturation of HRR is dependent on chromatin condensation. Therefore, the numbers of Rad51 foci at maximum in H3K9me3 positive regions (HC foci), in H3K9me3 negative regions (EC foci), as well as the total number of Rad51 foci (all foci) were plotted against the radiation dose (Fig. 22 A). The development of the maximum of Rad51 foci as a function of dose is comparable in all compartments. Independently of the co-localization of Rad51 in HC areas, the maximum number of Rad51 foci increases until IR doses between 2 and 4 Gy and stagnates or even decreases at higher doses.

To quantitatively estimate the contribution of homologous recombination to the repair of IR induced DSBs during the G_2 phase, the maximum numbers of Rad51 foci, which represent the numbers of DSBs processed by HRR, were divided by the maximum numbers of γH2AX foci, which reflect the approximate number of induced DSBs. As can be seen from Fig. 22 B, the engagement of HRR in DSB repair dramatically decreases with increasing the radiation dose. Whereas HRR processes ≥ 50% of DSBs after IR with low doses (0.5 Gy), irradiation with 2 Gy already reduces the contribution of HRR down to 20%. With progressively increasing DSB numbers with increasing IR doses, the fraction of DSBs processed by HRR is further reduced to less than 3% (16 Gy). The uniform development of HRR engagement calculated with

H3K9me3 overlapping and non-overlapping Rad51 and γH2AX foci suggests a general saturation of HRR, independently of chromatin condensation status.

In contrast, the maximum amount of total, as well as HC and EC RPA foci increase linearly with radiation dose, demonstrating that end resection is not suppressed at high radiation doses. These data support the assumption of a repair pathway switch from HRR to error-prone repair pathways as resected ends prevent c-NHEJ activity.

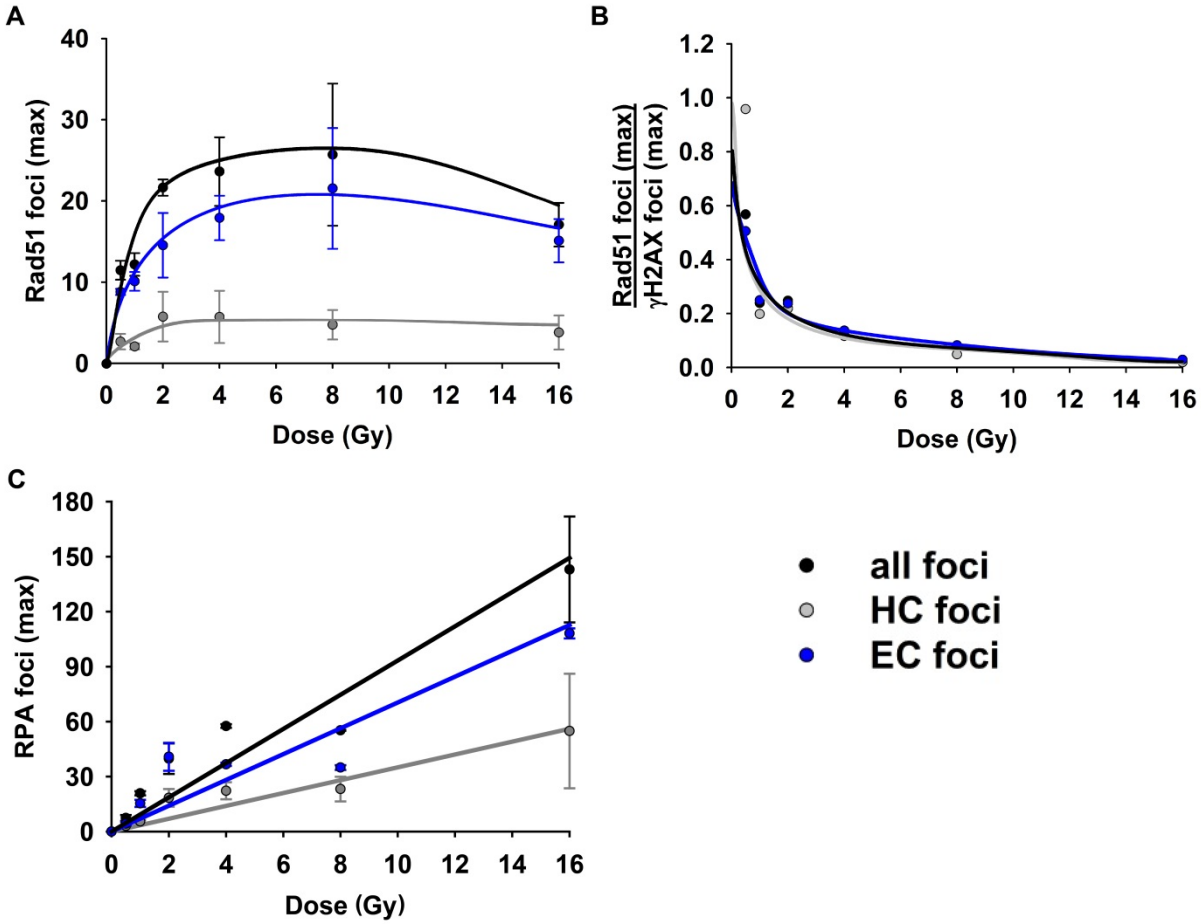

Figure 22: Saturation of HRR takes place independently of chromatin condensation status. (**A**) The maximum numbers of total Rad51 foci, Rad51 in HC and Rad51 foci in EC regions are plotted against the applied IR dose. Data points are the mean from 3-5 independent experiments and the error bars indicate the standard error of the mean values. (**B**) Quantitative estimation of HRR engagement in DSB repair was calculated by dividing the maximum Rad51 foci number by the maximum number of γH2AX foci. The maximum γH2AX foci number upon irradiation with more than 2 Gy is calculated by linear extrapolation (suppl. Tab. 16). (**C**) The maximum numbers of total RPA foci and RPA foci in HC and EC regions are plotted against the applied IR dose. Data points are the mean from 2 independent experiments and the error bars indicate the standard error of the mean values.

4.2 The formation of 53BP1 repair foci

53BP1 is a central component of DSB repair as it is known to recruit repair proteins and promoting checkpoint activation. The prevention of resection and the promotion of NHEJ attributed to 53BP1 make it an important player in DSB repair pathway choice. (Silverman et al., 2004, DiTullio Jr. et al., 2002, Wang et al., 2002, Bouwman et al., 2010, Bunting et al., 2010). Moreover, it has been shown that 53BP1 recruitment is required for heterochromatic DSB repair (Noon et al., 2010).

In order to investigate, whether the chromatin environment has an influence on 53BP1 foci formation, immunofluorescence experiments with antibodies specific for 53BP1 were carried out, together with the HC marker H3K9me3. Human A549 cells were irradiated with a wide range of radiation doses (0.5-16 Gy) to elucidate the recruitment of 53BP1 to DSBs, generated in hetero- and euchromatic regions, and to evaluate how 53BP1 recruitment into nuclear foci correlates with the number of initial DSBs induced during irradiation. For this set of experiments, cells were fixed and stained at several times after IR (30 min, 1, 3, 6, 9, 18 h) to acquire full repair kinetics. In Fig. 23 representative pictures of 53BP1 foci in H3K9me3 rich areas in irradiated A549 cell nuclei are shown. We observed that 53BP1 foci occur evenly in HC and EC areas.

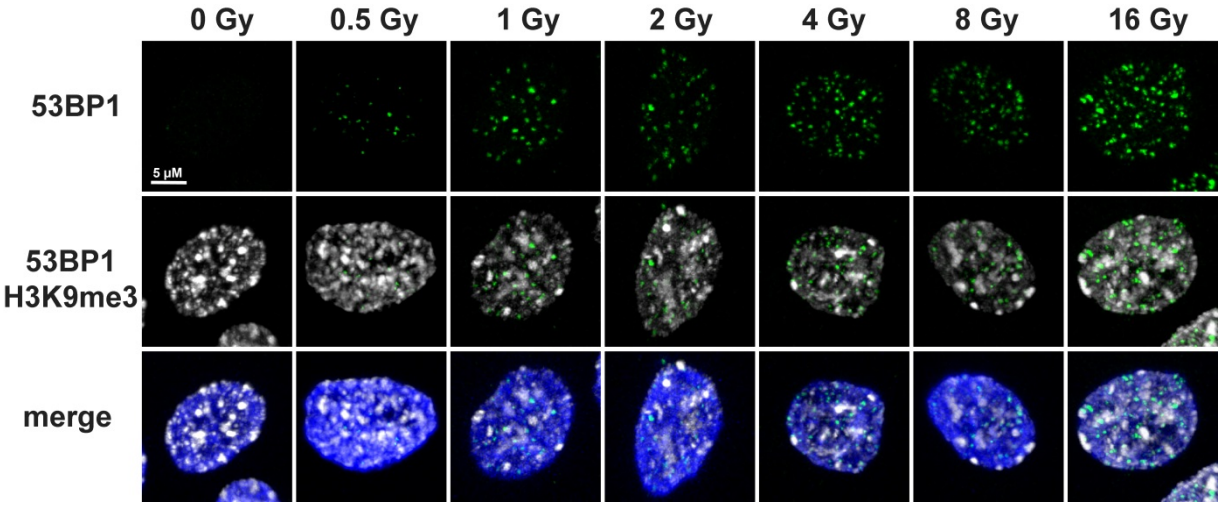

Figure 23: Formation of 53BP1 foci in heterochromatic and euchromatic regions in human A549 nuclei. Representative images of A549 nuclei fixed 1 h after irradiation with increasing radiation doses are shown. The DNA was stained with DAPI to visualize the cell nucleus. Co-immunostaining of 53BP1 foci together with the HC marker H3K9me3was applied to separate foci appearing in HC and EC areas.

To determine the amount of 53BP1 foci in HC and EC areas, foci were scored in HC and EC regions (Fig. 24). In comparison to γH2AX, Rad51 or RPA foci, we detected an increased formation of 53BP1 foci in HC areas. On average 53% of 53BP1 foci formed in H3K9me3 positive regions, which occupied on average only 27% of the total nuclear volume (proportion of HC and EC staining see suppl. Tab 15). This suggests that on average, 53BP1 foci had twice higher incidence in HC regions. We conclude that DSB repair in condensed regions requires 53BP1.

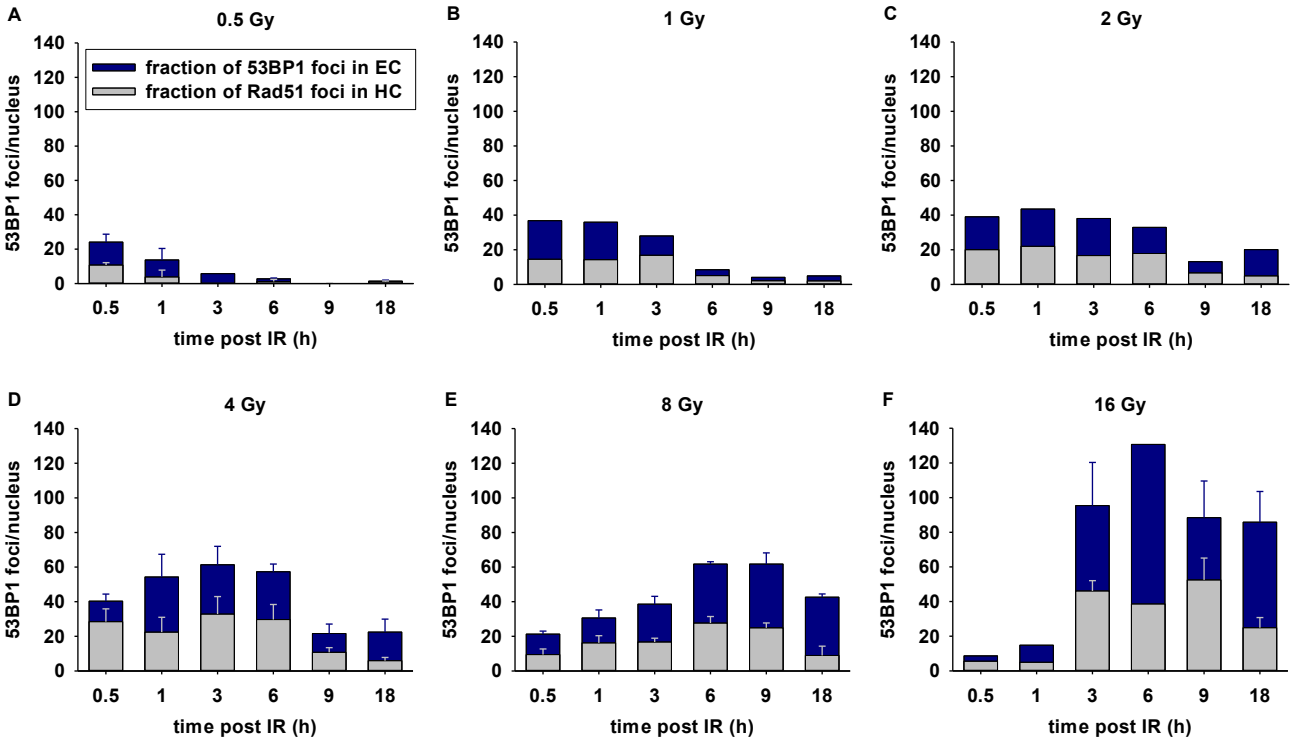

Figure 24: Amount of 53BP1 foci in condensed and decondensed chromatin regions in A549 nuclei. Exponentially growing A549 cells were irradiated with increasing radiation doses and fixed at different times after irradiation. Only late S and G_2 phase cells were analyzed. The numbers of 53BP1 foci in heterochromatic regions (H3K9me3 positive) are indicated by the grey bars, whereas the blue bars depict 53BP1 foci forming in euchromatin (H3K9me3 negative regions). Bars represent the mean from one to two independent experiments and the error bars indicate the standard error of the mean values. In average, 53BP1 foci were counted in 19 (+/- 6) nuclei per time point and experiment.

4.2.1 53BP1 foci persist after IR

During the analysis of hetero- and euchromatic 53BP1 foci in G_2 phase A549 cells, we observed a high and persistent 53BP1 foci number after irradiation of cells with high doses (≥ 4 Gy). To examine whether this was just a G_2-phase-specific phenomenon, or whether irradiated cells accumulate persistent 53BP1 foci independently of cell cycle phase, the entire population of exponentially growing A549 cells was analyzed. Similarly to the observations in G_2 phase cells, 53BP1 foci persisted after IR doses above 4 Gy in the entire population of exponentially growing A549 cells (Fig. 25). We further observed, that 53BP1 foci formation was delayed in cells irradiated with high radiation doses (8, 16 Gy), and that the maximum in the formation of 53BP1 foci was shifted to later time points (3 h after irradiation). In contrast, irradiation with doses ≤ 4 Gy induces a more rapid accumulation of 53BP1 into foci, with a maximum reached 1 h after IR.

To eliminate the possibility of a cell line specific phenomenon, the above experiments were repeated with the human fibroblast cell line, 82-6hTert and with human osteosarcoma U2OS cells. The results from these experiments are comparable with the findings in A549 cells (Fig. 25). We observed persistent 53BP1 foci at late time points after exposure to high doses, and a delayed reaching of the maximum of 53BP1 foci with increasing radiation dose in 82-6hTert and U2OS cells.

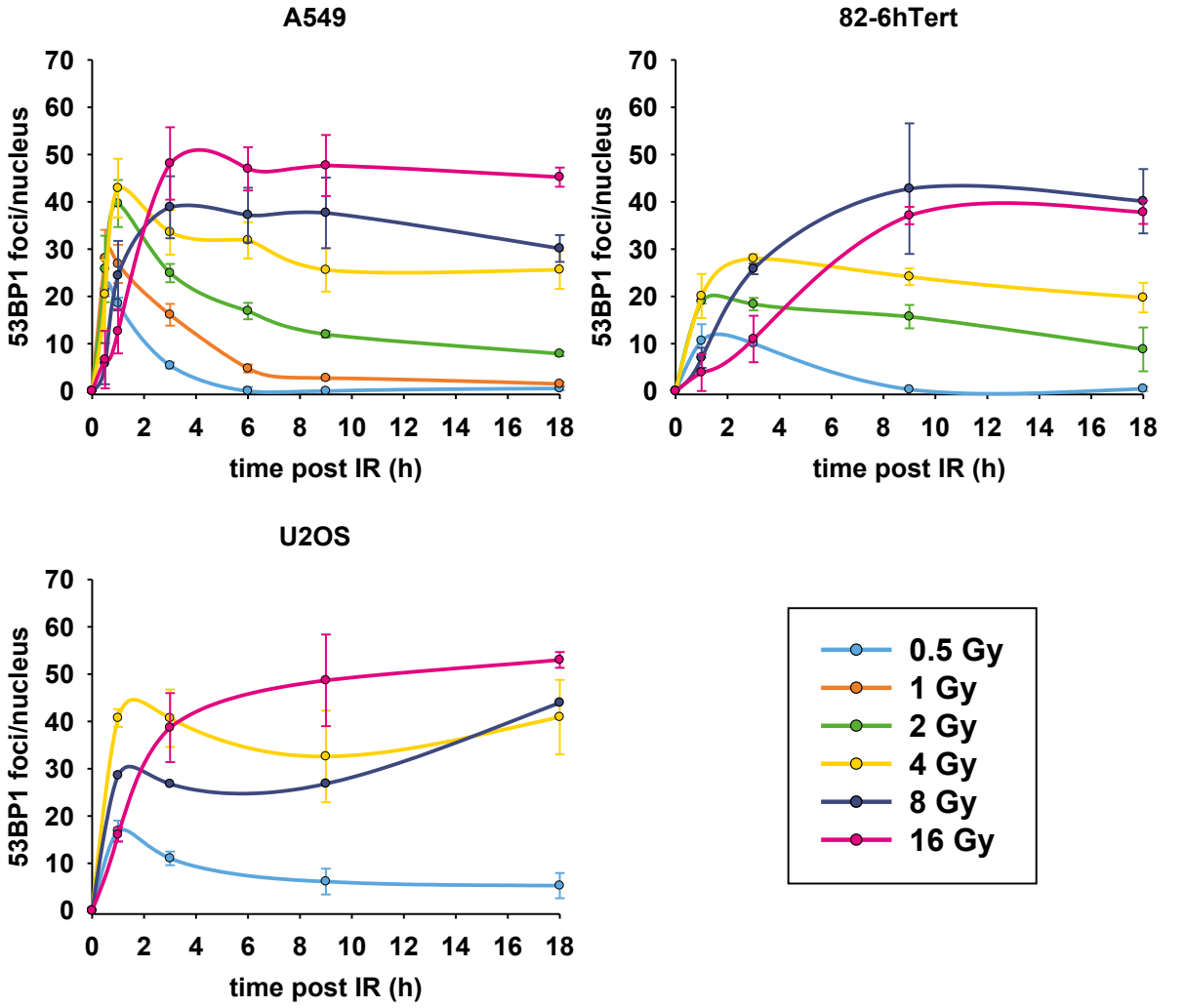

Figure 25: Repair kinetics of 53BP1 foci in A549, 82-6hTert and U2OS cells. Exponentially growing A549, 82-6hTert and U2OS cells were irradiated with varying doses and the formation of 53BP1 foci was analyzed at different times post IR (30 min-18 h). Data represent the mean from independent experiments and error bars indicate the standard error of the mean values (A549: n = 3-4, 82-6hTert: n = 2, U2OS: n = 2). On average, 53BP1 foci were counted in (82 +/- 21) (A549), 99 (+/- 38) (82-6hTert) and 105 (+/- 34) (U2OS) nuclei per time point and experiment.

4.2.2 Live cell imaging supports 53BP1 foci persistence

To verify the observation of persistent 53BP1 foci at late time points after high doses of IR, we used live cell imaging in cells expressing 53BP1-mCherry fusion protein. Previous experiments in our laboratory demonstrated that human U2OS cells are prone to be effectively transfected with various GFP expression plasmids. Furthermore, U2OS cells have regularly rounded nuclei, which is ideal for live microscopy studies. Both properties of U2OS cells were a decisive factor for their utilization as a model to investigate the formation of 53BP1 foci in live cell imaging experiments. Three days prior to transfection, U2OS cells were plated and allowed to reach ~ 70% confluency before transfection. By using the nucleofection method, cells were transfected with a 53BP1-mCherry plasmid and seeded in glass bottom live cell imaging chambers. One day after transfection, cells were irradiated and live cell imaging was started one hour after irradiation. In every chamber 2 fields were tracked every 15 or 30 min until 17 h post irradiation.

In approximately 35% of the cells well distinguishable and countable 53BP1 foci formed. Representative images are shown in Fig. 26 A. 53BP1 foci were counted manually in several nuclei (6-21 nuclei) and the average amount of 53BP1 foci per nucleus was plotted and presented in Fig. 26 B. We observed a constant decrease of 53BP1 foci over time after irradiation with 2 and 4 Gy, whereas in cells irradiated with 8 Gy a persistently high number of 53BP1 foci was detected. These findings are in accordance with the previous results from immunofluorescence experiments (Fig. 25).

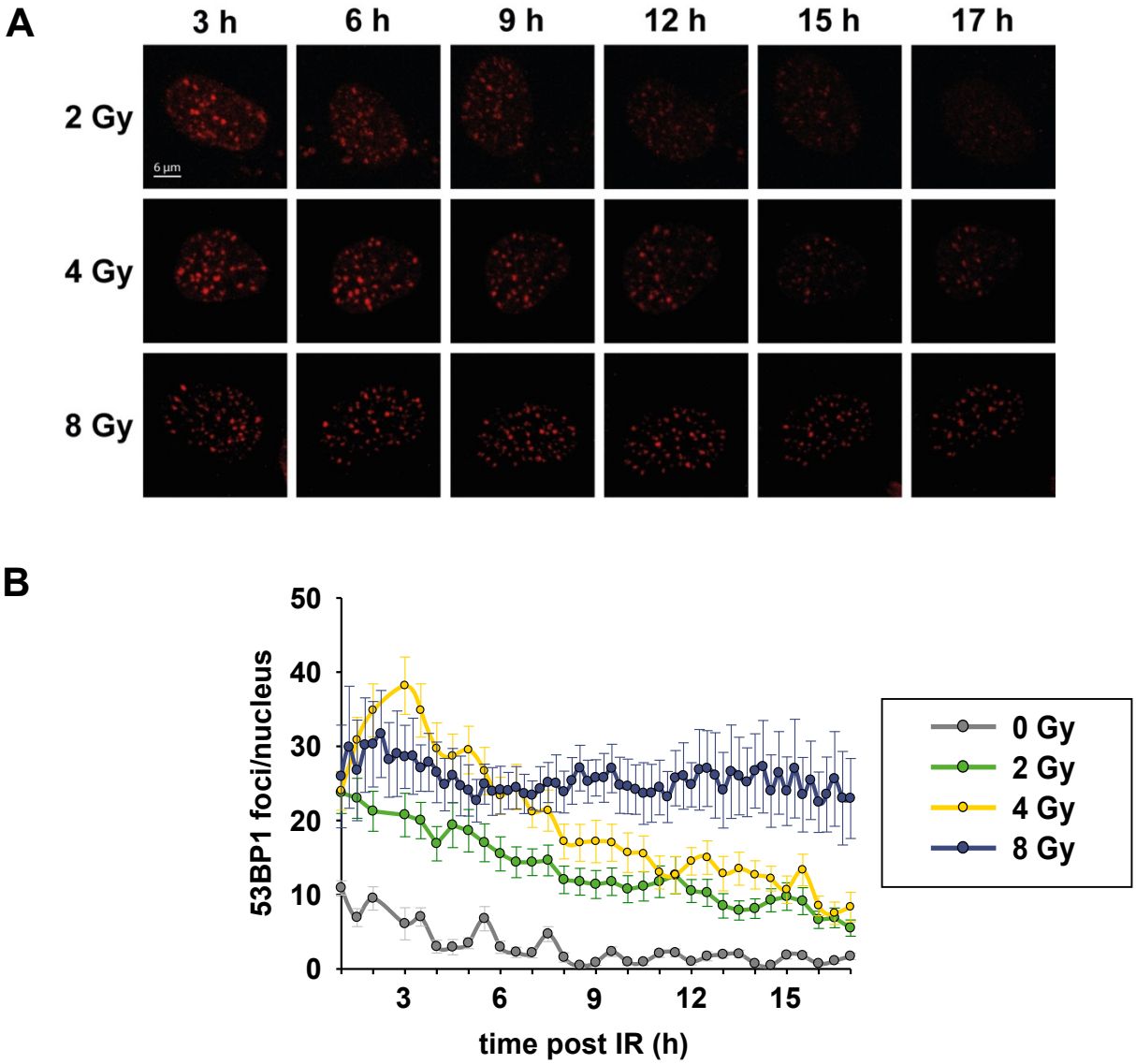

Figure 26: The formation of 53BP1 foci during live cell imaging in U2OS cells. U2OS cells were transfected with a 53BP1-mCherry plasmid 24 h prior to different doses of IR. One hour after irradiation live cell imaging with a confocal microscopy was started. (**A**) Representative images of U2OS cells with 53BP1 foci at different time points and after varying doses. (**B**) U2OS cells in two fields per live cell imaging chamber were tracked every 30 min (0, 2 and 4 Gy) or 15 min (8 Gy) until 17 h post irradiation. Data points represent the mean of 53BP1 foci per nucleus. Several nuclei were counted (0 Gy: 13 nuclei, 2 Gy: 8 nuclei; 4 Gy: 6 nuclei; 8 Gy: 21 nuclei) Error bars indicate the standard error between the single values. Experiment was performed once for 0, 2 and 4 Gy and twice for 8 Gy.

4.2.3 53BP1 foci formation saturates with increasing radiation dose

Beside the persistent and constant high 53BP1 foci numbers after irradiation at high doses, we also observed that the amount of 53BP1 foci did not increased linearly with increasing radiation dose. Rather, we discovered a saturation reminiscent to Rad51 foci formation

(Fig. 22 A). This saturation of 53BP1 foci formation with increasing radiation dose was detected in all three cell lines tested (Fig. 27).

Driven by this observation, we calculated the correlation of 53BP1 foci to γH2AX foci in the same way as we did for Rad51 foci (4.2.4). For each dose, the maximum number of 53BP1 foci determined by the repair kinetics (Fig. 24) was divided by the maximum number of γH2AX foci (exact values see suppl. Tab. 17). This calculation revealed, that the amount of 53BP1 foci in comparison to the amount of induced DSBs (represented by γH2AX foci) decreases with increasing radiation dose. This suggests that with increasing radiation dose the proportion of DSBs at which 53BP1 proteins accumulate gets reduced (Fig. 27 B). Already after exposure to 2 Gy, the maximum number of 53BP1 foci per nucleus covers only 50% of the induced DSBs. The amount of 53BP1 foci even drops below 20% of total DSBs at high radiation doses (8, 16 Gy).

The conspicuous parallels of Rad51 and 53BP1 foci saturation with increasing radiation dose and the accompanying decrease of Rad51 and 53BP1 foci fraction of total DSBs suggest that 53BP1 might be involved in the suppression of HRR at high radiation doses. Furthermore, as we assumed a repair pathway switch towards error-prone repair pathways (4.2.4), we suspect that 53BP1 plays a controlling role in these processes.

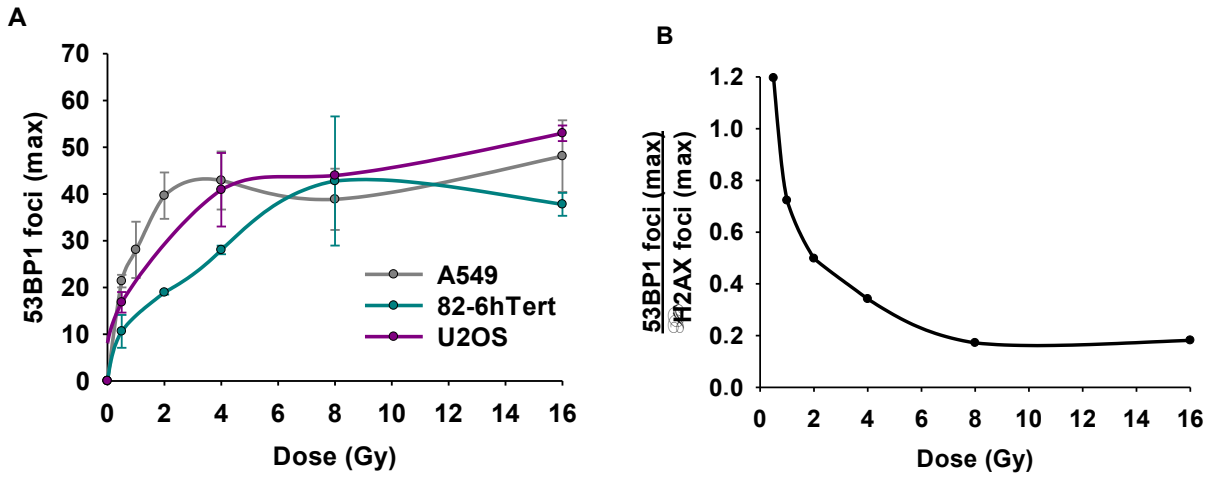

Figure 27: 53BP1 foci formation saturates with increasing radiation dose. (A) The maximum numbers of 53BP1 foci are plotted against the applied radiation doses. Data points represent the mean and error bars indicate the standard error of the mean values between independent experiments (A549: n = 3-4, 82-6hTert: n = 2, U2OS: n = 2). On average, 53BP1 foci were counted in 82 (+/- 21) (A549), 99 (+/- 38) (82-6hTert) and 105 (+/- 34) (U2OS) nuclei per time point and experiment. **(B)** The correlation of 53BP1 and γH2AX foci with increasing dose.

4.3 Modification of the chromatin architecture by hypertonic and hypotonic treatment and its influence on IRIF formation

To further examine the influence of chromatin structure on DSB processing and repair pathway choice we actively modified chromatin structure by growing cells in hypertonic or hypotonic cell culture medium. The increase or decrease of extracellular osmolarities are known to alter the cell volume and consequently the concentration of intracellular macromolecules (Finan et al., 2011). Hypertonic cell treatment leads to a loss of water and concomitant nucleus shrinkage. It was shown that hypertonic stress increases chromatin condensation and enlarges interchromatin compartments (Albiez et al., 2006).

In contrast, treatment with hypotonic medium leads to influx of water into the cell and nucleus. The size of the nucleus increases and hypotonic treatment results in evenly rounded nuclei. The effects of hypertonic and hypotonic treatment were shown to be reversible, if cells are in turn treated with isotonic medium (Albiez et al., 2006).

Here, we used hypertonic and hypotonic treatment to induce osmotic stress in order to modify the general chromatin architecture in the nucleus and study its influence on DSB processing and repair.

4.3.1 Effects of hypertonic and hypotonic treatment

To confirm the induction of the hyperosmotic stress in A549 cells, the standard cell culture medium McCoy's 5A was supplemented with NaCl. The molar concentration of NaCl in the medium was increased up to 300 mM, which doubled the isotonic concentration. A549 cells were seeded for two days in standard cell culture medium, before the hypertonic shock. Cells were incubated 10, 30 min and 1, 4 h with hypertonic medium, before fixation and DNA staining with DAPI. Even 10 min of incubation with hypertonic medium was enough to detect morphological chromatin alterations, evident as shrinkage of the nucleus and condensation of some of the chromatin areas. With increasing incubation time the nuclear volume further decreased and the appearance of interchromatin gaps was visible, which got larger with time (Fig. 28).

To decrease nuclear chromatin compaction, cells were treated with hypotonic medium. For this purpose, the standard cell culture medium McCoy's 5A was diluted with an equal amount of sterile water to decrease the osmotic concentration by a factor of two. The hypotonic treatment leads to an increase of nuclear size and an evenly distributed DAPI staining.

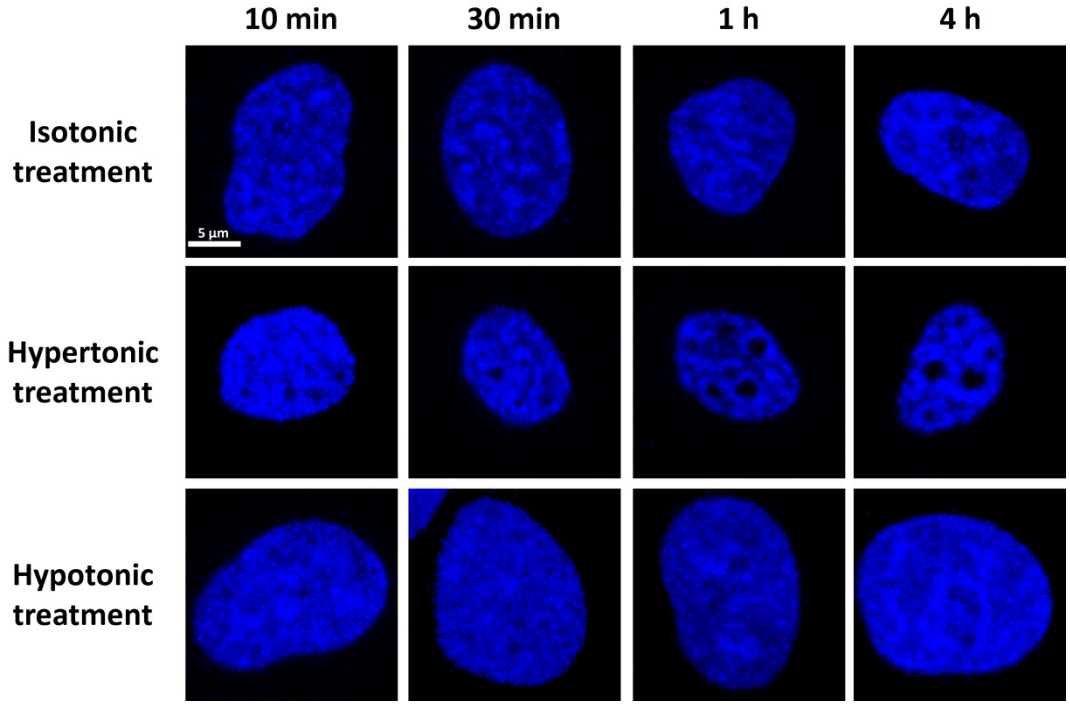

Figure 28: Appearance of A549 nuclei after osmotic shock. Exponentially growing A549 cells were treated in isotonic medium (standard cell culture medium), hypertonic medium (standard cell culture medium, supplemented with NaCl to double the osmotic concentration) and hypotonic medium (standard cell culture medium 1:1 diluted with sterile water to reduce the osmotic concentration by a factor of two). Cells were fixed at the indicated times and stained with DAPI. Hypertonic treatment leads to a nucleus shrinkage and increase in interchromatin gaps, whereas hypotonic treatment increases nuclear volume.

4.3.2 Hypertonic treatment increases γH2AX foci sizes and delays their disappearance

In order to examine the influence of general chromatin condensation induced by hypertonic treatment on DSB sensing and signaling, the formation of different IRIF was studied in hypertonically treated cells. A549 cells were exposed to IR and the standard cell culture medium was immediately replaced with hypertonic medium. For control conditions (isotonic treatment) we replaced the standard cell culture medium with fresh medium.

To analyze the phosphorylation of H2AX in response to irradiation at hypertonic treatment conditions, we used a global staining protocol in which the γH2AX signal was evaluated by flow cytometry. Flow cytometry is a high throughput technique which allows the analysis of a large number of cells (we have analyzed $3x10^4$ cells per treatment condition). Exponentially growing A549 cells were irradiated with different IR doses (2.5-20 Gy) and the standard growth medium was immediately replaced with hypertonic medium after exposure to IR. Cells were fixed and stained for flow cytometry 1 h post IR.

We compared the γH2AX fluorescence signals of isotonically and hypertonically treated cells and observed a strong increase in γH2AX intensities after hypertonic treatment. After irradiation with 2.5 and 5 Gy and following hypertonic treatment, the intensity of γH2AX signal was almost twice as high as the signal observed in isotonically maintained cells. Also irradiation with 10 and 20 Gy, remarkably enhanced γH2AX intensities in hypertonically treated cells (Fig. 29 A). This increase in γH2AX signals shows that hypertonic treatment enhances the amount of γH2AX. This can be rationalized by two scenarios: Either, hypertonic treatment increases the amount of induced DSBs, or more H2AX molecules get phosphorylated in the vicinity of DSBs.

In order to test these two hypotheses we used immunofluorescence staining and confocal microscopy to visualize the formation of γH2AX foci and to examine, whether the number of foci or their size is enhanced under hypertonic conditions. Exponentially growing A549 cells were irradiated with 2 Gy of X-rays and cell culture medium was immediately replaced with hypertonic medium. Cells were kept in hypertonic conditions for 1, 3 and 6 h before they were fixed and stained for immunofluorescence with antibodies against γH2AX. One hour after irradiation we observed a slight increase of γH2AX foci number per nucleus in hypertonic treated cells (Fig. 29 C). However, more prominent was the altered appearance of the γH2AX foci upon hypertonic treatment. The detected foci were noticeably larger and showed a more diffuse appearance (Fig. 29 B). This supports the suggestion, that under hypertonic conditions more H2AX molecules are phosphorylated in the vicinity of DSBs.

Moreover, the analysis of γH2AX foci number at later time points revealed no decrease of γH2AX foci in hypertonically treated cells. As the disappearance of γH2AX foci is commonly used as an indication of DSB repair, this observation suggests that hypertonic treatment suppresses DSB repair.

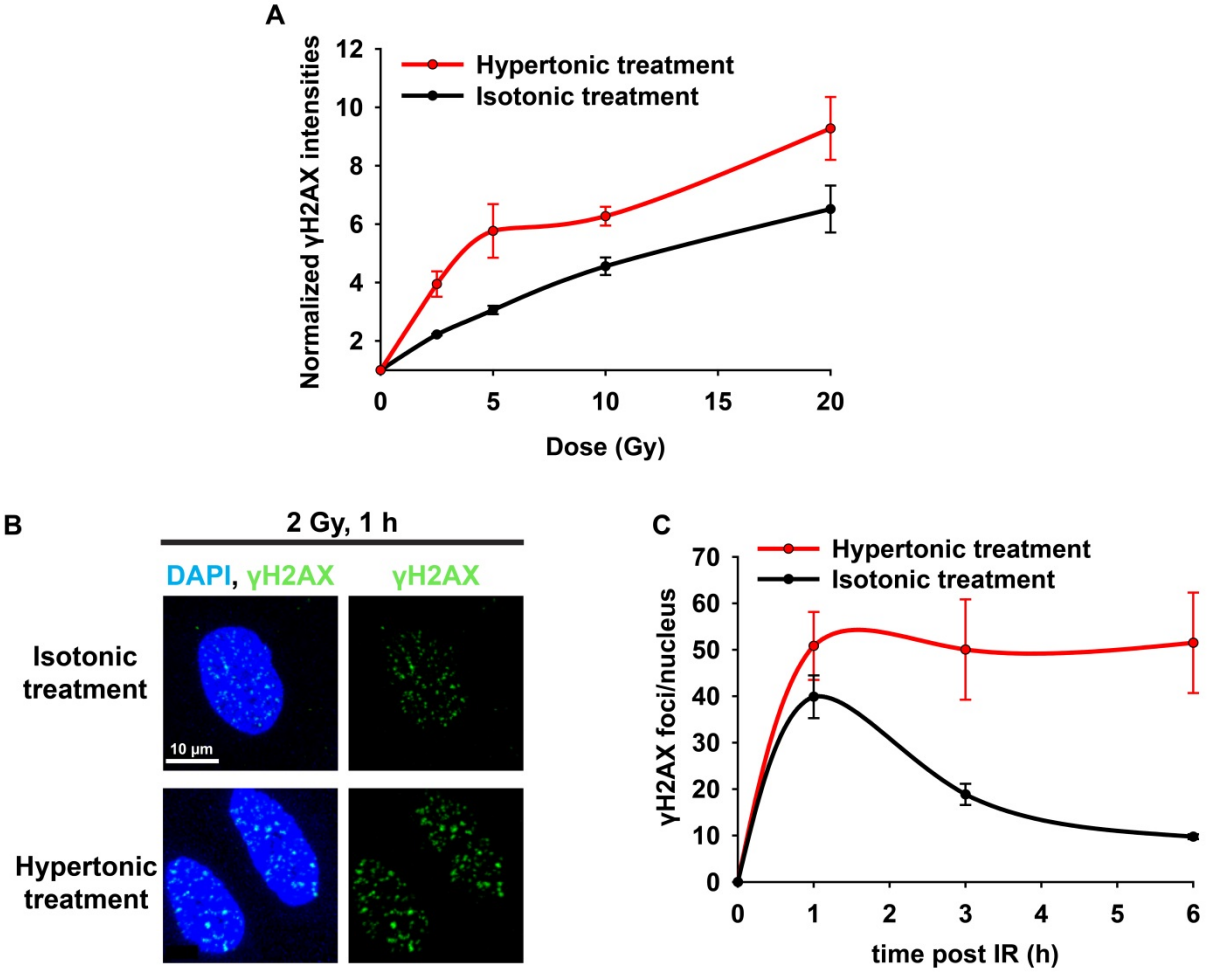

Figure 29: Hypertonic treatment enlarges γH2AX foci and delays their disappearance. (**A**) The influence of high salt medium treatment on the phosphorylation of H2AX after IR exposure was measured by flow cytometry. γH2AX intensities of irradiated cells were normalized to the non-irradiated control values and plotted against radiation dose. Data points represent the mean from two independent experiments and the error bars indicate the standard error of the mean values. Per condition $3x10^4$ cells were counted. (**B**) Representative pictures of γH2AX foci in isotonically and hypertonically treated cells 1 h after IR (2 Gy). (**C**) Repair kinetics of γH2AX foci measured 1, 3 and 6 h after IR (2 Gy) in hypertonically and isotonically treated exponentially growing cells. Data points represent the mean from at least two independent experiments (n = 2-4) and error bars indicate the standard error of the mean values. On average, γH2AX foci were counted in 227 (+/- 91) nuclei per time point and experiment.

4.3.3 Formation of 53BP1 foci is abrogated in hypertonically treated cells

In addition to γH2AX foci formation, we analyzed the occurrence of 53BP1 foci in hypertonically treated, irradiated cells. Under isotonic conditions the signaling cascade, which leads to 53BP1 accumulation at DSB is intact. Hence, 53BP1 is recruited downstream of H2AX phosphorylation and belongs to the second wave of repair proteins recruited to DSBs within a few minutes after damage induction.

Driven by the observation of increased γH2AX foci size and absent decay after hypertonic treatment, we studied the formation of the downstream repair mediator 53BP1. Incubation with hypertonic medium after irradiation with 2 Gy almost completely abrogated the formation of 53BP1 foci (Fig. 30). Even 6 h after irradiation 53BP1 foci were not forming, suggesting that hypertonic treatment suppresses the recruitment of 53BP1 to the DSB.

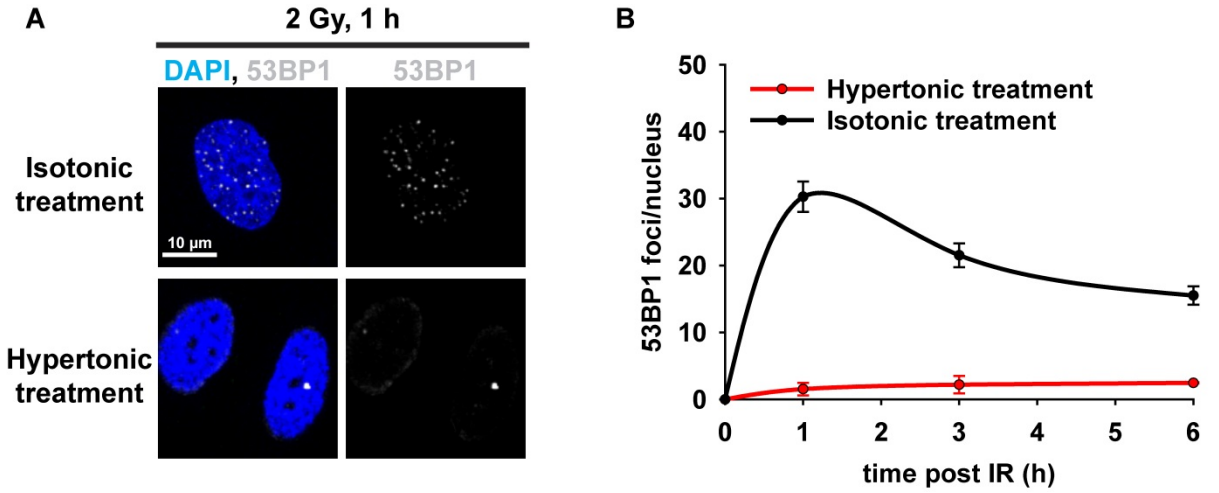

Figure 30: Hypertonic treatment suppresses the formation of 53BP1 foci. A549 cells were irradiated (2 Gy) and cell culture medium was changed to hypertonic medium. (**A**) Representative pictures of 53BP1 foci formation in isotonically (control) and hypertonically treated cells 1 h after IR. (**B**) Repair kinetics of 53BP1 foci 1, 3 and 6 h after IR in hypertonically and isotonically treated exponentially growing cells. Data points represent the mean from at least two independent experiments (n = 2-4) and error bars indicate the standard error of the mean values. On average, 53BP1 foci were counted in 227 (+/- 91) nuclei per time point and experiment.

4.3.4 Reduced formation of pATM foci in hypertonically treated cells

In order to reconcile the contradictory results of increased and prolonged γH2AX foci formation and abrogated 53BP1 foci, we analyzed the formation of phosphorylated ATM which is an upstream DSB repair signal compared to γH2AX and 53BP1. Upon DSB induction, ATM gets autophosphorylated and dissociates in active monomers which are recruited to the break, to facilitate the phosphorylation of H2AX - amongst several other substrates involved in the DDR. Five ATM autophosphorylation sites are known to be involved in DDR. The best described autophosphorylation site, which is commonly used as an indicator of ATM activation and is also used here as evidence of ATM activation, is the phosphorylation on Ser1981 (Kozlov et al., 2011). The accumulation of pATM at DSBs leads to the formation of nuclear foci, which can be detected by immunofluorescence experiments.

Under isotonic conditions, irradiation with 2 Gy leads to the accumulation of about 30 pATM foci 1 h after IR. The majority of pATM foci rapidly disappeared and 3 h after IR only 10 pATM foci remained. In contrast, hypertonic treatment after irradiation significantly reduces pATM formation and on average only 6 (1 h) and 1 (3 h) pATM foci were counted in the cell nuclei (Fig. 31).

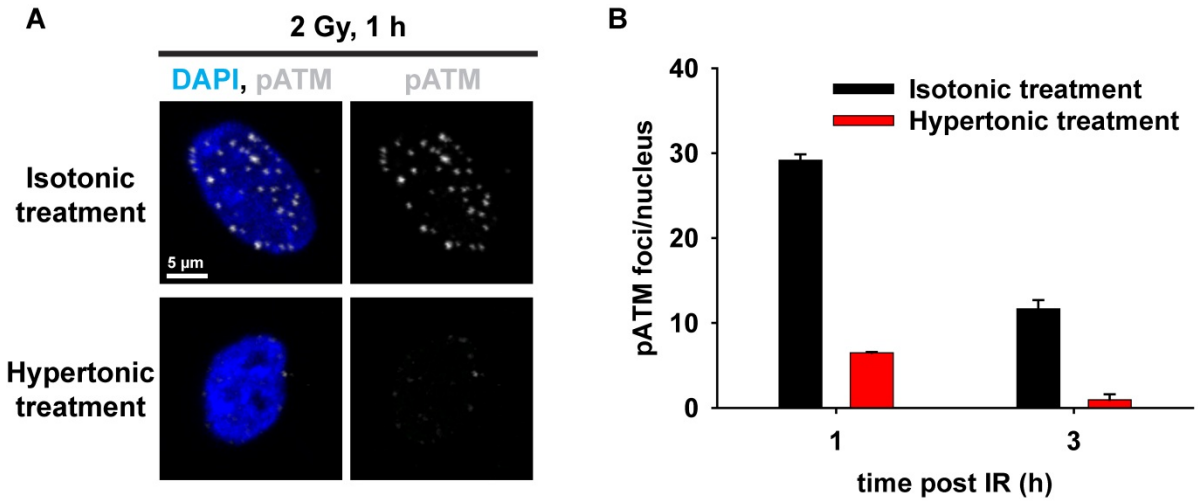

Figure 31: Hypertonic treatment suppresses pATM foci formation. A549 cells were irradiated (2 Gy) and the cell culture medium was changed to hypertonic medium. Cells were kept in hypertonic conditions until the fixation times. (**A**) Representative pictures of pATM foci formation in isotonically (control) and hypertonically treated cells 1 h after IR. (**B**) Average numbers of pATM foci per nucleus 1 and 3 h after IR in hypertonically and isotonically treated exponentially growing cells. Bars represent the mean from two independent experiments and error bars indicate the standard error of the mean values. On average, pATM foci were counted in 166 (+/- 48) nuclei per time point and experiment.

Taken together, we observed that hypertonic treatment after irradiation significantly suppresses the formation of pATM and 53BP1 foci. However, we detected an enhanced formation of γH2AX foci, which appear with increased foci sizes and which were not disappearing until 6 h post irradiation.

4.3.5 Hypotonic treatment suppresses γH2AX foci formation but facilitates the formation of 53BP1 foci

Hypotonic treatment is known to induce a general chromatin relaxation. To study the influence of hypotonic treatment on DSB sensing and processing, A549 cell were exposed to IR, immediately incubated in hypotonic medium and the formation of IRIF was analyzed. For hypotonic treatment we used standard cell culture medium, which was diluted with an equal amount of sterile water. For control conditions (isotonic treatment) we replaced the standard cell culture medium with fresh medium.

Cells were exposed to 2 Gy of X-rays and the medium was immediately changed to either hypotonic or isotonic medium until the cells were fixed for immunostaining (1, 3 and 6 h). Incubation in hypotonic medium significantly suppressed the formation of γH2AX foci in the first hours after IR (Fig. 32 A, B). In cells which were analyzed at later time points (6 h) post irradiation, several γH2AX foci were detected (on average 17 foci/nucleus). However, this amount was far lower from the maximum reached in isotonically treated cells (in average 40 foci/nucleus, 1 h post IR). This result suggests that hypotonic treatment suppresses the formation of γH2AX foci.

Additionally, the development of 53BP1 foci in irradiated and hypotonically treated cells was investigated. In contrast to the results obtained for γH2AX foci, we detected marked formation of 53BP1 foci 1h post irradiation (Fig. 32 A, C). However, the number of 53BP1 foci was reduced in hypotonically treated cells (on average 19 53BP1 foci/nucleus) in comparison to isotonically treated control cells (on average 30 53BP1 foci/nucleus). Co-staining of γH2AX and 53BP1 revealed that the few γH2AX foci, accumulated in hypotonically treated cells, almost completely overlapped with 53BP1 foci. Thus, under these conditions, 53BP1 foci form on DSB sites where γH2AX failed to form (Fig. 32 A).

Notably, the number of 53BP1 foci forming in irradiated and hypotonically treated cells failed to decline at later time points (3 and 6 h, Fig. 32 C), suggesting abrogated DSB repair.

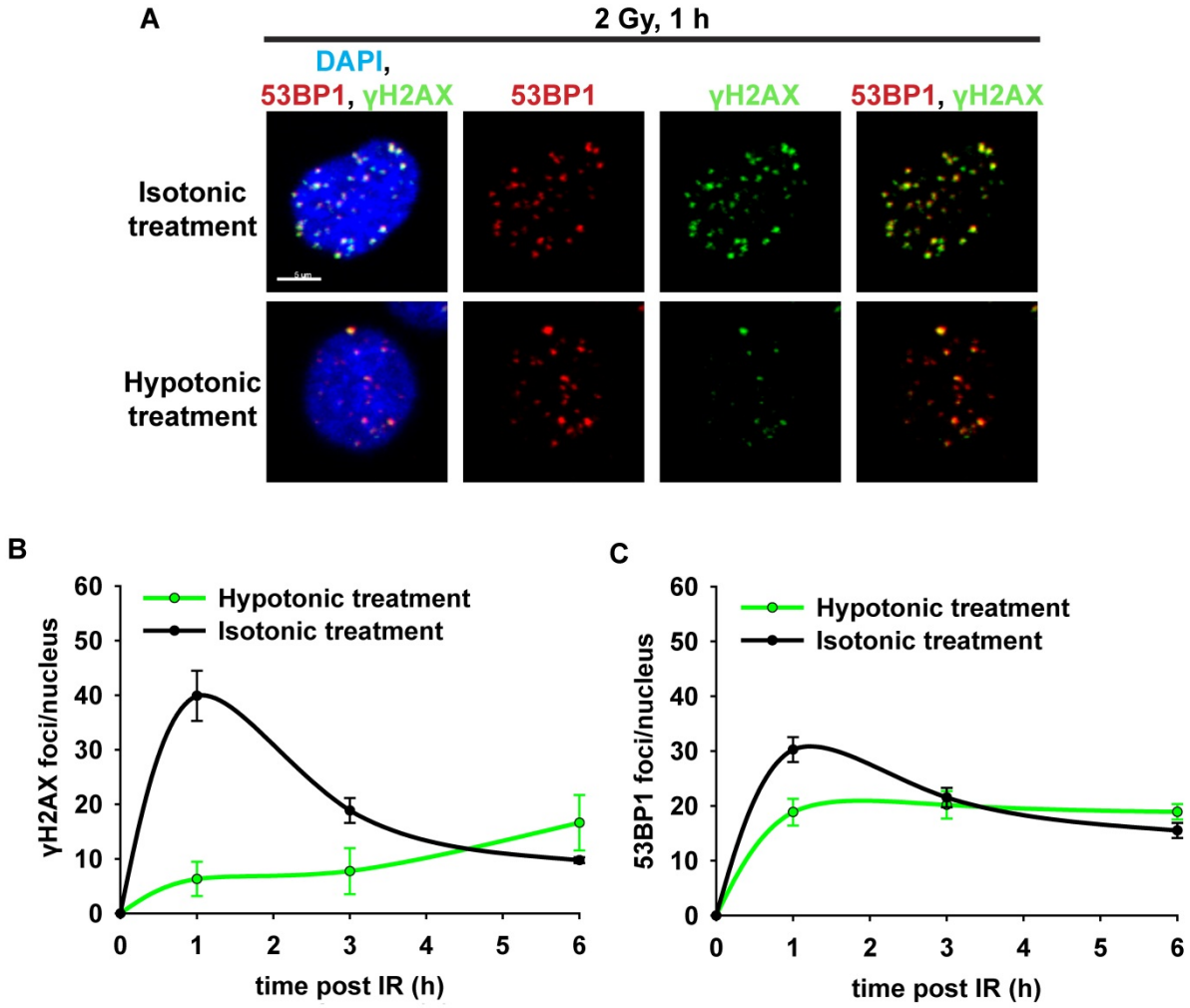

Figure 32: 53BP1 foci form without the formation of γH2AX foci in hypotonically treated cells. A549 cells were irradiated (2 Gy) and the cell culture medium was changed to hypotonic medium. Cells were kept in hypotonic conditions until fixation. (**A**) Representative images of γH2AX and 53BP1 foci formation in isotonically (control) and hypotonically treated cells 1 h after IR. (**B**) Average numbers of γH2AX foci per nucleus 1, 3 and 6 h after IR in hypotonically and isotonically treated exponentially growing cells. (**C**) Average numbers of 53BP1 foci per nucleus 1, 3 and 6 h after IR in hypotonically and isotonically treated cells. Data points represent the mean from at least two independent experiments (n = 2-4) and error bars indicate the standard error of the mean values. In average, foci were counted in 204 (+/- 81) nuclei per time point and experiment.

4.3.6 Hypotonic treatment slightly decreases pATM foci formation

To examine whether the reduced number of γH2AX foci derives from incomplete activation of ATM, we analyzed the formation of pATM foci in hypotonically treated cells. In irradiated and isotonically treated control cells we counted on average 29 pATM foci per nucleus 1 h post IR. Hypotonic treatment reduced the size and the intensities of pATM foci to the extent that a reduced number of pATM foci (on average 18 foci per nucleus) were detected (Fig. 33).

The number of pATM foci decreased to 10 foci per nucleus 3 h post IR, a value that is very similar to that measured in the untreated controls. We conclude that the suppression of γH2AX foci formation in hypotonically treated cells can be partially explained by a reduced ATM activation. However, as a substantial amount of pATM foci was still observed, the almost complete suppression of γH2AX foci formation must have additional causes.

Taken together, the above results show that under hypotonic conditions ATM can be activated and pATM foci accumulate, albeit at reduced size and numbers. Yet, the formation of γH2AX foci is significantly suppressed, whereas 53BP1 foci form on DSB sites where γH2AX failed to form.

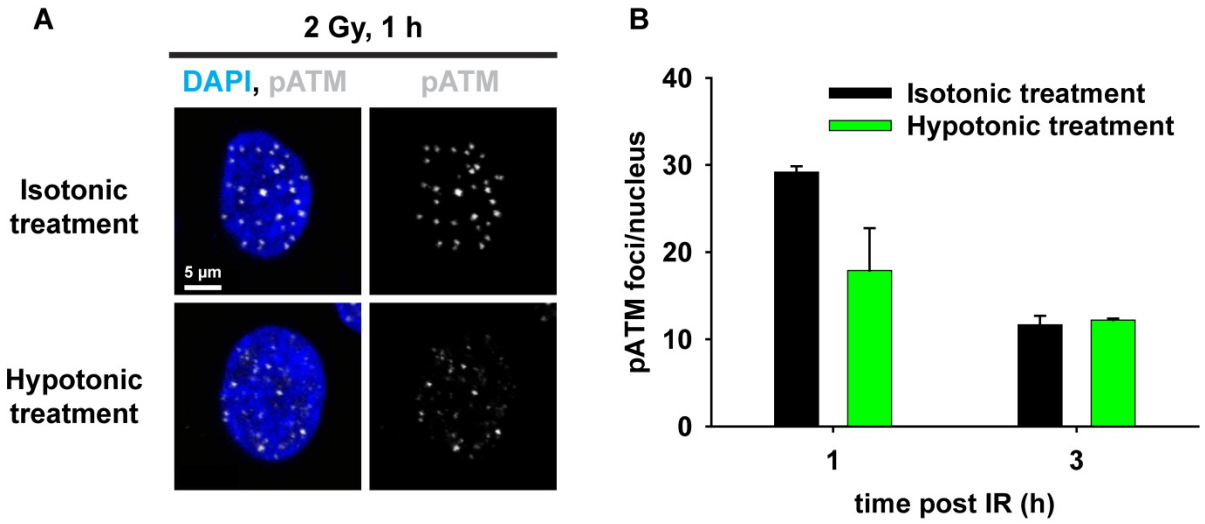

Figure 33: Hypotonic treatment reduces pATM foci formation. A549 cells were irradiated (2 Gy) and the cell culture medium was changed to hypotonic medium. Cells were kept under hypotonic conditions until the fixation. (**A**) Representative images of pATM foci formation in isotonically (control) and hypotonically treated cells 1 h after IR. (**B**) Average numbers of pATM foci per nucleus 1 and 3 h after IR in hypotonically and isotonically treated exponentially growing cells. Bars represent the mean from two independent experiments and error bars indicate the standard error of the mean values. On average, pATM foci were counted in 138 (+/- 21) nuclei per time point and experiment.

4.3.7 HRR is abrogated by hypertonic or hypotonic treatment

To study if modified chromatin condensation as generated by hypertonic or hypotonic treatment has an influence on repair pathway choice, we analyzed formation of Rad51 foci.

Exponentially growing A549 cells were irradiated with increasing doses of IR (2, 4, 8 and 16 Gy) and transferred to hypertonic, hypotonic or isotonic medium until analysis by

immunofluorescence. To distinguish between HRR proficient late S and G_2 phase cells and G_1 and early S phase cells, only cyclin B1 positive cells were analyzed.

As we expected, 3 h post IR the Rad51 recombinase started to accumulate into nuclear foci in isotonically treated control cells at every dose tested. In contrast, at both treatment conditions, hypertonic as well as hypotonic, the formation of Rad51 foci was dramatically reduced in irradiated cells (Fig. 34). Considering Rad51 foci formation as an indicator of HRR, these results suggest the abrogation of HRR under hypertonic and hypotonic conditions.

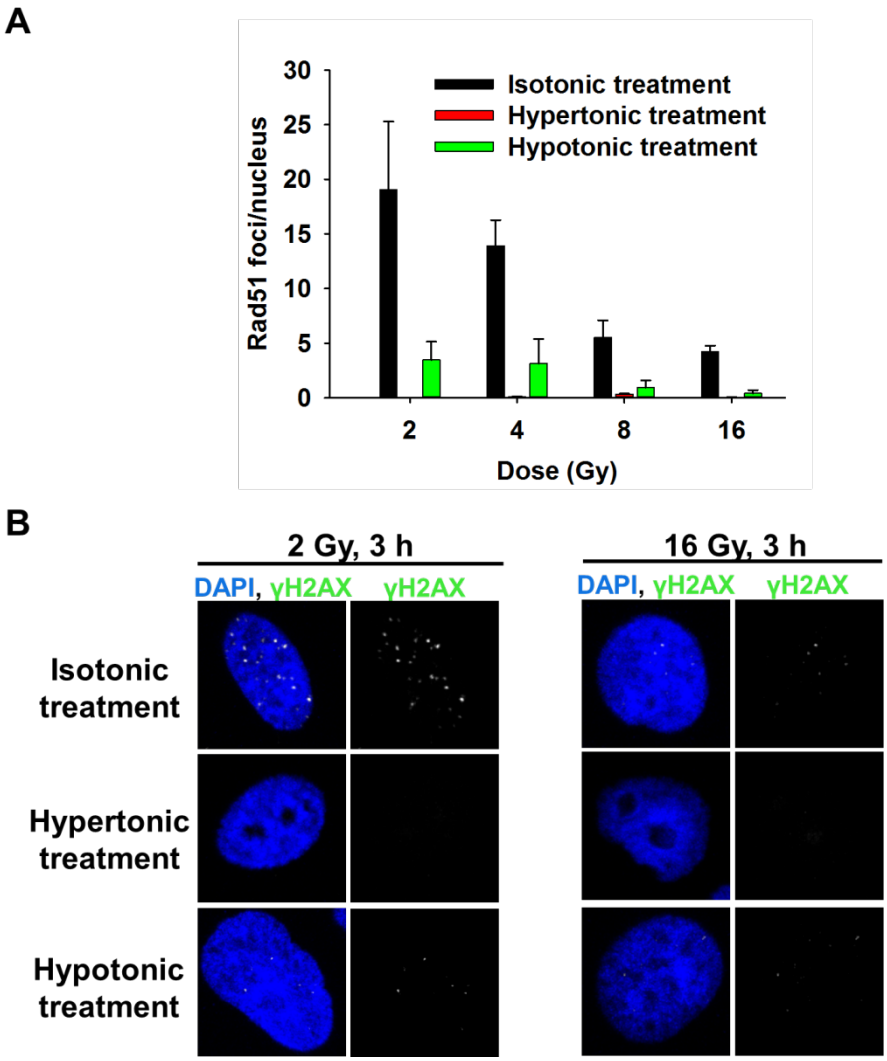

Figure 34: The formation of Rad51 foci is suppressed in hypertonically and hypotonically treated cells. Exponentially growing A549 cells were irradiated with increasing doses and the cell culture medium was changed to either hypertonic or hypotonic medium. Cells were kept under hypertonic or hypotonic conditions until fixation 3 h post IR. Only cyclin B1 positive cells were analyzed. (**A**) Average numbers of Rad51 foci per cell nucleus 3 h after IR in cells maintained in hypertonic, hypotonic or isotonic medium. On average, Rad51 foci were scored in 26 (+/- 10) nuclei per experiment and error bars indicate the standard error of the mean values from two independent experiments. (**B**) Representative pictures of Rad51 foci formation in cells maintained in isotonic, hypertonic or hypotonic media for 3 h after IR with 2 and 16 Gy.

To confirm the functional abrogation of HRR following hypertonic or hypotonic treatment, we have used the DR-GFP reporter assay. In these experiments U2OS 282C cells with a stable integration of a reporter construct, specifically designed to measure HRR activity after induction of I-*Sce*I mediated DSB, was used. The integrated construct consists of two modified GFP gene sequences, oriented as direct repeats and was hence named DR-GFP. The schematic of the reporter is presented in Fig. 35 A. The *Sce*GFP gene contains the complete GFP sequence but is interrupted by an I-*Sce*I cutting site and a premature stop-codon. The iGFP gene is an inactive copy of the GFP gene as its sequence is 5' and 3' truncated. Consequently, the U2OS 282C DR-GFP cells cannot express a functional GFP, either from the *Sce*GFP or iGFP gene. To target the I-*Sce*I cutting site, cells were transfected with an I-*Sce*I expression plasmid. The expression of the endonuclease I-*Sce*I leads to the induction of a DSB in the *Sce*GFP gene. If this DSB undergoes HRR by using the iGFP gene as homologous sequence, the I-*Sce*I site and the premature stop-codon in the *Sce*GFP gene are lost and a functional GFP gene forms. Cells which repair the I-*Sce*I induced DSB by HRR can be detected due to the GFP fluorescence signal using flow cytometry.

To validate the repair reporter system, we first tested how inhibition of HRR or c-NHEJ affects the GFP signal. B02 is a specific inhibitor of human Rad51 (Huang et al., 2011) and c-NHEJ can be suppressed by NU7441, which selectively inhibits DNA-PK. We transfected U2OS 282C DR-GFP cells with the I-*Sce*I expression plasmid using electroporation and allowed cell attachment and recovery for two hours after transfection before inhibitors were added. As expected, inhibition of HRR by B02 (25 μM) reduced GFP positive cells by more than 90% from 12.71% for DMSO treated control cells to 1.2% GFP positive cells for B02 treated cells (Fig. 35 B, C). The chemical inhibition of DNA-PKcs by NU7441 (5 μM) leads to an increase of GFP signal, suggesting that c-NHEJ suppresses HRR (Fig. 35 B, C).

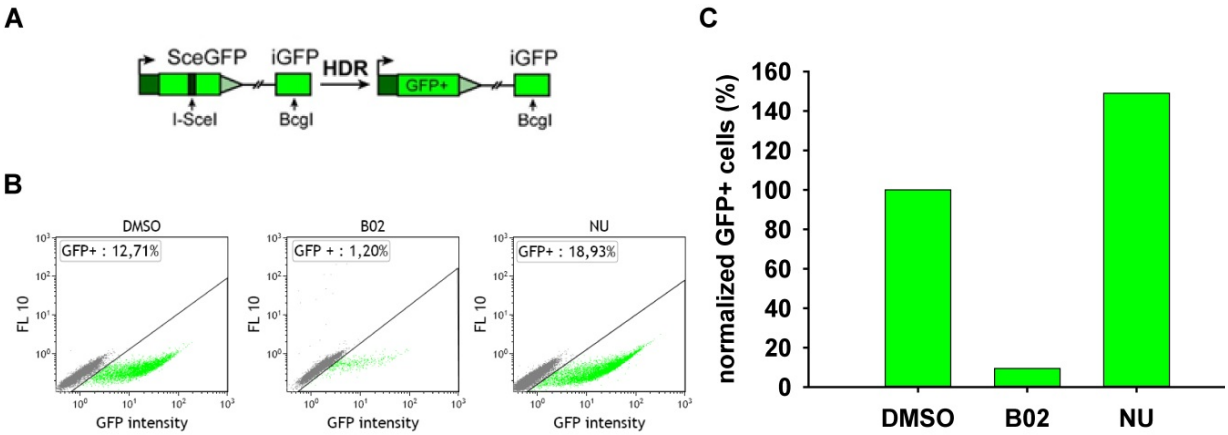

Figure 35: Validation of the HRR reporter assay. (**A**) Schematic drawing of the DR-GFP construct. (**B**) Exponentially growing U2OS 282C DR-GFP cells were transfected with an I-*Sce*I expressing plasmid. Two hours after transfection cells were treated with DMSO, B02 (25µM) or NU7441 (5µM) and 24 h after transfection $3x10^4$ cells were measured by flow cytometry. Dot plots with the set threshold to discriminate GFP positive cells are shown. (**C**) The percentage of GFP positive cells in DMSO treated control cells and after B02 and NU7441 treatment.

In order to study the effect of hypertonic and hypotonic treatment on HRR frequency with the HRR reporter assay, we first had to test if the treatment with hypertonic or hypotonic medium has an influence on the overall GFP protein expression and its correct folding, which would limit the significance of the results obtained from the reporter assay. Therefore, we used the pmaxGFP plasmid as a positive control and analyzed the maxGFP signals in isotonically, hypertonically and hypotonically treated cells. Exponentially growing U2OS cells were transfected with the pmaxGFP plasmid and 2 h after transfection an equal amount of medium, containing 600 mM NaCl or sterile water was added to the cells, resulting in increased or decreased osmotic pressure. Normal (isotonic) medium was added to the control cells. 24 h after transfection, cells were collected and maxGFP expression was analyzed by flow cytometry.

In isotonically treated control samples, cell viability was high (> 97%) and almost all viable cells (> 90%) expressed the maxGFP protein (Fig. 36). In contrast, hypertonic treatment dramatically reduced the viability of cells to 25%. Furthermore the ability to express the maxGFP protein was strongly suppressed as in only 35% of the viable cells a GFP signal was detected (Fig. 36). However, hypotonic treatment had no influence on cell viability and protein expression as we observed the same amounts of live cells (> 97%) and the same levels of GFP positive signals (> 90%) as in isotonically treated control cells.

This preliminary test demonstrated that for hypertonically treated cells, results of the HRR reporter assay must be interpreted with caution, as hypertonic treatment reduces cell survival and protein expression. However, hypotonic treatment is well tolerated and consequently, results of the HRR reporter assay should be valid without restrictions.

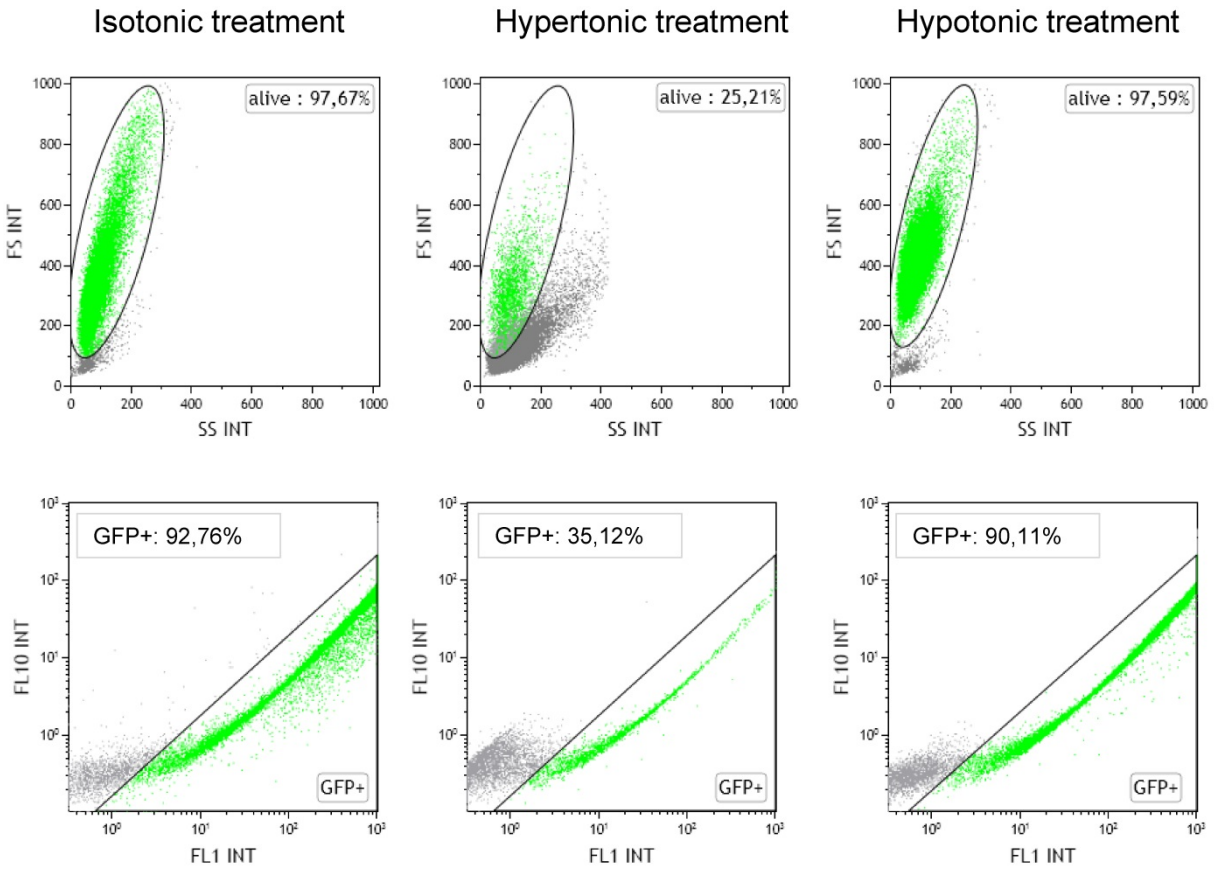

Figure 36: Influence of hypertonic and hypotonic treatment on cell survival and protein expression. To test whether hypertonic or hypotonic treatment influences protein expression and folding, exponentially growing U2OS 279A EJ2-GFP cells were transfected with a pmaxGFP plasmid via electroporation. Two hours after transfection, an equal amount of medium containing 600 mM NaCl or sterile water was added to increase or decrease the osmotic pressure by a factor of two. An equal amount of normal (isotonic) medium was added to control cells. 24 h after transfection, cells were collected and the maxGFP expression was analyzed by flow cytometry in $2x10^4$– $3x10^4$ cells. **Upper row**: Dot plots show the live cell fraction. **Lower row**: Dot plots of live cells with the set threshold to discriminate GFP positive cells.

To study the effect of hypertonic and hypotonic treatment on HRR, the HRR reporter assay was used. U2OS 282C DR-GFP cells were transfected with the I-*Sce*I expression plasmid by electroporation and were plated afterwards in normal cell culture medium to allow cell attachment and recovery. Hypertonic and hypotonic conditions were applied as described

above and cells were collected 24 h after transfection for GFP fluorescence analysis by flow cytometry.

We detected a strong reduction of GFP positive cells in hypertonically and hypotonically treated cells as compared to isotonically treated control cells (Fig. 37). In hypertonically treated cells, repair by homologous recombination was almost completely suppressed and in hypotonically treated cells GFP positive cells were reduced by 83% in comparison to the control cells. These results are in accordance to the above findings, showing strongly reduced Rad51 foci formation under the same conditions (Fig. 34). Taken together, these observations suggest a severe reduction of HRR in hypertonically and hypotonically treated cells.

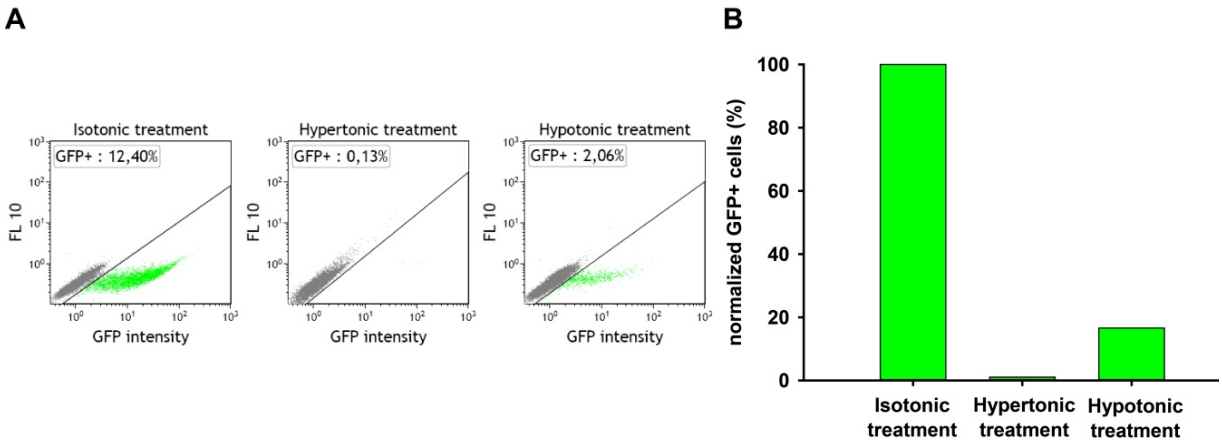

Figure 37: Hypertonic or hypotonic treatments strongly reduces HRR. The HRR reporter assay was used to examine the impact of hypertonic and hypotonic treatment on HRR. Experiments were carried out as described in the text. (**A**) Dot plots with the set thresholds to discriminate GFP positive cells. (**B**) The percentage of GFP positive cells in isotonic controls and in hypertonically or hypotonically treated cells.

4.3.8 Hypotonic treatment has no influence on RPA foci formation

In the previous section (4.3.7) we demonstrated a significant reduction of Rad51 foci accumulation after IR when cells are incubated in hypertonic or hypotonic medium. DNA end resection is an upstream event of Rad51 loading and decisive to shunting DSB repair towards HRR. To find out, how DNA end resection is influenced in hypertonically or hypotonically treated cells, we investigated the formation of RPA foci. Exponentially growing A549 cells were irradiated with different doses of IR (2, 4, 8 and 16 Gy) and transferred to hypertonic, hypotonic or isotonic medium. Since we expected RPA foci development 3 h post IR at every tested dose, we selected this time point for cell fixation and the cells were incubated under

hypertonic or hypotonic conditions for this period of time. To distinguish HRR proficient late S and G_2 phase cells, the cell cycle marker cyclin B1 was used and only cyclin B1 positive cells were analyzed.

In hypertonically treated cells, we observed a complete suppression of RPA foci formation (Fig. 38). In contrast, hypotonic treatment had no influence on the development of RPA foci. For each radiation dose, almost the same number of RPA foci was scored per cell nucleus (Fig. 38 A) and foci sizes and intensities were comparable to those of isotonically treated cells (Fig. 38 B).

In summary, we revealed a strong suppression of RPA and Rad51 foci formation in hypertonically treated cells, suggesting inhibition of HRR. In hypotonically treated cells, we also detected reduced formation of Rad51 foci; however RPA foci formation was not altered. This suggests that resection is not impaired by hypotonic treatment, although later steps of HRR are compromised. As resected DSBs cannot be repaired by c-NHEJ, we hypothesized that resected DSBs in hypotonically treated cells are directed to alt-EJ. In the next section we tested this hypothesis using two repair reporter systems for NHEJ events.

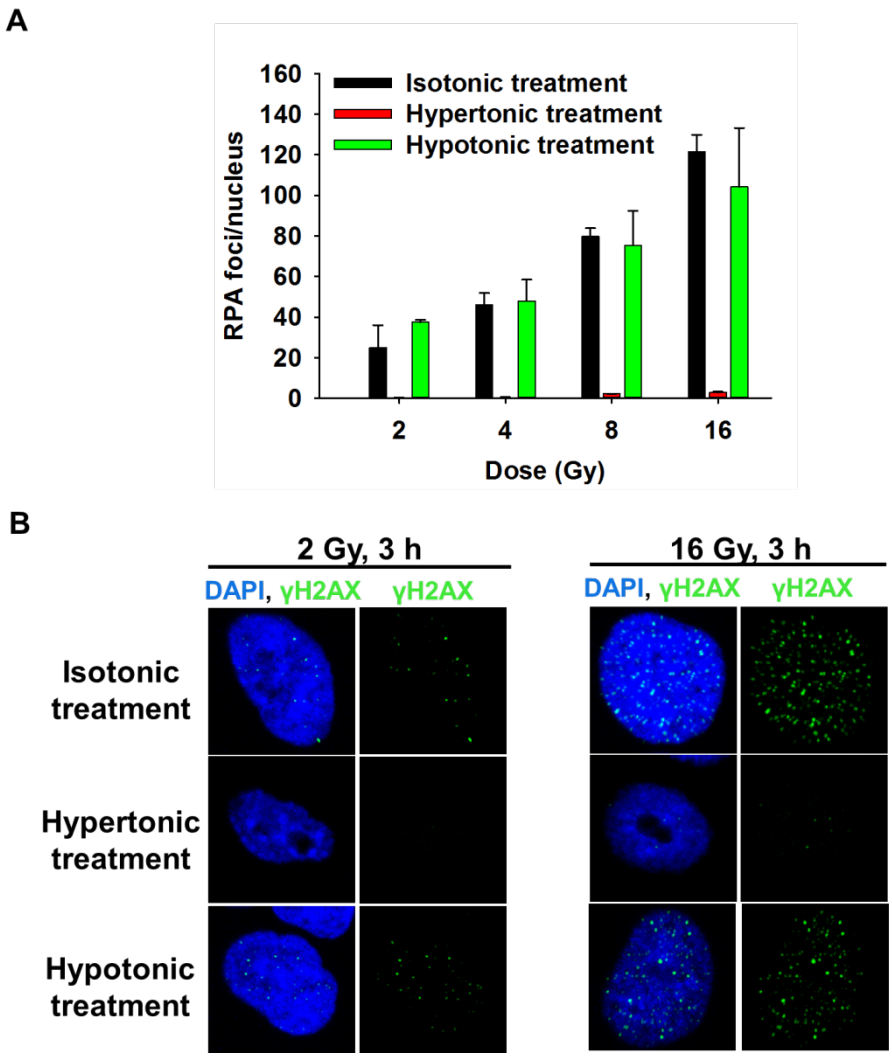

Figure 38: Formation of RPA foci in hypertonically or hypotonically treated cells. Exponentially growing A549 cells were irradiated with different radiation doses and the cell culture medium was changed to either hypertonic or hypotonic medium. Cells were kept in hypertonic and hypotonic conditions until fixation 3 h later. Only late S and G_2 phase cells were analyzed and identified by cyclin B1 staining. (**A**) Average numbers of RPA foci per cell nucleus 3 h after IR in hypertonically, hypotonically and isotonically treated cells. On average, Rad51 foci were counted in 21 (+/- 6) nuclei per experiment and error bars indicate the standard error of the mean values from two independent experiments. (**B**) Representative images of RPA foci formation in isotonically, hypertonically and hypotonically treated cells 3 h after IR with 2 and 16 Gy.

4.3.9 Hypertonic and hypotonic treatment and its effect on NHEJ

To investigate the effect of hypertonic and hypotonic treatment on DSB repair by NHEJ we used two different U2OS reporter cell lines, each harboring a genome-integrated reporter construct. The EJ5-GFP reporter cell line contains a reporter construct which is used to

measure NHEJ events, which are accompanied by extensive deletions. A schematic drawing of the EJ5-GFP construct is shown in Fig. 39 A. In this construct, a full length GFP open reading frame is separated from its promotor by a puromycin (puro) gene. Two I-*Sce*I cutting sites flank the puro gene region. Upon I-*Sce*I expression, two DSBs are introduced. If the puro sequence is lost, the two distal ends are rejoined and GFP signal can be detected.

With the EJ2-GFP reporter cell line, microhomology dependent alt-EJ events can be detected. The reporter construct (Fig. 39 D) contains a GFP sequence, fused to an N-terminal tag sequence. The tag and GFP sequence are interrupted by an I-*Sce*I cutting site and a stop codon which are flanked by 8 nucleotides of microhomology. The repair of the DSB at the I-*Sce*I site by microhomology-dependent alt-EJ restores the GFP reading frame and GFP positive cells can be detected.

The results of the U2OS EJ5-GFP reporter cell line are shown in Fig. 39 B, C. In hypertonically treated cells almost no GFP positive cells were detected, whereas in hypotonically treated cells the amount of GFP positive cells was reduced to 45% of those detected in isotonically treated cells.

The measurement of the U2OS EJ2-GFP reporter cells showed also a strong reduction of GFP positive cells after hypertonic treatment, whereas in hypotonically treated cells the GFP signal was only reduced by 26% compared to the control signal in isotonically treated cells. Together with the results obtained from the U2OS DR-GFP reporter cell line (Fig. 38), these findings demonstrated that hypertonic treatment completely inhibits DSB repair by HRR and distal c-NHEJ. Only some repair events by microhomology dependent alt-EJ were detectable after hypertonic treatment, but with a strongly reduced frequency in comparison to control cells.

In hypotonically treated cells, repair events were detected with all three reporter cell lines. Nevertheless, the repair frequencies in hypotonically treated cells were reduced in comparison to the isotonically treated control cells. The strongest inhibitory effect of hypotonic treatment on DSB repair was measured with the HRR reporter cell line, which revealed an 83% reduction of HRR in hypotonically treated cells (Fig. 37). The least affected repair pathway in hypotonically treated cells was the microhomology dependent alt-EJ (Fig. 39 F) which was only reduced by 26%.

Thus, we demonstrated that hypertonic or hypotonic treatment impairs DSB repair. However, the different repair pathways exhibit different tolerance levels towards osmotic modifications

and we revealed that the most tolerant repair pathway towards osmotic changes is the microhomology dependent alt-EJ.

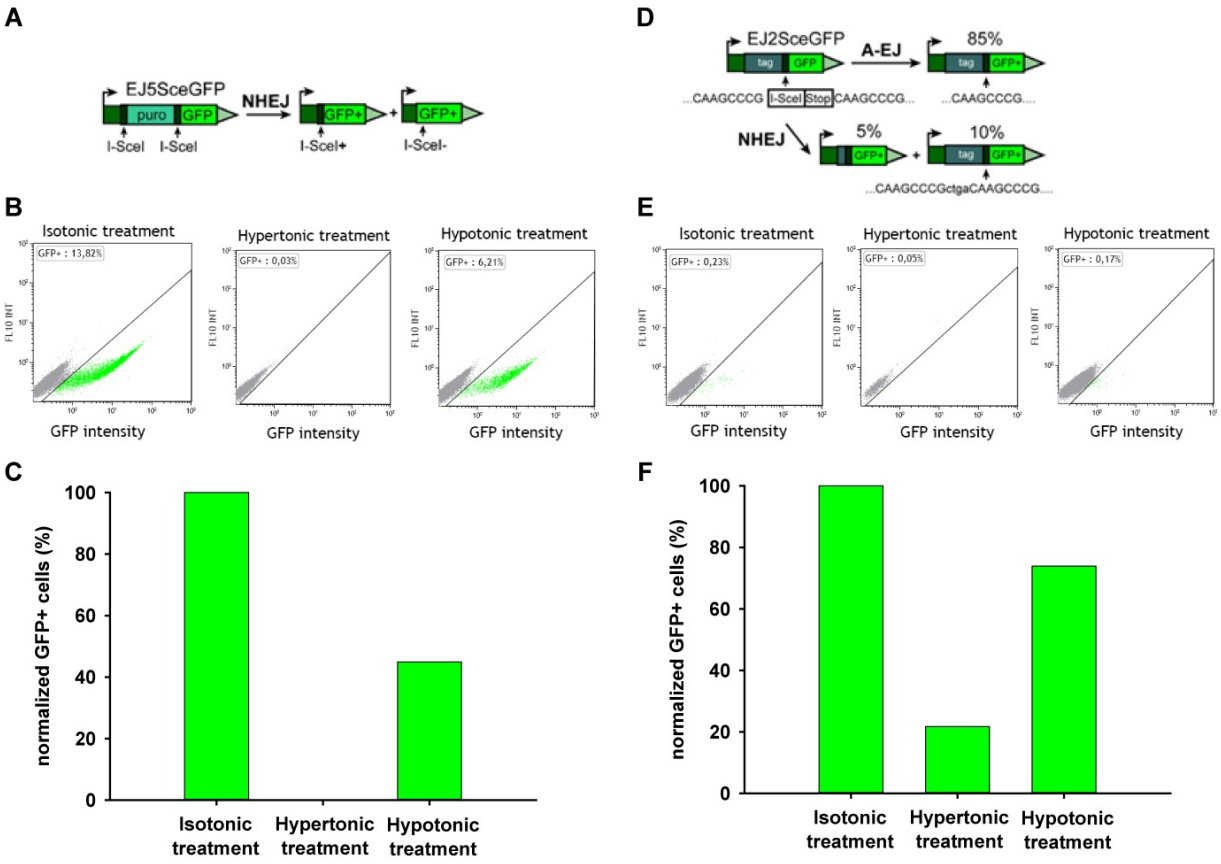

Figure 39: Effects of hypertonic or hypotonic treatment on NHEJ events measured with the reporter cell lines U2OS EJ5-GFP and U2OS EJ2-GFP. (**A**) Schematic drawing of the EJ5-GFP construct. (**B**) Exponentially growing U2OS EJ5-GFP cells were transfected with an I-*Sce*I expressing plasmid. Two hours after transfection, osmotic concentrations of the cell culture medium were modified towards hypertonic (300 mM NaCl) and hypotonic (~ 75 mM NaCl) conditions. Up to $3x10^4$ cells were measured by flow cytometry. Dot plots with the set threshold to discriminate GFP positive cells are shown. (**C**) Normalized results for U2OS EJ5-GFP cells. The number of GFP positive cells, normalized to the number of GFP positive cells in the isotonic control is plotted for each treatment. (**D**) Schematic drawing of the EJ2-GFP construct. (**E**) Flow cytometry results of the U2OS EJ2-GFP cell line. Same experimental setup as described in (**B**). (**F**) Normalized results for U2OS EJ2-GFP cells.

4.4 Inhibition of methyltransferase SUV39H1 and its influence on DSB repair

The histone methyltransferase SUV39H1 is known to play an important role in heterochromatin organization as it methylates H3K9 and its loss impairs heterochromatin structures and genome stability (Peters et al., 2001). Chaetocin is a specific inhibitor of SUV39H1 and leads to a decrease of di- and trimethylated histone H3 at lysine 9 (Greiner et

al., 2005). In this study, chaetocin was used to investigate the role of SUV39H1 in DSB repair and how DSB signaling and repair are affected by inhibition of SUV39H1.

First, we tested the effect of varying chaetocin doses and treatment times on H3K9me3 region-volumes, cell growth and cell cycle distribution in A549 cells. With immunofluorescence staining, we could detect that a 6 h treatment significantly reduced the level of H3K9me3 in A549 cell nuclei (Fig. 40 A, B). At this time point, cell growth (Fig. 40 C) and the cell cycle distribution (Fig. 40 D) was not affected and we decided to use a 6 h pre-treatment with chaetocin in the following experiments.

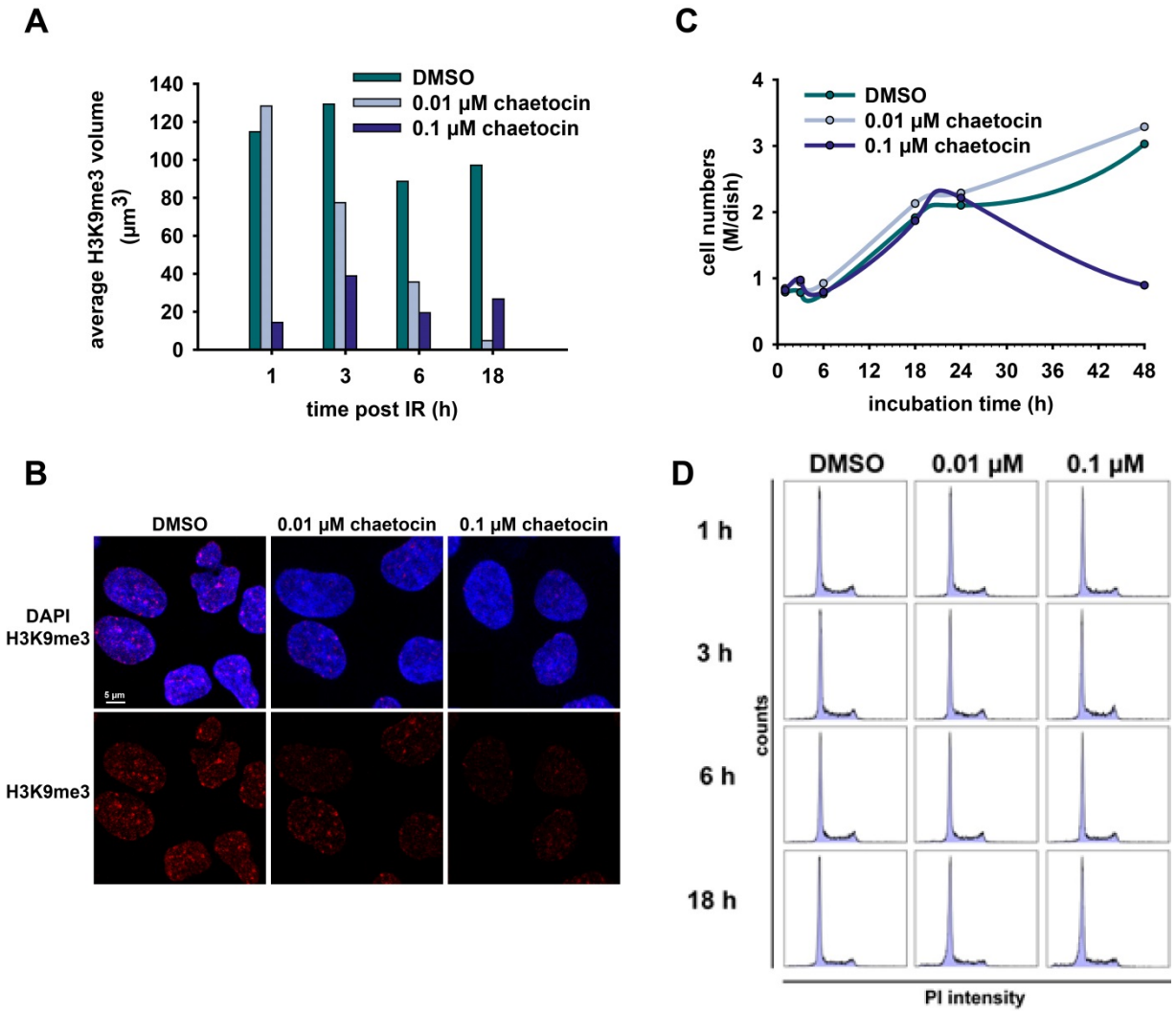

Figure 40: Chaetocin treatment reduces the level of H3K9me3. A549 cells were incubated with chaetocin for different times and H3K9me3 levels, cell numbers and cell cycle distribution were analyzed. (**A**) Immunofluorescence staining with an antibody against H3K9me3 demonstrated that chaetocin treatment reduces the amount of H3K9me3 volume in A549 nuclei. (**B**) Representative images of cells treated 6h with DMSO (control) or chaetocin (0.01, 0.1 µM). (**C**) The impact of chaetocin treatment on cell numbers. (**D**) The impact of chaetocin treatment on cell cycle distribution.

4.4.1 Chaetocin treatment and its influence on γH2AX and 53BP1 foci formation after IR

To study the formation of γH2AX and 53BP1 foci after inhibition of SUV39H1, A549 cells were pre-treated for 6 h with chaetocin and irradiated with 2 Gy. Cells were kept in chaetocin-containing medium until fixation and analysis.

In control cells we observed clearly forming, overlapping γH2AX and 53BP1 foci (Fig. 41 A). After chaetocin treatment, γH2AX foci sizes increased but were still co-localizing with 53PB1 foci. Quantification revealed that within 30 minutes post irradiation similar numbers of γH2AX foci formed in control and chaetocin treated cells. Chaetocin treatment slightly inhibited the decay of γH2AX foci observed 1 h after irradiation in control cells. However, 3 h after irradiation the number of γH2AX foci in chaetocin treated cells was similar to untreated control cells (Fig. 41 B). Moreover, chaetocin treatment had no effect on 53BP1 foci formation (Fig. 41 C). 53BP1 foci developed and disappeared with similar kinetics in chaetocin and in DMSO treated control cells.

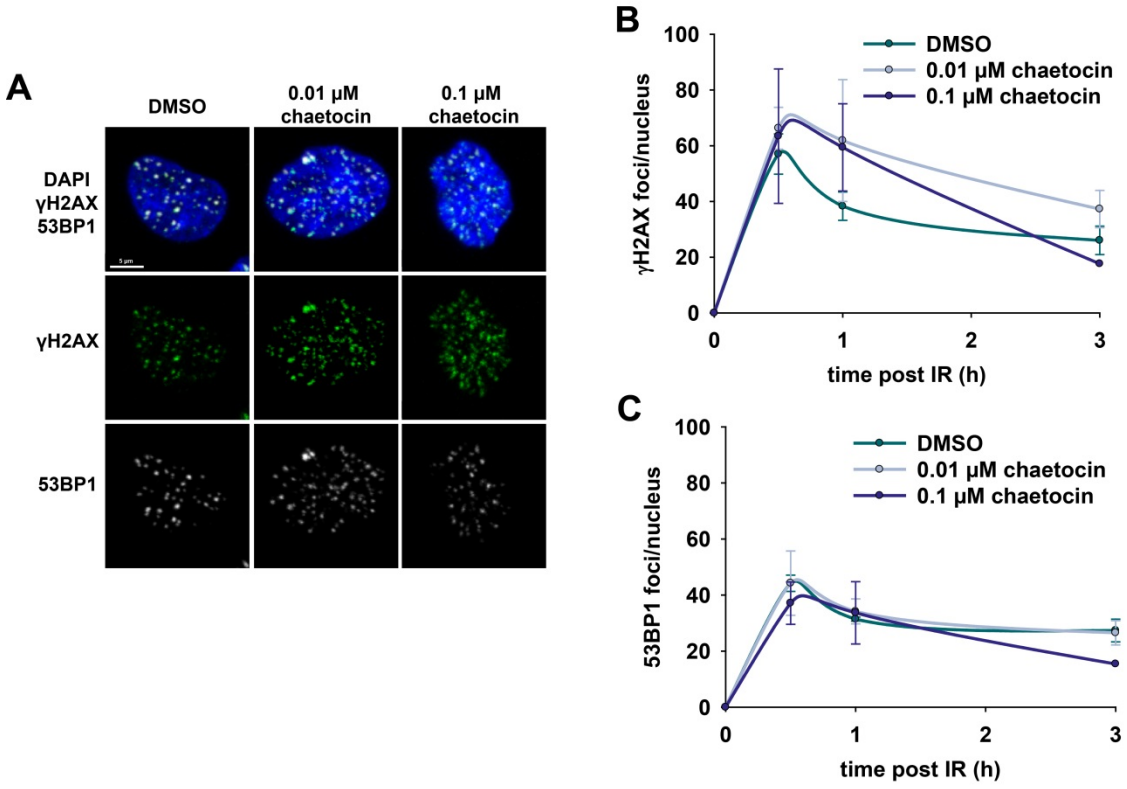

Figure 41: Development of γH2AX and 53BP1 foci after irradiation in the presence of chaetocin. A549 cells were pre-treated with 0.01 µM chaetocin, 0.1 µM chaetocin or DMSO 6 h before they were exposed to 2 Gy of IR. (**A**) Average numbers of γH2AX foci per nucleus in chaetocin treated cells and control cells. (**B**) Numbers of 53BP1 foci per nucleus after chaetocin treatment in comparison to DMSO treated control cells. Data points represent the mean from two independent experiments and error bars indicate the standard error of the mean values. On average, foci were scored in 186 (+/- 27) nuclei per time point and experiment.

4.4.2 Chaetocin treatment and its effect on HRR

Overall, inhibition of SUV39H1 by chaetocin had very little effect on the formation of γH2AX and 53BP1 foci. The decay of γH2AX foci is generally interpreted as an indicator of DSB repair. The clear decay of γH2AX foci numbers in chaetocin treated cells 3 h after irradiation with kinetics similar to untreated control cells suggests, that DSB repair is not affected by chaetocin. To examine the influence of chaetocin on HRR, we analyzed Rad51 foci formation. A549 cells were pre-treated for 6 h with chaetocin, exposed to increasing radiation doses and fixed 3h later. Only late S and G_2 phase cells were analyzed and were selected by cyclin B1 staining. Fig. 42 shows a clear trend for a reduction in Rad51 foci level after chaetocin treatment in a concentration dependent manner. Specifically, after 2 and 8 Gy, the amount of Rad51 foci was reduced by 60% and 80%, respectively in cells treated with 0.1 µM chaetocin. These findings indicate that chaetocin treatment and the consequent inhibition of SUV39H1 reduces the rate of HRR.

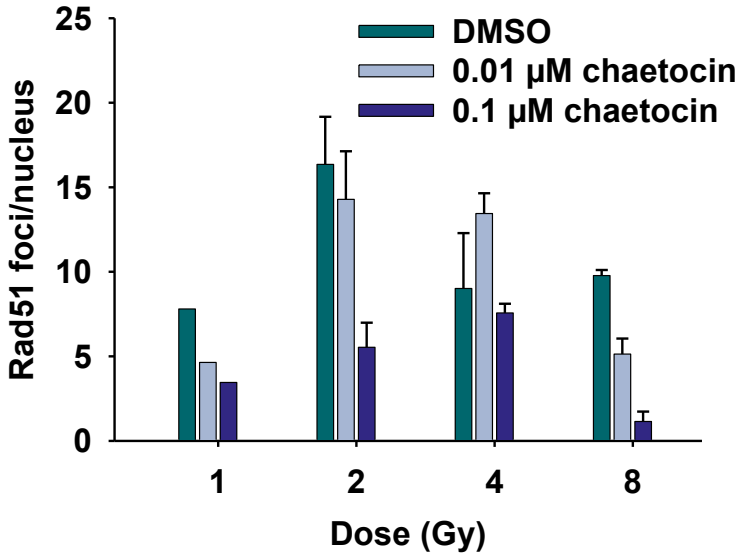

Figure 42: Reduction of Rad51 foci formation after irradiation in the presence of chaetocin. A549 cells were pre-treated with 0.01 µM chaetocin, 0.1 µM chaetocin or DMSO 6 h before they were exposed to increasing doses of IR. Cells were fixed 3 h after irradiation and stained for immunofluorescence analysis. Only cyclin B1 positive cells were analyzed. Bars represent the mean from two independent experiments and error bars indicate the standard error of the mean values. On average, Rad51 foci were counted in 19 (+/- 5) nuclei per time point and experiment.

To further investigate the potential of chaetocin to down regulate HRR, we used the HRR DR-GFP reporter assay to measure the frequency of HRR after DSB induction in U2OS 282C cells. The experiment was performed as described above (4.3.7).

The measurement of GFP positive cells by flow cytometry revealed only a minimal reduction of HRR frequency after 0.01 µM chaetocin treatment. However, incubation with increasing concentration of chaetocin (0.1 µM) almost completely abrogated DSB repair by homologous recombination (Fig. 43). These results confirm the above measured reduction of HRR through Rad51 foci formation analysis, especially after treatment with 0.1 µM chaetocin and support the assumption that cell treatment with chaetocin suppresses HRR.

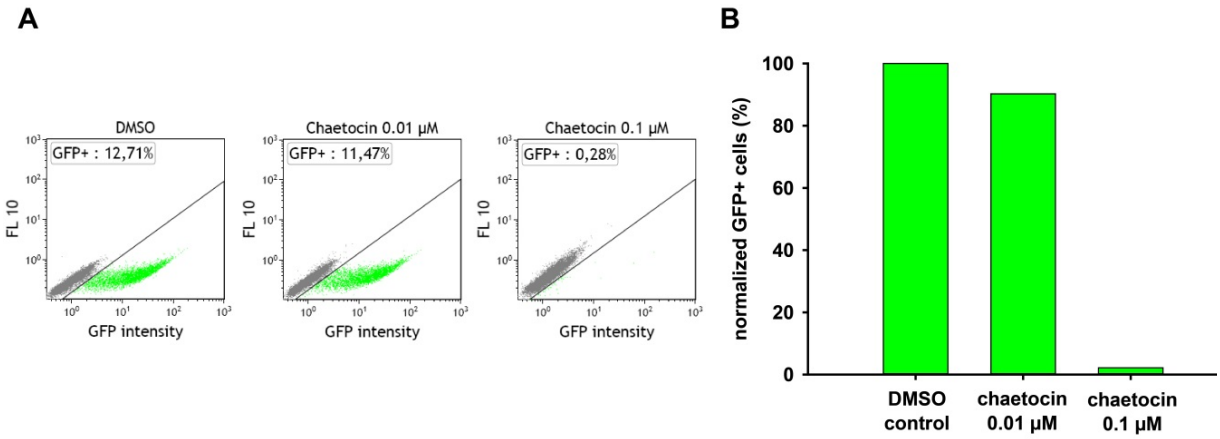

Figure 43: Chaetocin treatment reduces HRR. The HRR reporter assay was used to examine the impact of chaetocin treatment on HRR. U2OS 282C DR-GFP cells were transfected with the I-*Sce*I expression plasmid by electroporation. Two hours after transfection chaetocin (0.01 or 0.1 µM) was added into the medium. Cells were collected 24 h after transfection for GFP fluorescence analysis by flow cytometry. (**A**) Dot plots with the set threshold to discriminate GFP positive cells. (**B**) The number of GFP positive cells, normalized to the number of GFP positive cells in the DMSO control is plotted for each treatment.

5. Discussion

The purpose of this work was to examine the influence of chromatin organization on DSB repair pathway selection with a focus on the contribution of HRR. DSBs were generated by exposing cells to IR. In order to evaluate the rate of HRR in different chromatin compartments, we systematically examined the formation of various IRIF in heterochromatic or euchromatic regions.

As we aimed to specifically analyze the involvement of HRR in DSB repair, we only considered cells in late S or G_2 phase of the cell cycle, where all three repair pathways HRR, c-NHEJ and alt-EJ are active. CLSM was the method of choice, which allowed us to analyze foci development in three dimensional high resolution images. To discriminate the formation of IRIF in HC and EC regions, we used co-immunostaining with specific chromatin markers. H3K9me3 antibody staining was applied as a marker of constitutive heterochromatin. H3K9me3 is preferentially detected in gene poor regions, characterized with tandem repeat sequences including satellite repeats in telomeres and pericentromeres. Moreover, H3K9me3 is considered to be a permanent repression signal, which occurs through the action of H3K9 methylases SUV39H1 and SUV39H2 (Kim and Kim, 2012, Peters et al., 2001). The euchromatin marker H3K9ac is associated with transcriptional activity and its appearance in promoter regions is associated with low nucleosome density in the vicinity of transcription start sites (Nishida et al., 2006).

Additionally to the analysis of IRIF in HC and EC regions, we modified chromatin structure and examined its consequences on DSB signaling and repair. Hypertonic treatment after IR exposure, established enhanced chromatin condensation conditions during the repair process, whereas hypotonic treatment generated decondensed chromatin states. To target specific chromatin remodeling processes during DSB repair, we inhibited the methyltransferase SUV39H1 with chaetocin and investigated how this inhibition correlates with DSB processing.

The effect of chaetocin, as well as the impact of chromatin condensation and decondensation after treatment with hypertonic or hypotonic media on DSB repair was analyzed by the formation of IRIF by specific proteins as well as using different GFP reporter assays. These

methods are powerful and generally accepted tools to measure DSB signaling and repair. However, the limitations of each method have to be taken into consideration when interpreting the obtained results.

The quantification of repair foci after DSB induction by IR over several hours provides information about damage induction and repair (e.g. γH2AX, 53BP1 foci), as well as repair pathway choice, e.g. HRR by analyzing RPA, or Rad51 foci. Although, the formation of nuclear foci only indirectly visualizes the formation of DSB and the activation of the DSB repair processes, it is a powerful tool for the investigation of biological responses to IR. In comparison to physical methods of analysis of DSB induction and repair, e.g. PFGE, IRIF experiments revealed some discrepancies between foci formation and the actual physical presence of DSBs: Whereas the maximum of γH2AX foci is reached between 30 min and 1 h, PFGE results demonstrate, that more than 50% of DSBs are rejoined at that time (Kinner et al., 2008). Nevertheless, the numbers of γH2AX foci correlate with the theoretically predicted and physically evaluated numbers of DSBs produced per Gy per cell (Kinner et al., 2008).

In addition, the use of I-*Sce*I reporter assays allowed us to analyze the activity of specific repair pathways (Bennardo et al., 2008). However, it is important to mention that the chemical alterations at the DSB ends, generated by IR are very different in comparison to those generated by restriction endonucleases. IR induces complex breaks with chemical modifications, which have to be further processed to enable religation. Moreover, the major characteristic of IR, the formation of ionization clusters, results in increased DSB complexity by inducing clustered lesions. In contrast, restriction endonucleases produce “clean” ends with a 5’-phosphate and a 3’-OH group allowing direct religation (Schipler and Iliakis, 2013).

5.1 DSB induction in heterochromatic and euchromatic regions

In order to evaluate the induction of DSBs in HC and EC regions we first analyzed the formation and decay of γH2AX foci in HC and EC regions. The scoring of maximum numbers of γH2AX foci in the entire nucleus was in accordance with the expected amounts of induced DSBs which is 40 DSBs/Gy in G_2 phase cells. On average, we detected 17% of γH2AX foci in H3K9me3 positive regions (Fig. 16). Surprisingly, heterochromatic γH2AX kinetics were almost identical with euchromatic γH2AX kinetics and revealed a rapid DSB processing in highly condensed regions after reaching the maximum foci formation within one hour post

irradiation. Furthermore, the disappearance of HC γH2AX foci followed kinetics similar to those observed in EC regions (Fig. 16). These findings were unexpected as it has been published that DSB repair within HC was slower in comparison to EC repair (Riballo et al., 2004, Goodarzi et al., 2008). However, a recent study in *Drosophila* cells revealed an equally fast accumulation, as well as reduction rate of γH2Av (the homologue of γH2AX) in HC and EC regions, supporting our findings of comparable repair kinetics (Chiolo et al., 2011). Moreover, Chiolo et al. demonstrated that the fast reduction of γH2Av foci in HC was due to a relocation of heterochromatic DSBs to outside heterochromatin (Chiolo et al., 2011). A similar relocation of DSB processing site from its initial location to the periphery of heterochromatin was found in murine and human cells after single-ion exposure (Jakob et al., 2011). Hence, DSB relocations and chromatin decondensation processes upon DSB induction are reasonable explanations for the fast decay of γH2AX foci in HC regions observed in our experiments.

The equal distribution of γH2AX foci in HC (17%) and EC (83%) areas according to the proportion of HC (12%) and EC (88%) in the nucleus suggests an even induction of DSBs in condensed and decondensed regions. Indeed, the sensitivity of structurally and functionally different chromatin structures to DSB induction is a still hotly debated question.

Already in 1969 a study of Natarajan and Ahnström assumed, that the initial DSB induction occurs with the same frequencies in EC and HC regions (Natarajan and Ahnstrom, 1969). In recent years, several publications demonstrated an increased sensitivity of EC to DSB induction (Cowell et al., 2007, Karagiannis et al., 2007). Comparing DSB induction in two chromatin regions of identical length but with different gene densities revealed enhanced DSB induction in EC (Falk et al., 2008). It was concluded that the higher abundance of proteins in HC has a radio-protecting function by scavenging hydroxyl radicals (Xue et al., 1994, Falk et al., 2010). In contrast, it was shown that chemical modulation of chromatin conformation towards more compacted chromatin radio-sensitizes tumor cells, suggesting a higher sensitivity of condensed regions towards IR (Biade et al., 2001). In line with this, an increased induction of DSBs in HC can be rationalized by the increased DNA content per unit volume in HC as it is known that the amount of DSBs rises linearly with DNA content.

As we cannot definitely quantify the exact DNA content of H3K9me3 positive and negative regions, we are not able to predict, whether the DSB amount induced per unit of DNA length in H3K9me3 positive and negative regions is different. However, the even distribution of

γH2AX foci formation in EC and HC areas suggests an equal induction of DSBs in condensed and decondensed chromatin regions.

5.2 The rate of HRR is equal in heterochromatic and euchromatic regions identified by specific H3 marker staining

The decay of γH2AX foci 1 h post irradiation indicates effective DSB processing in EC as well as in HC regions but reveals no information regarding the involved repair pathways. Therefore, the formation of RPA and Rad51 foci was used to detect DNA end resection and HRR activity. On average, 34% of RPA and 20% of Rad51 foci occurred in H3K9me3 positive regions (4.1.3). These results were confirmed using the H3K9ac marker to stain EC, demonstrating that the majority of Rad51 foci occurred in EC regions (Fig. 19). Considering, that in eukaryotic cell HC makes 10-25% of total chromatin, the percentage of HRR associated foci in heterochromatic regions is similar to the percentage of HC in the cell nucleus. This leads to the conclusion that the distribution of HRR-activity-indicative foci is in accordance to the percentage of HC and EC: i.e. HRR is chosen with equal probability in H3K9me3 positive heterochromatic regions and H3K9ac positive euchromatic regions.

Previous publications suggested a pronounced activity of HRR at HC induced DSBs, as it was demonstrated that the slow repair component in G_2 is dependent on ATM and HRR factors like BRCA2 (Beucher et al., 2009). ATM activity was required to phosphorylate KAP1 which triggers global chromatin relaxation; thus, the conclusion that the majority of HRR takes place in HC generated DSBs (Ziv et al., 2006, Goodarzi et al., 2008, Shibata et al., 2011).

However, a recent study, published during the preparation of the current thesis, revealed that DSBs induced in active genes are also repaired by HRR, as it was shown that the transcription elongation-associated mark H3K36me3 functions as a target for HRR (Aymard et al., 2014). This publication discovered, that preexisting chromatin structure functions in DSB repair pathway choice and the authors proposed a “DSB repair choice histone code” (Aymard et al., 2014, Clouaire and Legube, 2015). The systematic analysis of RPA and Rad51 foci formation in H3K9me3 and H3K9ac positive regions, shown in the present thesis, revealed no role, at least with the currently used methods, for H3K9me3 or H3K9ac in directing the repair pathways towards HRR, as we observed an almost equal distribution of RPA and Rad51 foci accumulation in HC and EC regions. Nevertheless, we cannot exclude that the limited

resolution of confocal laser scanning microscopy compromised the exact colocalization of IRIF and chromatin markers. In order to exclude H3K9me3 and H3K9ac chromatin modifications as possible regulators of HRR, ChIP-seq could be used as a further approach, since this method was already successfully applied in the studies of Aymard et al. to identify H3K36me3 as a recruitment site for Rad51 (Aymard et al., 2014).

From the perspective of the distinct repair mechanisms and processes underpinning the three different repair pathways, it is tempting to assume that the structural conditions of HC favors DSB repair by c-NHEJ above HRR. The dense packing of chromatin could present a barrier for the DNA end resection required for HRR. On the other hand, the presence of repetitive DNA sequences within HC could complicate recombination events. Furthermore, a priority of the cell to repair heterochromatic regions, which contain mostly non-coding sequences or inactivated genes, with an error-free repair pathway, is implausible. The condensed structure could rather present an advantage for c-NHEJ as the two ends are held in close proximity, which facilitates fast ligation.

5.3 Saturation of HRR is independent of chromatin condensation

Recent findings from our laboratory revealed a saturation of HRR with increasing radiation dose (1.2.7). It was shown, that below 0.5-1 Gy, the majority of DSBs are repaired by HRR and the maximum amount of Rad51 foci was detected after 2-4 Gy, with higher doses not inducing higher Rad51 foci accumulation. The findings of an equal distribution of Rad51 foci in HC and EC regions strengthens the assumption, that after irradiation at low doses the majority of DSBs in G_2 phase cells are repaired by HRR.

Moreover, the ratio of maximum HC Rad51 foci to HC γH2AX, as well as EC Rad51 foci to EC γH2AX after different doses, demonstrated the same reduction of HRR activity at HC and EC DSBs with increasing dose. The results reveal once more that HRR plays a major role at low radiation doses without preference for DSBs induced in highly condensed regions. They also revealed that the decline of HRR with increasing radiation dose is independent of chromatin condensation in the neighborhood of the induced DSB.

In contrast to the saturation of Rad51 foci, the amount of RPA foci increased almost linearly with increasing radiation dose, indicating active DNA end resection at higher doses, although HRR activity was compromised. Since DNA end resection is an exclusion criterion of

c-NHEJ, resected breaks have to utilize mutagenic repair pathways like alt-EJ or SSA. This suggests a DNA repair pathway shift towards error-prone repair mechanisms in G_2 phase cells at higher doses. The reason why HRR reaches a plateau and why DSB repair shifts towards error-prone repair pathways is yet not clear. A possible role of 53BP1 in this context is discussed in the next section.

5.4 53BP1 as a regulator of repair pathway switch

The comprehensive analysis of 53BP1 foci revealed surprisingly persistent 53BP1 foci after exposure to radiation doses higher than 4 Gy. This response is not a peculiarity of a single cell line, but it is observed in all cell lines investigated (Fig. 25). These observations were also supported by the live cell imaging experiments (Fig. 26).

The dose response curves demonstrated a saturation of 53BP1 foci number at higher radiation doses, similar qualitatively to the saturation of Rad51 foci number, although 53BP1 foci number saturation occurs at higher doses (4-8 Gy) than that of Rad51 foci (2-4 Gy). Furthermore, the correlation of 53BP1 foci to γH2AX foci (Fig. 27 B) revealed, that the amount of 53BP1 foci, in comparison to the amount of induced DSBs, decreases with increasing radiation dose, similar to the calculation of Rad51 foci to γH2AX foci (Fig. 22 B).

In comparison to the Rad51 data, the decrease of 53BP1 foci to γH2AX foci ratio was attenuated. Nevertheless, the calculation demonstrates that the proportion of DSBs at which 53BP1 accumulates is reduced at higher radiation doses. These conspicuous parallels of Rad51 and 53BP1 foci saturation with increasing radiation dose and the associated decrease of Rad51 and 53BP1 foci versus total DSBs suggest that 53BP1 recruitment to DSBs is under the same control as Rad51. According to current models 53BP1 itself has a regulating role in HRR suppression and pathway switch.

It should be mentioned that the formation of 53BP1 foci was analyzed in exponentially growing cells and was not restricted to late S and G_2 phase cells. Nevertheless, preliminary results (data not shown) of 53BP1 foci scored in late S and G_2 phase cells also suggests saturation of 53BP1 foci. 53BP1 is known to suppress resection in G_1 and gets removed in a cell cycle regulated manner by BRCA1, to allow DNA end resection and HRR (Bothmer et al., 2010, Bunting et al., 2010). However, 53BP1 was demonstrated to be required for HRR of HC

DSBs, as it promotes phosphorylation of KAP1 that promotes HC relaxation (Kakarougkas et al., 2013).

Unpublished data from our laboratory with 53BP1 deficient cells support the model that 53BP1 is involved in suppressing HRR, as in these cells a significant increase of Rad51 foci was observed. Moreover, preliminary results (data not shown) indicated increasing co-localization of 53BP1 foci with RPA and Rad51 over time after high IR doses (≥ 8 Gy), supporting the model that 53BP1 has a role in the saturation of HRR. To further investigate the role of 53BP1 in the control of repair pathway switch, co-localization studies as well as extended analysis of HRR in 53BP1 deficient cells should be carried out.

5.5 Altered formation of IRIF in hypertonically treated cells

Hypertonic treatment is known to induce chromatin condensation (Dettor et al., 1972, Albiez et al., 2006, Falk et al., 2008). In order to investigate the influence of increased chromatin condensation on the repair of IR induced DSBs, cells were cultivated post irradiation in medium with doubled ionic strength (300 mM NaCl) and the formation of IRIF was analyzed.

We observed an increase of γH2AX intensity, reflected in enlarged foci size. Moreover, γH2AX foci number did not decay post irradiation, suggesting inhibition of DSB repair under hypertonic conditions (Fig. 29). In contrast to the prominent accumulation of γH2AX foci, the formation of 53BP1 and pATM foci was almost completely abrogated under hypertonic conditions (Fig. 30, Fig. 31). Furthermore, the formation of HRR associated RPA and Rad51 foci was completely inhibited, and repair reporter assays demonstrated an almost complete abrogation of the activity of all repair pathways tested.

The significant increase of H2AX phosphorylation in irradiated and hypertonically treated cells was already reported in a study of Reitsema and colleagues (Reitsema et al., 2004). Unexpectedly, we could not detect a parallel activation of ATM and an associated formation of pATM foci, although ATM is considered to be the major kinase, phosphorylating H2AX after IR exposure (Burma et al., 2001).

Studies in ATM deficient cells or with ATM inhibitors revealed, that predominantly DNA-PK but not ATR, can phosphorylate H2AX to a similar extend as ATM after exposure to IR (Stiff et al., 2004). A further study of Reitsema et al. also indicated that DNA-PK is responsible for the enhanced phosphorylation of H2AX under hypertonic conditions (Reitsema et al., 2005).

These authors developed the model that hypertonic treatment inhibits DSB rejoining and enhances γH2AX foci formation by maintaining active DNA-PK at unrepaired DSBs.

The suppression of 53BP1 foci formation (Fig. 30) strengthens the hypothesis that DSB signaling is interrupted in hypertonically treated cells. 53BP1 is recruited downstream of H2AX phosphorylation and belongs to the second wave of repair proteins recruited to DSBs. 53BP1 recruitment requires, in addition to phosphorylation of H2AX, the accumulation of MDC1 and chromatin ubiquitylation by RNF8 and RNF168 at the break site. The complete loss of RPA and Rad51 foci additionally indicates that the repair of DSBs is inhibited at very early stages. Further experiments investigating the formation of MDC1 or RNF8 and RNF168 foci would help to identify at which step DSB repair is blocked in hypertonically treated cells. However, it has to be mentioned that the increased ionic concentration "*per se"* could be responsible for the altered formation of IRIF and not only the associated chromatin condensation. High concentration of ions might inhibit the activity of many enzymes and may disturb interactions between proteins or between proteins and DNA (Falk et al., 2008).

It was shown, that hyper-condensation induced by high saline solutions suppresses binding between proteins and that it also reduces the dissociation rate of proteins already bound to DNA. These effects are in addition to the chromatin condensation, expected to affect chromatin access and binding of chromatin proteins (Martin and Cardoso, 2010).

In summary, hypertonic treatment after IR dramatically alters IRIF formation as demonstrated by enlarged γH2AX foci and suppressed 53BP1, pATM, RPA and Rad51 foci formation. All these effects are in line with an inhibition of DSB repair in hypertonically treated cells. The potential of hypertonic treatment to sensitize cells to ionizing radiation was shown (Dettor et al., 1972, Raaphorst et al., 1977). Moreover, the injection of hypertonic saline into liver tumors in rabbits reduced tumor growth and prolonged survival time (Lin et al., 2005). Further investigations have to be performed combining hypertonic treatment and IR to deepen our understanding of the potential of hypertonic treatment to affect cell radiosensitivity to killing.

5.6 Altered formation of IRIF in hypotonically treated cells

Hypotonic treatment (~ 75 mM NaCl) post irradiation was applied to study the effect of chromatin decondensation on the repair of DSBs. Destabilized chromatin structure by reduced ion concentration was already successfully used to identify chromatin condensation as a

determinant of alt-EJ repression in plateau-phase cells (Moscariello and Iliakis, 2013). Here we showed that hypotonic treatment slightly reduced the formation of 53BP1 foci and pATM foci, whereas it strongly suppresses the formation of γH2AX foci. Moreover, formation of RPA foci was not altered, demonstrating efficient resection in hypotonically treated cells, despite the fact that almost no Rad51 foci were detected.

Overall, these results indicate that hypotonic treatment, in contrast to hypertonic treatment, has a lower impact on initial DSB signaling and repair processes, as pATM, 53BP1 and even RPA foci are detected in hypotonically treated cells. However, the persistence of 53BP1 foci at later time points post IR, as well as the lack of Rad51 foci point to incomplete DSB repair.

The strongly suppressed formation of γH2AX foci was surprising, particularly because pATM and 53BP1 foci formation remained almost unaltered. This suggests that suppressed phosphorylation of H2AX was not due to inactive ATM. It is possible that under hypotonic conditions, ATM is not able to phosphorylate enough H2AX molecules to generate distinguishable γH2AX foci. Since 53BP1 foci numbers reached control levels, the phosphorylation of H2AX, if at all present, has to be sufficient to recruit 53BP1 to the break site, as it was shown that 53BP1 foci formation is dependent on γH2AX (Celeste et al., 2002, Celeste et al., 2003). However, the data can be also interpreted that 53BP1 can be recruited to DSBs in the absence of γH2AX, at least under hypotonic conditions.

In addition, the results of GFP reporter repair assays show incomplete DSB repair under hypotonic conditions, with a strong reduction of HRR activity (83%) and NHEJ repair (45%) but only a slight reduction (23%) of microhomology dependent alt-EJ mechanisms. Considering hypotonic treatment as a chromatin decondensation agent, this suggests that microhomology dependent alt-EJ repair is very tolerant to chromatin decondensation, whereas HRR and NHEJ benefit from stable chromatin structure.

5.7 Chaetocin treatment reduces HRR

Chaetocin was shown to specifically inhibit the histone methyltransferase SUV39H1 as it acts as a competitive inhibitor for S-adenosylmethionine and leads to a reduction of di- and trimethylation of H3 at lysine 9 (Greiner et al., 2005, Wang et al., 2014). In order to target particular chromatin remodeling processes during DSB repair, we inhibited the methyltransferase SUV39H1 by chaetocin and studied the effect of this inhibition on the

development of IRIF. We observed a strong decrease of H3K9me3 levels in A549 cells after 6 h incubation with chaetocin (Fig. 40), and used this pre-treatment condition to analyze IR induced repair foci formation.

Inhibition of SUV39H1 by chaetocin had almost no effect on the initial formation of γH2AX and 53BP1 foci within the first 3 h post irradiation (Fig. 41). Moreover, the decay of γH2AX foci to a level similar to control 3 h after IR suggests effective repair under chaetocin treatment. However, Rad51 foci formation was repressed, which hints towards inhibition of HRR (Fig. 42). This observation is somewhat counterintuitive, as we expected chromatin relaxation to enable DNA end resection and to facilitate strand invasion and thus also HRR. The reduction of HRR after inhibition of SUV39H1 hints towards a role of SUV39H1 in HRR. However this statement is highly speculative and the possible involvement and function of SUV39H1 in HRR has to be proven in further experiments.

5.8 Histone modifications are critical targets of repair proteins

Histone modifications are critical targets of repair proteins and are therefore important in regulating DSB repair. The recruitment of 53BP1 is known to be dependent on H4K20me2 and H4K20me1 due to the tandem Tudor domain of 53BP1 specifically recognizing these chromatin modifications (Botuyan et al., 2006, Panier and Boulton, 2014). Moreover, the stable recruitment of 53BP1 to damaged chromatin requires ubiquitylation of H2A as the UDR motif binds to H2AK15ub (Fradet-Turcotte et al., 2013). The reduction of H3K9me3 through inhibition of SUV39H1 showed no effect on 53BP1 recruitment.

Nevertheless, H3K9me3 plays an important role in DSB repair coordination through the activation of the acetyltransferase Tip60, since the chromodomain of Tip60 binds to H3K9me3 (Sun et al., 2009). In turn, Tip60 acetylates ATM which was shown to stimulate ATM activity (Sun et al., 2005). Moreover, Tip60 acetylates H4 and was shown to diminish 53BP1 binding to H4K20me2 and to promote HRR (Tang et al., 2013). In line with this, we observed a reduction in Rad51 foci development after chaetocin treatment, and also measured reduced HRR activity with the reporter assay.

A recent study even revealed an increase of H3K9me3 levels after induction of DSBs: Ayrapetov and colleagues showed a rapid loading of a complex containing KAP1, HP1 and SUV39H1 onto chromatin at DSB sites that provides a transient increase of H3K9me3

(Ayrapetov et al., 2014). On the one hand, the authors suggest a stabilizing effect of the modification on damaged chromatin by the transient formation of repressive/condensed chromatin structures. They further speculate that the dynamic change of H3K9me3 levels is one of the earliest signaling events required for processing of DSBs by activating Tip60 and promoting ATM activity. Indeed, they demonstrated an increased radiosensitivity in cells lacking SUV39H1, which was due to reduced HRR, whereas NHEJ activity was not significantly altered. These results are consistent with our findings.

6. Summary

Higher eukaryotes have evolved mechanistically distinct repair pathways to remove DSBs from the genome: c-NHEJ, HRR and alt-EJ. The probability to faithfully repair the DSB is strongly dependent on the utilized repair pathway and HRR is the only known error-free repair pathway, whereas c-NHEJ and especially alt-EJ are known to induce sequence alterations or even translocations. How the repair pathway selection is regulated in the cell is currently under investigation and in the present work we specifically focused on HRR activity regulation and on chromatin structure as a parameter influencing repair pathway choice.

DSB repair was systematically evaluated by analyzing the formation of different IRIF in heterochromatic and euchromatic chromatin regions and we concentrated our analysis on late S and G_2 phase cells to track HRR activity. The results of γH2AX foci formation demonstrated clear incidence in EC and HC regions. To specifically visualize DNA end resection and HRR activity, we examined formation of RPA and Rad51 foci. We demonstrated that the choice towards HRR is not regulated by chromatin structure. Indeed, we observed proportional distribution of RPA and Rad51 foci in EC and HC regions.

Moreover, the numbers of Rad51 foci saturated with increasing radiation dose independently of chromatin condensation status, supporting recent findings from our laboratory revealing a saturation of HRR with increasing radiation dose. However, RPA foci in HC and EC regions increased almost linearly, demonstrating active resection at high doses, which suggests a repair pathway switch towards error-prone repair mechanisms. The dose response curves of 53BP1 foci show a similar saturation as Rad51 foci and we observed persistence of 53BP1 foci after high radiation doses. These findings suggest a regulating role of 53BP1 in the process of HRR saturation.

In order to study DSB repair under altered chromatin condensation conditions, we applied hypertonic or hypotonic treatments. Hypertonic treatment causes an increase in chromatin condensation and impaired DSB repair. Although we detected enlarged γH2AX foci formation in hypertonically treated cells, the formation of pATM, 53BP1, RPA and Rad51 foci was almost completely suppressed. Treatment in hypotonic medium, on the other hand relaxed chromatin and was better tolerated during DSB repair. This was shown by the almost unaltered formation of 53BP1, pATM and RPA foci. Unexpectedly, γH2AX foci formation

was suppressed in hypotonically treated cells, which indicates that 53BP1 and RPA are able to accumulate at the break site without extensive phosphorylation of H2AX. With the help of repair reporter assays we detected the highest repair reduction with the HRR reporter assay under hypertonic and hypotonic conditions, demonstrating that HRR is highly sensitive to changes in chromatin structure. Notably, inhibition of the histone methyltransferase SUV39H1 with chaetocin also strongly suppressed HRR.

Thus, the results obtained in the present thesis strongly support an HRR saturation with increasing radiation dose and demonstrate a regulatory role of 53BP1 in this process. Moreover, chromatin modifications were successfully established as key regulatory parameters of HRR.

7. References

ALBIEZ, H., CREMER, M., TIBERI, C., VECCHIO, L., SCHERMELLEH, L., DITTRICH, S., KUPPER, K., JOFFE, B., THORMEYER, T., VON HASE, J., YANG, S., ROHR, K., LEONHARDT, H., SOLOVEI, I., CREMER, C., FAKAN, S. & CREMER, T. 2006. Chromatin domains and the interchromatin compartment form structurally defined and functionally interacting nuclear networks. *Chromosome research : an international journal on the molecular, supramolecular and evolutionary aspects of chromosome biology,* 14**,** 707-33.

ALEXEEV, A. A., MAZIN, A. V. & KOWALCZYKOWSKI, S. C. 2003. Rad54 protein possesses chromatin-remodeling activity stimulated by the Rad51-ssDNA nucleoprotein filament. *Nature Structural Biology,* 10**,** 182-186.

ALEXIADIS, V. & KADONAGA, J. T. 2002. Strand pairing by Rad54 and Rad51 is enhanced by chromatin. *Genes & Development,* 16**,** 2767-2771.

ANDERSON, L., HENDERSON, C. & ADACHI, Y. 2001. Phosphorylation and Rapid Relocalization of 53BP1 to Nuclear Foci upon DNA Damage. *Molecular and Cellular Biology,* 21**,** 1719-1508.

AUDEBERT, M., SALLES, B. & CALSOU, P. 2004. Involvement of Poly(ADP-ribose) Polymerase-1 and XRCC1/DNA Ligase III in an Alternative Route for DNA Double-strand Breaks Rejoining. *Journal of Biological Chemistry,* 279**,** 55117-55126.

AYMARD, F., BUGLER, B., SCHMIDT, C. K., GUILLOU, E., CARON, P., BRIOIS, S., IACOVONI, J. S., DABURON, V., MILLER, K. M., JACKSON, S. P. & LEGUBE, G. 2014. Transcriptionally active chromatin recruits homologous recombination at DNA double-strand breaks. *Nature Structural & Molecular Biology,* 21**,** 366-374.

AYOUB, N., JEYASEKHARAN, A. D. & VENKITARAMAN, A. R. 2009. Mobilization and recruitment of HP1: a bimodal response to DNA breakage. *Cell Cycle,* 8**,** 2945-50.

AYRAPETOV, M. K., GURSOY-YUZUGULLU, O., XU, C., XU, Y. & PRICE, B. D. 2014. DNA double-strand breaks promote methylation of histone H3 on lysine 9 and transient formation of repressive chromatin. *Proceedings of the National Academy of Sciences of the United States of America,* 111**,** 9169-9174.

BAKKENIST, C. J. & KASTAN, M. B. 2003. DNA damage activates ATM through intermolecular autophosphorylation and dimer dissociation. *Nature,* 421**,** 499-506.

BANK, E. M. & GRUENBAUM, Y. 2011. The nuclear lamina and heterochromatin: a complex relationship. *Biochem Soc Trans,* 39**,** 1705-9.

BARTEK, J. & LUKAS, J. 2003. Chk1 and Chk2 kinases in checkpoint control and cancer. *Cancer Cell,* 3**,** 421-429.

BEKKER-JENSEN, S., LUKAS, C., MELANDER, F., BARTEK, J. & LUKAS, J. 2005. Dynamic assembly and sustained retention of 53BP1 at the sites of DNA damage are controlled by Mdc1/NFBD1. *Journal of Cell Biology,* 170**,** 201-211.

BEKKER-JENSEN, S. & MAILAND, N. 2010. Assembly and function of DNA double-strand break repair foci in mammalian cells. *DNA Repair,* 9**,** 1219-1228.

BELLON, S., SHIKAZONO, N., CUNNIFFE, S., LOMAX, M. & O'NEILL, P. 2009. Processing of thymine glycol in a clustered DNA damage site: mutagenic or cytotoxic. *Nucleic Acids Research,* 37**,** 4430-4440.

BENNARDO, N., CHENG, A., HUANG, N. & STARK, J. M. 2008. Alternative-NHEJ Is a Mechanistically Distinct Pathway of Mammalian Chromosome Break Repair. *PLoS Genetics,* 4**,** e1000110.

BEUCHER, A., BIRRAUX, J., TCHOUANDONG, L., BARTON, O., SHIBATA, A., CONRAD, S., GOODARZI, A. A., KREMPLER, A., JEGGO, P. A. & LÖBRICH, M. 2009. ATM and Artemis promote homologous recombination of radiation-induced DNA double-strand breaks in G2. *EMBO Journal,* 28**,** 3413-3427.

BIADE, S., STOBBE, C. C., BOYD, J. T. & CHAPMAN, J. D. 2001. Chemical agents that promote chromatin compaction radiosensitize tumour cells. *International Journal of Radiation Biology,* 77**,** 1033-1042.

BOTHMER, A., ROBBIANI, D. F., FELDHAHN, N., GAZUMYAN, A., NUSSENZWEIG, A. & NUSSENZWEIG, M. C. 2010. 53BP1 regulates DNA resection and the choice between classical and alternative end joining during class switch recombination. *Journal of Experimental Medicine,* 207**,** 855-865.

BOTUYAN, M. V., LEE, J., WARD, I. M., KIM, J.-E., THOMPSON, J. R., CHEN, J. & MER, G. 2006. Structural Basis for the Methylation State-Specific Recognition of Histone H4-K20 by 53BP1 and Crb2 in DNA Repair. *Cell,* 127**,** 1361-1373.

BOUWMAN, P., ALY, A., ESCANDELL, J. M., PIETERSE, M., BARTKOVA, J., VAN DER GULDEN, H., HIDDINGH, S., THANASOULA, M., KULKARNI, A., YANG, Q., HAFFTY, B. G., TOMMISKA, J., BLOMQVIST, C., DRAPKIN, R., ADAMS, D. J., NEVANLINNA, H., BARTEK, J., TARSOUNAS, M., GANESAN, S. & JONKERS, J. 2010. 53BP1 loss rescues BRCA1 deficiency and is associated with triple-negative and BRCA-mutated breast cancers. *Nature Structural & Molecular Biology,* advance online publication**,** doi:10.1038/nsmb.1831.

BUIS, J., STONEHAM, T., SPEHALSKI, E. & FERGUSON, D. O. 2012. Mre11 regulates CtIP-dependent double-strand break repair by interaction with CDK2. *Nature Structural & Molecular Biology,* 19**,** 246-252.

BUNTING, S. F., CALLÉN, E., WONG, N., CHEN, H.-T., POLATO, F., GUNN, A., BOTHMER, A., FELDHAHN, N., FERNANDEZ-CAPETILLO, O., CAO, L., XU, X., DENG, C.-X., FINKEL, T., NUSSENZWEIG, M., STARK, J. M. & NUSSENZWEIG, A. 2010. 53BP1 Inhibits Homologous Recombination in Brca1-Deficient Cells by Blocking Resection of DNA Breaks. *Cell,* 141**,** 243-254.

BURMA, S., CHEN, B. P., MURPHY, M., KURIMASA, A. & CHEN, D. J. 2001. ATM phosphorylates histone H2AX in response to DNA double-strand breaks. *Journal of Biological Chemistry,* 276**,** 42462-42467.

CALLEN, E., DI VIRGILIO, M., KRUHLAK, MICHAEL J., NIETO-SOLER, M., WONG, N., CHEN, H.-T., FARYABI, ROBERT B., POLATO, F., SANTOS, M., STARNES, LINDA M., WESEMANN, DUANE R., LEE, J.-E., TUBBS, A., SLECKMAN, BARRY P., DANIEL, JEREMY A., GE, K., ALT, FREDERICK W., FERNANDEZ-CAPETILLO, O., NUSSENZWEIG, MICHEL C. & NUSSENZWEIG, A. 2013. 53BP1 Mediates Productive and Mutagenic DNA Repair through Distinct Phosphoprotein Interactions. *Cell,* 153**,** 1266-1280.

CAO, L., XU, X., BUNTING, S. F., LIU, J., WANG, R.-H., CAO, L. L., WU, J. J., PENG, T.-N., CHEN, J., NUSSENZWEIG, A., DENG, C.-X. & FINKEL, T. 2009. A Selective Requirement for 53BP1 in the Biological Response to Genomic Instability Induced by Brca1 Deficiency. *Molecular Cell,* 35**,** 534-541.

CELESTE, A., FERNANDEZ-CAPETILLO, O., KRUHLAK, M. J., PILCH, D. R., STAUDT, D. W., LEE, A., BONNER, R. F., BONNER, W. M. & NUSSENZWEIG, A. 2003. Histone H2AX phosphorylation is dispensable for the initial recognition of DNA breaks. *Nature Cell Biology,* 5**,** 675-679.

CELESTE, A., PETERSEN, S., ROMANIENKO, P. J., FERNANDEZ-CAPETILLO, O., CHEN, H. T., SEDELNIKOVA, O. A., REINA-SAN-MARTIN, B., COPPOLA, V., MEFFRE, E., DIFILIPPANTONIO, M. J., REDON, C., PILCH, D. R., OLARU, A., ECKHAUS, M., CAMERINI-OTERO, R. D., TESSAROLLO, L., LIVAK, F., MANOVA, K., BONNER, W. M., NUSSENZWEIG, M. C. & NUSSENZWEIG, A. 2002. Genomic instability in mice lacking histone H2AX. *Science,* 296**,** 922-927.

CHAPMAN, J. R., BARRAL, P., VANNIER, J.-B., BOREL, V., STEGER, M., TOMAS-LOBA, A., SARTORI, A. A., ADAMS, I. R., BATISTA, F. D. & BOULTON, S. J. 2013. RIF1 Is Essential for 53BP1-Dependent Nonhomologous End Joining and Suppression of DNA Double-Strand Break Resection. *Molecular Cell,* 49**,** 858-871.

CHEN, L., NIEVERA, C. J., LEE, A. Y.-L. & WU, X. 2008. Cell Cycle-dependent Complex Formation of BRCA1-CtIP-MRN Is Important for DNA Double-strand Break Repair. *Journal of Biological Chemistry,* 283**,** 7713-7720.

CHIOLO, I., MINODA, A., COLMENARES, SERAFIN U., POLYZOS, A., COSTES, SYLVAIN V. & KARPEN, GARY H. 2011. Double-Strand Breaks in Heterochromatin Move Outside of a Dynamic HP1a Domain to Complete Recombinational Repair. *Cell,* 144**,** 732-744.

CLOUAIRE, T. & LEGUBE, G. 2015. DNA double strand break repair pathway choice: a chromatin based decision? *Nucleus,* 6**,** 107-113.

COSTELLOE, T., LOUGE, R., TOMIMATSU, N., MUKHERJEE, B., MARTINI, E., KHADAROO, B., DUBOIS, K., WIEGANT, W. W., THIERRY, A., BURMA, S., VAN ATTIKUM, H. & LLORENTE, B. 2012. The yeast Fun30 and human SMARCAD1 chromatin remodellers promote DNA end resection. *Nature,* 489**,** 581-584.

COWELL, I. G., SUNTER, N. J., SINGH, P. B., AUSTIN, C. A., DURKACZ, B. W. & TILBY, M. J. 2007. γH2AX foci form preferentially in euchromatin after ionising-radiation. *PLoS ONE,* 2**,** e1057.

CREMER, T. & CREMER, C. 2001. Chromosome territories, nuclear architecture and gene regulation in mammalian cells. *Nat Rev Genet,* 2**,** 292-301.

DALEY, J. M. & SUNG, P. 2014. 53BP1, BRCA1, and the Choice between Recombination and End Joining at DNA Double-Strand Breaks. *Molecular and Cellular Biology,* 34**,** 1380-1388.

DATTA, K., JARUGA, P., DIZDAROGLU, M., NEUMANN, R. D. & WINTERS, T. A. 2006. Molecular Analysis of Base Damage Clustering Associated with a Site-Specific Radiation-Induced DNA Double-Strand Break. *Radiation Research,* 166**,** 767-781.

DATTA, K., NEUMANN, R. D. & WINTERS, T. A. 2005. Characterization of complex apurinic/apyrimidinic-site clustering associated with an authentic site-specific radiation-induced DNA double-strand break. *Proceedings of the National Academy of Sciences of the United States of America,* 102**,** 10569-10574.

DECKBAR, D., JEGGO, P. A. & LÖBRICH, M. 2011. Understanding the limitations of radiation-induced cell cycle checkpoints. *Critical Reviews in Biochemistry and Molecular Biology,* 46**,** 271-283.

DELLA-MARIA, J., ZHOU, Y., TSAI, M.-S., KUHNLEIN, J., CARNEY, J. P., PAULL, T. T. & TOMKINSON, A. E. 2011. Human Mre11/Human Rad50/Nbs1 and DNA Ligase IIIα/XRCC1 Protein Complexes Act Together in an Alternative Nonhomologous End Joining Pathway. *Journal of Biological Chemistry,* 286**,** 33845-33853.

DELPIRE, E., DUCHÊNE, C., GOESSENS, G. & GILLES, R. 1985. Effects of osmotic shocks on the ultrastructure of different tissues and cell types. *Experimental Cell Research,* 160**,** 106-116.

DETTOR, C. M., DEWEY, W. C., WINANS, L. F. & NOEL, J. S. 1972. Enhancement of X-ray damage in synchronous Chinese hamster cells by hypertonic treatments. *Radiation Research,* 52**,** 352-372.

DINANT, C. & LUIJSTERBURG, M. S. 2009. The Emerging Role of HP1 in the DNA Damage Response. *Molecular and Cellular Biology,* 29**,** 6335-6340.

DITULLIO JR., R. A., MOCHAN, T. A., VENERE, M., BARTKOVA, J., SEHESTED, M., BARTEK, J. & HALAZONETIS, T. D. 2002. 53BP1 functions in an ATM-dependent checkpoint pathway that is constitutively activated in human cancer. *Nature Cell Biology,* 4**,** 998-1002.

DOBBS, T. A., PALMER, P., MANIOU, Z., LOMAX, M. E. & O'NEILL, P. 2008. Interplay of two major repair pathways in the processing of complex double-strand DNA breaks. *DNA Repair,* 7**,** 1372-1383.

DOIL, C., MAILAND, N., BEKKER-JENSEN, S., MENARD, P., LARSEN, D. H., PEPPERKOK, R., ELLENBERG, J., PANIER, S., DUROCHER, D., BARTEK, J., LUKAS, J. & LUKAS, C. 2009. RNF168 Binds and Amplifies Ubiquitin Conjugates on Damaged Chromosomes to Allow Accumulation of Repair Proteins. *Cell,* 136**,** 435-446.

DUEVA, R. & ILIAKIS, G. 2013. Alternative pathways of non-homologous end joining (NHEJ) in genomic instability and cancer. *Translational Cancer Research,* 2**,** 163-177.

ECCLES, L. J., O'NEILL, P. & LOMAX, M. E. 2011. Delayed repair of radiation induced clustered DNA damage: Friend or foe? *Mutation Research/Fundamental and Molecular Mechanisms of Mutagenesis,* 711**,** 134-141.

ENDOH, D., OKUI, T., KON, Y. & HAYASHI, M. 2001. Hypertonic treatment inhibits radiation-induced nuclear translocation of the Ku proteins G22p1 (Ku70) and Xrcc5 (Ku80) in rat fibroblasts. *Radiation Research,* 155**,** 320-327.

ESCRIBANO-DIAZ, C., ORTHWEIN, A., FRADET-TURCOTTE, A., XING, M., YOUNG, J. T. F., TKAC, J., COOK, M. A., ROSEBROCK, A. P., MUNRO, M., CANNY, M. D., XU, D. & DUROCHER, D. 2013. A Cell Cycle-Dependent Regulatory Circuit Composed of 53BP1-RIF1 and BRCA1-CtIP Controls DNA Repair Pathway Choice. *Molecular Cell,* 49**,** 872-883.

FALCK, J., MAILAND, N., SYLJUASEN, R. G., BARTEK, J. & LUKAS, J. 2001. The ATM-Chk2-Cdc25A checkpoint pathway guards against radioresistant DNA synthesis. *Nature,* 410**,** 842-847.

FALK, M., LUKASOVA, E. & KOZUBEK, S. 2010. Higher-order chromatin structure in DSB induction, repair and misrepair. *Mutation Research/Reviews in Mutation Research,* 704**,** 88-100.

FALK, M., LUKÁSOVÁ, E. & KOZUBEK, S. 2008. Chromatin structure influences the sensitivity of DNA to γ-radiation. *Biochimica et Biophysica Acta (BBA) - Molecular Cell Research,* 1783**,** 2398-2414.

FENG, L., FONG, K.-W., WANG, J., WANG, W. & CHEN, J. 2013. RIF1 Counteracts BRCA1-mediated End Resection during DNA Repair. *Journal of Biological Chemistry,* 288**,** 11135-11143.

FERNANDEZ-CAPETILLO, O., CELESTE, A. & NUSSENZWEIG, A. 2003. Focusing on foci: H2AX and the recruitment of DNA-damage response factors. *Cell Cycle,* 2**,** 426-427.

FERNANDEZ-CAPETILLO, O., LEE, A., NUSSENZWEIG, M. & NUSSENZWEIG, A. 2004. H2AX: the histone guardian of the genome. *DNA Repair,* 3**,** 959-967.

FINAN, J. D., LEDDY, H. A. & GUILAK, F. 2011. Osmotic stress alters chromatin condensation and nucleocytoplasmic transport. *Biochemical and biophysical research communications,* 408**,** 230-5.

FRADET-TURCOTTE, A., CANNY, M. D., ESCRIBANO-DIAZ, C., ORTHWEIN, A., LEUNG, C. C. Y., HUANG, H., LANDRY, M.-C., KITEVSKI-LEBLANC, J., NOORDERMEER, S. M., SICHERI, F. & DUROCHER, D. 2013. 53BP1 is a reader of the DNA-damage-induced H2A Lys[thinsp]15 ubiquitin mark. *Nature,* 499**,** 50-54.

GEORGAKILAS, A. G., O'NEILL, P. & STEWART, R. D. 2012. Induction and Repair of Clustered DNA Lesions: What do we know so far? *Radiation Research,* 180**,** 100-109.

GHEZRAOUI, H., PIGANEAU, M., RENOUF, B., RENAUD, J.-B., SALLMYR, A., RUIS, B., OH, S., TOMKINSON, A. E., HENDRICKSON, ERIC A., GIOVANNANGELI, C., JASIN, M. & BRUNET, E. 2014. Chromosomal Translocations in Human Cells Are Generated by Canonical Nonhomologous End-Joining. *Molecular Cell,* 55**,** 829-842.

GOODARZI, A. A., JEGGO, P. & LOBRICH, M. 2010. The influence of heterochromatin on DNA double strand break repair: Getting the strong, silent type to relax. *DNA Repair,* 9**,** 1273-1282.

GOODARZI, A. A., NOON, A. T., DECKBAR, D., ZIV, Y., SHILOH, Y., LÖBRICH, M. & JEGGO, P. A. 2008. ATM signaling facilitates repair of DNA double-strand breaks associated with heterochromatin. *Molecular Cell,* 31**,** 167-177.

GOSPODINOV, A., VAISSIERE, T., KRASTEV, D. B., LEGUBE, G., ANACHKOVA, B. & HERCEG, Z. 2011. Mammalian Ino80 Mediates Double-Strand Break Repair through Its Role in DNA End Strand Resection. *Molecular and Cellular Biology,* 31**,** 4735-4745.

GREINER, D., BONALDI, T., ESKELAND, R., ROEMER, E. & IMHOF, A. 2005. Identification of a specific inhibitor of the histone methyltransferase SU(VAR)3-9. *Nat Chem Biol,* 1**,** 143-5.

GRIGORYEV, S. A. & WOODCOCK, C. L. 2012. Chromatin organization - the 30 nm fiber. *Exp Cell Res,* 318**,** 1448-55.

HAAF, T., GOLUB, E. I., REGGY, G., RADDING, C. M. & WARD, D. C. 1995. Nuclear foci of mammalian Rad51 recombination protein in somatic cells after DNA damage and its localization in synaptonemal complexes. *Proceedings of the National Academy of Sciences of the United States of America,* 92**,** 2298-2302.

HADA, M. & GEORGAKILAS, A. G. 2008. Formation of Clustered DNA Damage after High-LET Irradiation: A Review. *Journal of Radiation Research,* 49**,** 203-210.

HALL, E. J. & GIACCIA, A. J. 2006. *Radiobiology for the Radiologist,* Philadelphia, Baltimore, New York, London, Buenos Aires, Hong Kong, Sydney, Tokyo, Lippincott Williams & Wilkins.

HENNER, W. D., GRUNBERG, S. M. & HASELTINE, W. A. 1982. Sites and structure of γ radiation-induced DNA strand breaks. *Journal of Biological Chemistry,* 257**,** 11750-11754.

HENNER, W. D., RODRIGUEZ, L. O., HECHT, S. M. & HASELTINE, W. A. 1983. Gamma-ray Induced deoxyribonucleic acid strand breaks. *Journal of Biological Chemistry,* 258**,** 711-713.

HUANG, F., MOTLEKAR, N. A., BURGWIN, C. M., NAPPER, A. D., DIAMOND, S. L. & MAZIN, A. V. 2011. Identification of Specific Inhibitors of Human RAD51 Recombinase Using High-Throughput Screening. *ACS Chemical Biology,* 6**,** 628-635.

HUEN, M. S. Y., GRANT, R., MANKE, I., MINN, K., YU, X., YAFFE, M. B. & CHEN, J. 2007. RNF8 transduces the DNA-damage signal via histone ubiquitylation and checkpoint protein assembly. *Cell,* 131**,** 901-914.

HUERTAS, P. & JACKSON, S. P. 2009. Human CtIP Mediates Cell Cycle Control of DNA End Resection and Double Strand Break Repair. *Journal of Biological Chemistry,* 284**,** 9558-9565.

HUYEN, Y., ZGHEIB, O., DITULLIO JR., R. A., GORGOULIS, V. G., ZACHARATOS, P., PETTY, T. J., SHESTON, E. A., MELLERT, H. S., STAVRIDI, E. S. & HALAZONETIS, T. D. 2004. Methylated lysine 79 of histone H3 targets 53BP1 to DNA double-strand breaks. *Nature,* 432**,** 406-411.

IKURA, T., OGRYZKO, V. V., GRIGORIEV, M., GROISMAN, R., WANG, J., HORIKOSHI, M., SCULLY, R., QIN, J. & NAKATANI, Y. 2000. Involvement of the TIP60 histone acetylase complex in DNA repair and apoptosis. *Cell,* 102**,** 463-473.

ILIAKIS, G. 2009. Backup pathways of NHEJ in cells of higher eukaryotes: Cell cycle dependence. *Radiotherapy and Oncology,* 92**,** 310-315.

ILIAKIS, G., OKAYASU, R., VARLOTTO, J., SHERNOFF, C. & WANG, Y. 1993. Hypertonic treatment during premature chromosome condensation allows visualization of interphase chromosome breaks repaired with fast kinetics in irradiated CHO cells. *Radiation Research,* 135**,** 160-170.

ILIAKIS, G., WANG, H., PERRAULT, A. R., BOECKER, W., ROSIDI, B., WINDHOFER, F., WU, W., GUAN, J., TERZOUDI, G. & PANTELIAS, G. 2004. Mechanisms of DNA double strand break repair and chromosome aberration formation. *Cytogenetic and Genome Research,* 104**,** 14-20.

ILIAKIS, G., WANG, Y., GUAN, J. & WANG, H. 2003. DNA damage checkpoint control in cells exposed to ionizing radiation. *Oncogene,* 22**,** 5834-5847.

ILIAKIS, G., WU, W., WANG, M., TERZOUDI, G. I. & PANTELIAS, G. E. 2007. Backup Pathways of Nonhomologous End Joining May Have a Dominant Role in the Formation of Chromosome Aberrations. *In:* OBE, G., VIJAYALAXMI (ed.) *Chromosomal Alterations.* Berlin, Heidelberg, New York: Springer Verlag.

IYENGAR, S. & FARNHAM, P. J. 2011. KAP1 Protein: An Enigmatic Master Regulator of the Genome. *Journal of Biological Chemistry,* 286**,** 26267-26276.

JACKSON, S. P. & BARTEK, J. 2009. The DNA-damage response in human biology and disease. *Nature,* 461**,** 1071-1078.

JAKOB, B., SPLINTER, J., CONRAD, S., VOSS, K.-O., ZINK, D., DURANTE, M., LÖBRICH, M. & TAUCHER-SCHOLZ, G. 2011. DNA double-strand breaks in heterochromatin elicit fast repair protein recruitment, histone H2AX phosphorylation and relocation to euchromatin. *Nucleic Acids Research,* 39**,** 6489-6499.

JEGGO, P. A. & DOWNS, J. A. 2014. Roles of chromatin remodellers in DNA double strand break repair. *Experimental Cell Research,* 329**,** 69-77.

JEGGO, P. A., GEUTING, V. & LÖBRICH, M. 2011. The role of homologous recombination in radiation-induced double-strand break repair. *Radiotherapy and Oncology,* 101**,** 7-12.

JENSEN, R. B., CARREIRA, A. & KOWALCZYKOWSKI, S. C. 2010. Purified human BRCA2 stimulates RAD51-mediated recombination. *Nature,* 467**,** 678-683.

JONES, G. D., BOSWELL, T. V. & WARD, J. F. 1994. Effects of postirradiation temperature on the yields of radiation-induced single- and double-strand breakage in SV40 DNA. *Radiation Research,* 138**,** 291-296.

KABOTYANSKI, E. B., GOMELSKY, L., HAN, J.-O., STAMATO, T. D. & ROTH, D. B. 1998. Double-strand break repair in Ku86- and XRCC4-deficient cells. *Nucleic Acids Research,* 26**,** 5333-5342.

KAKAROUGKAS, A., ISMAIL, A., KLEMENT, K., GOODARZI, A. A., CONRAD, S., FREIRE, R., SHIBATA, A., LOBRICH, M. & JEGGO, P. A. 2013. Opposing roles for 53BP1 during homologous recombination. *Nucleic Acids Research,* 41**,** 9719-9731.

KARAGIANNIS, T. C., KN, H. & EL-OSTA, A. 2007. Disparity of histone deacetylase inhibition on repair of radiation-induced DNA damage on euchromatin and constitutive heterochromatin compartments. *Oncogene,* 26**,** 3963-3971.

KIM, H., CHEN, J. & YU, X. 2007. Ubiquitin-Binding Protein RAP80 Mediates BRCA1-Dependent DNA Damage Response. *Science,* 316**,** 1202-1205.

KIM, J. & KIM, H. 2012. Recruitment and biological consequences of histone modification of H3K27me3 and H3K9me3. *ILAR J,* 53**,** 232-9.

KINNER, A., WU, W., STAUDT, C. & ILIAKIS, G. 2008. γ-H2AX in recognition and signaling of DNA double-strand breaks in the context of chromatin. *Nucleic Acids Research,* 36**,** 5678-5694.

KOLAS, N. K., CHAPMAN, J. R., NAKADA, S., YLANKO, J., CHALWAN, R., SWEENEY, F. D., PANIER, S., MENDEZ, M., WILDENHAIN, J., THOMSON, T. M., PELLETIER, L., JACKSON, S. P. & DUROCHER, D. 2007. Orchestration of the DNA-damage response by the RNF8 ubiquitin ligase. *Science,* 318**,** 1637-1640.

KOZLOV, S. V., GRAHAM, M. E., JAKOB, B., TOBIAS, F., KIJAS, A. W., TANUJI, M., CHEN, P., ROBINSON, P. J., TAUCHER-SCHOLZ, G., SUZUKI, K., SO, S., CHEN, D. & LAVIN, M. F. 2011. Autophosphorylation and ATM Activation. *Journal of Biological Chemistry,* 286**,** 9107-9119.

KRUHLAK, M. J., CELESTE, A., DELLAIRE, G., FERNANDEZ-CAPETILLO, O., MULLER, W. G., MCNALLY, J. G., BAZETT-JONES, D. P. & NUSSENZWEIG, A. 2006. Changes in chromatin structure and mobility in living cells at sites of DNA double-strand breaks. *Journal of Cell Biology,* 172**,** 823-834.

KÜHNE, M., RIBALLO, E., RIEF, N., ROTHKAMM, K., JEGGO, P. A. & LÖBRICH, M. 2004. A Double-Strand Break Repair Defect in ATM-Deficient Cells Contributes to Radiosensitivity. *Cancer Research,* 64**,** 500-508.

LEMAITRE, C., FISCHER, B., KALOUSI, A., HOFFBECK, A. S., GUIROUILH-BARBAT, J., SHAHAR, O. D., GENET, D., GOLDBERG, M., BETRAND, P., LOPEZ, B., BRINO, L. & SOUTOGLOU, E. 2012. The nucleoporin 153, a novel factor in double-strand break repair and DNA damage response. *Oncogene,* 31**,** 4803-4809.

LEMAÎTRE, C. & SOUTOGLOU, E. 2014. Double strand break (DSB) repair in heterochromatin and heterochromatin proteins in DSB repair. *DNA Repair,* 19**,** 163-168.

LI, S., TING, N. S. Y., ZHENG, L., CHEN, P.-L., ZIV, Y., SHILOH, Y., LEE, E. Y.-H. P. & LEE, W.-H. 2000. Functional link of BRCA1 and ataxia telangiectasia gene product in DNA damage response. *Nature,* 406**,** 210-215.

LIEBER, M. R. 2010. NHEJ and its backup pathways in chromosomal translocations. *Nature Structural & Molecular Biology,* 17**,** 393-395.

LIN, Y. C., CHEN, J. H., HAN, K. W. & SHEN, W. C. 2005. Ablation of liver tumor by injection of hypertonic saline. *AJR Am J Roentgenol,* 184**,** 212-9.

LIU, J., DOTY, T., GIBSON, B. & HEYER, W.-D. 2010. Human BRCA2 protein promotes RAD51 filament formation on RPA-covered single-stranded DNA. *Nature Structural & Molecular Biology,* 17**,** 1260-1262.

LUKAS, C., MELANDER, F., STUCKI, M., FALCK, J., BEKKER-JENSEN, S., GOLDBERG, M., LERENTHAL, Y., JACKSON, S. P., BARTEK, J. & LUKAS, J. 2004. Mdc1 couples DNA double-strand break recognition by Nbs1 with its H2AX-dependent chromatin retention. *EMBO Journal,* 23**,** 2674-2683.

MA, Y., PANNICKE, U., SCHWARZ, K. & LIEBER, M. R. 2002. Hairpin Opening and Overhang Processing by an Artemis/DNA-Dependent Protein Kinase Complex in Nonhomologous End Joining and V(D)J Recombination. *Cell,* 108**,** 781-794.

MAHANEY, B. L., HAMMEL, M., MEEK, K., TAINER, J. A. & LEES-MILLER, S. P. 2013. XRCC4 and XLF form long helical protein filaments suitable for DNA end protection and alignment to facilitate DNA double strand break repair. *Biochem Cell Biol,* 91**,** 31-41.

MAILAND, N., BEKKER-JENSEN, S., FAUSTRUP, H., MELANDER, F., BARTEK, J., LUKAS, C. & LUKAS, J. 2007. RNF8 ubiquitylates histones at DNA double-strand breaks and promotes assembly of repair proteins. *Cell,* 131**,** 887-900.

MAILAND, N., FALCK, J., LUKAS, C., SYLJUASEN, R. G., WELCKER, M., BARTEK, J. & LUKAS, J. 2000. Rapid destruction of human Cdc25A in response to DNA damage [In Process Citation]. *Science,* 288**,** 1425-1429.

MAISON, C. & ALMOUZNI, G. 2004. HP1 and the dynamics of heterochromatin maintenance. *Nat Rev Mol Cell Biol,* 5**,** 296-304.

MARTIN, R. M. & CARDOSO, M. C. 2010. Chromatin condensation modulates access and binding of nuclear proteins. *FASEB Journal,* 24**,** 1066-1072.

MAZIN, A. V., MAZINA, O. M., BUGREEV, D. V. & ROSSI, M. J. 2010. Rad54, the motor of homologous recombination. *DNA Repair,* 9**,** 286-302.

MLADENOV, E. & ILIAKIS, G. 2011. Induction and Repair of DNA Double Strand Breaks: The Increasing Spectrum of Non-homologous End Joining Pathways. *Mutation Research,* 711**,** 61-72.

MOSCARIELLO, M. & ILIAKIS, G. 2013. Effects of chromatin decondensation on alternative NHEJ. *DNA Repair,* 12**,** 972-981.

MOSCARIELLO, M., WIELOCH, R., KUROSAWA, A., LI, F., ADACHI, N., MLADENOV, E. & ILIAKIS, G. 2015. Role for Artemis nuclease in the repair of radiation-induced DNA double strand breaks by alternative end joining. *DNA Repair,* 31**,** 29-40.

MUNOZ, I. M., JOWSEY, P. A., TOTH, R. & ROUSE, J. 2007. Phospho-epitope binding by the BRCT domains of hPTIP controls multiple aspects of the cellular response to DNA damage. *Nucleic Acids Research,* 35**,** 5312-5322.

MURR, R., LOIZOU, J. I., YANG, Y.-G., CUENIN, C., LI, H., WANG, Z.-Q. & HERCEG, Z. 2006. Histone acetylation by Trrap-Tip60 modulates loading of repair proteins and repair of DNA double-strand breaks. *Nature Cell Biology,* 8**,** 91-99.

NATARAJAN, A. T. & AHNSTROM, G. 1969. Heterochromatin and chromosome aberrations. *Chromosoma,* 28**,** 48-61.

NIMONKAR, A. V., GENSCHEL, J., KINOSHITA, E., POLACZEK, P., CAMPBELL, J. L., WYMAN, C., MODRICH, P. & KOWALCZYKOWSKI, S. C. 2011. BLM-DNA2-RPA-MRN and EXO1-BLM-RPA-MRN constitute two DNA end resection machineries for human DNA break repair. *Genes & Development,* 25**,** 350-362.

NIMONKAR, A. V., ÖZSOY, A. Z., GENSCHEL, J., MODRICH, P. & KOWALCZYKOWSKI, S. C. 2008. Human exonuclease 1 and BLM helicase interact to resect DNA and initiate DNA repair. *Proceedings of the National Academy of Sciences of the United States of America,* 105**,** 16906-16911.

NISHIDA, H., SUZUKI, T., KONDO, S., MIURA, H., FUJIMURA, Y. & HAYASHIZAKI, Y. 2006. Histone H3 acetylated at lysine 9 in promoter is associated with low nucleosome density in the vicinity of transcription start site in human cell. *Chromosome Res,* 14**,** 203-11.

NOON, A. T., SHIBATA, A., RIEF, N., LOBRICH, M., STEWART, G. S., JEGGO, P. A. & GOODARZI, A. A. 2010. 53BP1-dependent robust localized KAP-1 phosphorylation is essential for heterochromatic DNA double-strand break repair. *Nature Cell Biology,* 12**,** 177-184.

OCHI, T., BLACKFORD, A. N., COATES, J., JHUJH, S., MEHMOOD, S., TAMURA, N., TRAVERS, J., WU, Q., DRAVIAM, V. M., ROBINSON, C. V., BLUNDELL, T. L. & JACKSON, S. P. 2015. PAXX, a paralog of XRCC4 and XLF, interacts with Ku to promote DNA double-strand break repair. *Science,* 347**,** 185-188.

OLINS, A. L. & OLINS, D. E. 1974. Spheroid chromatin units (v bodies). *Science,* 183**,** 330-2.

PANIER, S. & BOULTON, S. J. 2014. Double-strand break repair: 53BP1 comes into focus. *Nature Reviews. Molecular Cell Biology,* 15**,** 7-18.

PARK, J.-H., PARK, E.-J., LEE, H.-S., KIM, S. J., HUR, S.-K., IMBALZANO, A. N. & KWON, J. 2006. Mammalian SWI/SNF complexes facilitate DNA double-strand break repair by promoting γ-H2AX induction. *EMBO Journal,* 25**,** 3986-3997.

PAUL, K., WANG, M., MLADENOV, E., BENCSIK-THEILEN, A. A., BEDNAR, T., WU, W., ARAKAWA, H. & ILIAKIS, G. 2013. DNA ligases I and III cooperate in alternative non-homologous end-joining in vertebrates. *PLoS ONE,* 8**,** e59505.

PEI, H., ZHANG, L., LUO, K., QIN, Y., CHESI, M., FEI, F., BERGSAGEL, P. L., WANG, L., YOU, Z. & LOU, Z. 2011. MMSET regulates histone H4K20 methylation and 53BP1 accumulation at DNA damage sites. *Nature,* 470**,** 124-128.

PETERS, A. H., O'CARROLL, D., SCHERTHAN, H., MECHTLER, K., SAUER, S., SCHOFER, C., WEIPOLTSHAMMER, K., PAGANI, M., LACHNER, M., KOHLMAIER, A., OPRAVIL, S., DOYLE, M., SIBILIA, M. & JENUWEIN, T. 2001. Loss of the Suv39h histone methyltransferases impairs mammalian heterochromatin and genome stability. *Cell,* 107**,** 323-37.

PETUKHOVA, G., VAN KOMEN, S., VERGANO, S., KLEIN, H. & SUNG, P. 1999. Yeast Rad54 Promotes Rad51-dependent Homologous DNA Pairing via ATP Hydrolysis-driven Change in DNA Double Helix Conformtion. *Journal of Biological Chemistry,* 274**,** 29453-29462.

POLO, S. E. & JACKSON, S. P. 2011. Dynamics of DNA damage response proteins at DNA breaks: a focus on protein modifications. *Genes & Development,* 25**,** 409-433.

POVIRK, L. F. 2012. Processing of Damaged DNA Ends for Double-Strand Break Repair in Mammalian Cells. *ISRN Molecular Biology,* 2012**,** Article: ID 345805.

RAAPHORST, G. P., FREY, H. E. & KRUUV, J. 1977. Effect of salt solutions on radiosensitivity of mammalian cells III. Treatment with hypertonic solutions. *International Journal of Radiation Biology,* 32**,** 109-126.

RADERSCHALL, E., GOLUB, E. I. & HAAF, T. 1999. Nuclear foci of mammalian recombination proteins are located at single-stranded DNA regions formed after DNA damage. *Proceedings of the National Academy of Sciences, (USA),* 96**,** 1921-1926.

REITSEMA, T., KLOKOV, D., BAN, X00E, TH, J. P. & OLIVE, P. L. 2005. DNA-PK is responsible for enhanced phosphorylation of histone H2AX under hypertonic conditions. *DNA Repair,* 4**,** 1172-1181.

REITSEMA, T. J., BANATH, J. P., MACPHAIL, S. H. & OLIVE, P. L. 2004. Hypertonic Saline Enhances Expression of Phosphorylated Histone H2AX after Irradiation. *Radiation Research,* 161**,** 402-408.

RIBALLO, E., KÜHNE, M., RIEF, N., DOHERTY, A., SMITH, G. C. M., RECIO, M.-J., REIS, C., DAHM, K., FRICKE, A., KREMPLER, A., PARKER, A. R., JACKSON, S. P., GENNERY, A., JEGGO, P. A. & LÖBRICH, M. 2004. A pathway of double-strand break rejoining dependent upon ATM, artemis, and proteins locating to γ-H2AX foci. *Molecular Cell,* 16**,** 715-724.

ROBERTS, S. A., STRANDE, N., BURKHALTER, M. D., STROM, C., HAVENER, J. M., HASTY, P. & RAMSDEN, D. A. 2010. Ku is a 5'-dRP/AP lyase that excises nucleotide damage near broken ends. *Nature,* 464**,** 1214-1217.

ROGAKOU, E. P., BOON, C., REDON, C. & BONNER, W. M. 1999. Megabase chromatin domains involved in DNA double-strand breaks *in vivo*. *Journal of Cell Biology,* 146**,** 905-915.

ROGAKOU, E. P., PILCH, D. R., ORR, A. H., IVANOVA, V. S. & BONNER, W. M. 1998. DNA double-stranded breaks induce histone H2AX phosphorylation on serine 139. *Journal of Biological Chemistry,* 273**,** 5858-5868.

ROTHKAMM, K., BARNARD, S., MOQUET, J., ELLENDER, M., RANA, Z. & BURDAK-ROTHKAMM, S. 2015. DNA damage foci: Meaning and significance. *Environmental and Molecular Mutagenesis,* 56**,** 491-504.

SARTORI, A. A., LUKAS, C., COATES, J., MISTRIK, M., FU, S., BARTEK, J., BAER, R., LUKAS, J. & JACKSON, S. P. 2007. Human CtIP promotes DNA end resection. *Nature,* 450**,** 509-514.

SCHIPLER, A. & ILIAKIS, G. 2013. DNA double-strand-break complexity levels and their possible contributions to the probability for error-prone processing and repair pathway choice. *Nucleic Acids Research,* 41**,** 7589-7605.

SHIBATA, A., CONRAD, S., BIRRAUX, J., GEUTING, V., BARTON, O., ISMAIL, A., KAKAROUGKAS, A., MEEK, K., TAUCHER-SCHOLZ, G., LOBRICH, M. & JEGGO, P. A. 2011. Factors determining DNA double-strand break repair pathway choice in G2 phase. *EMBO Journal,* 30**,** 1079-1092.

SILVERMAN, J., TAKAI, H., BUONOMO, S. B. C., EISENHABER, F. & DE LANGE, T. 2004. Human Rif1, ortholog of a yeast telomeric protein, is regulated by ATM and 53BP1 and functions in the S-phase checkpoint. *Genes & Development,* 18**,** 2108-2119.

SINGH, S. K., BENCSIK-THEILEN, A., MLADENOV, E., JAKOB, B., TAUCHER-SCHOLZ, G. & ILIAKIS, G. 2013. Reduced contribution of thermally labile sugar lesions to DNA double strand break formation after exposure to heavy ions. *Radiation Oncology,* 8**,** 77.

SINGH, S. K., WANG, M., STAUDT, C. & ILIAKIS, G. 2011. Post-irradiation chemical processing of DNA damage generates double-strand breaks in cells already engaged in repair. *Nucleic Acids Research,* 39**,** 8416-8429.

SINGH, S. K., WU, W., WU, W., WANG, M. & ILIAKIS, G. 2009. Extensive Repair of DNA Double-Strand Breaks in Cells Deficient in the DNA-PK Dependent Pathway of NHEJ after Exclusion of Heat-Labile Sites. *Radiation Research,* 172**,** 152-164.

SOBHIAN, B., SHAO, G., LILLI, D. R., CULHANE, A. C., MOREAU, L. A., XIA, B., LIVINGSTON, D. M. & GREENBERG, R. A. 2007. RAP80 targets BRCA1 to specific ubiquitin structures at DNA damage sites. *Science,* 316**,** 1198-1202.

SORIA, G. & ALMOUZNI, G. 2013. Differential contribution of HP1 proteins to DNA end resection and homology-directed repair. *Cell Cycle,* 12**,** 422-429.

SORIA, G., POLO, SOPHIE E. & ALMOUZNI, G. 2012. Prime, Repair, Restore: The Active Role of Chromatin in the DNA Damage Response. *Molecular Cell,* 46**,** 722-734.

STIFF, T., O'DRISCOLL, M., RIEF, N., IWABUCHI, K., LÖBRICH, M. & JEGGO, P. A. 2004. ATM and DNA-PK function redundantly to phosphorylate H2AX after exposure to ionizing radiation. *Cancer Research,* 64**,** 2390-2396.

STUCKI, M., CLAPPERTON, J. A., MOHAMMAD, D., YAFFE, M. B., SMERDON, S. J. & JACKSON, S. P. 2005. MDC1 directly binds phosphorylated histone H2AX to regulate cellular responses to DNA double-strand breaks. *Cell,* 123**,** 1213-1226.

SUN, Y., JIANG, X., CHEN, S., FERNANDES, N. & PRICE, B. D. 2005. A role for the Tip60 histone acetyltransferase in the acetylation and activation of ATM. *Proceedings of the National Academy of Sciences of the United States of America,* 102**,** 13182-13187.

SUN, Y., JIANG, X., XU, Y., AYRAPETOV, M. K., MOREAU, L. A., WHETSTINE, J. R. & PRICE, B. D. 2009. Histone H3 methylation links DNA damage detection to activation of the tumour suppressor Tip60. *Nature Cell Biology,* 11**,** 1376-1382.

SUZUKI, K., OKADA, H., YAMAUCHI, M., OKA, Y., KODAMA, S. & WATANABE, M. 2006. Qualitative and Quantitative Analysis of Phosphorylated ATM Foci Induced by Low-Dose Ionizing Radiation. *Radiation Research,* 165**,** 499-504.

TANG, J., CHO, N. W., CUI, G., MANION, E. M., SHANBHAG, N. M., BOTUYAN, M. V., MER, G. & GREENBERG, R. A. 2013. Acetylation limits 53BP1 association with damaged chromatin to promote homologous recombination. *Nature Structural & Molecular Biology,* 20**,** 317-325.

TERATO, H., WATARI, H., SHIMAZAKI, Y., HIRAYAMA, R., FURUSAWA, Y. & IDE, H. 2008. Analysis for complexity of clustered DNA damage generated by heavy ion beams. *Nucleic Acids Symp Ser (Oxf)***,** 443-4.

THOMPSON, L. H. 2012. Recognition, signaling, and repair of DNA double-strand breaks produced by ionizing radiation in mammalian cells: the molecular choreography. *Mutation Research,* 751**,** 158-246.

TOKUYAMA, Y., FURUSAWA, Y., IDE, H., YASUI, A. & TERATO, H. 2015. Role of isolated and clustered DNA damage and the post-irradiating repair process in the effects of heavy ion beam irradiation. *Journal of Radiation Research,* 56**,** 446-455.

UZIEL, T., LERENTHAL, Y., MOYAL, L., ANDEGEKO, Y., MITTELMAN, L. & SHILOH, Y. 2003. Requirement of the MRN complex for ATM activation by DNA damage. *EMBO Journal,* 22**,** 5612-5621.

WANG, B., MATSUOKA, S., BALLIF, B. A., ZHANG, D., SMOGORZEWSKA, A., GYGI, S. P. & ELLEDGE, S. J. 2007. Abraxas and RAP80 Form a BRCA1 Protein Complex Required for the DNA Damage Response. *Science,* 316**,** 1194-1198.

WANG, B., MATSUOKA, S., CARPENTER, P. B. & ELLEDGE, S. J. 2002. 53BP1, a Mediator of the DNA Damage Checkpoint. *Science,* 298**,** 1435-1438.

WANG, H., ROSIDI, B., PERRAULT, R., WANG, M., ZHANG, L., WINDHOFER, F. & ILIAKIS, G. 2005. DNA Ligase III as a Candidate Component of Backup Pathways of Nonhomologous End Joining. *Cancer Research,* 65**,** 4020-4030.

WANG, H., WANG, X., ZHANG, P. & WANG, Y. 2008. The Ku-dependent non-homologous end-joining but not other repair pathway is inhibited by high linear energy transfer ionizing radiation. *DNA Repair,* 7**,** 725-733.

WANG, H., ZENG, Z.-C., BUI, T.-A., SONODA, E., TAKATA, M., TAKEDA, S. & ILIAKIS, G. 2001a. Efficient rejoining of radiation-induced DNA double-strand breaks in vertebrate cells deficient in genes of the RAD52 epistasis group. *Oncogene,* 20**,** 2212-2224.

WANG, H., ZHAO-CHONG, Z., PERRAULT, A. R., CHENG, X., QIN, W. & ILIAKIS, G. 2001b. Genetic evidence for the involvement of DNA ligase IV in the DNA-PK-dependent pathway of non-homologous end joining in mammalian cells. *Nucleic Acids Research,* 29**,** 1653-1660.

WANG, M., KERN, A. M., HÜLSKÖTTER, M., GRENINGER, P., SINGH, A., PAN, Y., CHOWDHURY, D., KRAUSE, M., BAUMANN, M., BENES, C. H., EFSTATHIOU, J. A., SETTLEMAN, J. & WILLERS, H. 2014. EGFR-Mediated Chromatin Condensation Protects KRAS-Mutant Cancer Cells against Ionizing Radiation. *Cancer Research,* 74**,** 2825-2834.

WEINFELD, M., MANI, R. S., ABDOU, I., ACEYTUNO, R. D. & GLOVER, J. N. M. 2011. Tidying up loose ends: the role of polynucleotide kinase/phosphatase in DNA strand break repair. *Trends in Biochemical Sciences,* 36**,** 262-271.

WINDHOFER, F., WU, W., WANG, M., SINGH, S. K., SAHA, J., ROSIDI, B. & ILIAKIS, G. 2007. Marked dependence on growth state of backup pathways of NHEJ. *International Journal of Radiation Oncology Biology Physics,* 68**,** 1462-1470.

WU, W., WANG, M., WU, W., SINGH, S. K., MUSSFELDT, T. & ILIAKIS, G. 2008. Repair of radiation induced DNA double strand breaks by backup NHEJ is enhanced in G2. *DNA Repair,* 7**,** 329-338.

XING, M., YANG, M., HUO, W., FENG, F., WEI, L., JIANG, W., NING, S., YAN, Z., LI, W., WANG, Q., HOU, M., DONG, C., GUO, R., GAO, G., JI, J., ZHA, S., LAN, L., LIANG, H. & XU, D. 2015. Interactome analysis identifies a new paralogue of XRCC4 in non-homologous end joining DNA repair pathway. *Nature Communications,* 6**,** 6233.

XU, D., MUNIANDY, P., LEO, E., YIN, J., THANGAVEL, S., SHEN, X., II, M., AGAMA, K., GUO, R., FOX, D., MEETEI, A. R., WILSON, L., NGUYEN, H., WENG, N.-P., BRILL, S. J., LI, L., VINDIGNI, A., POMMIER, Y., SEIDMAN, M. & WANG, W. 2010. Rif1 provides a new

DNA-binding interface for the Bloom syndrome complex to maintain normal replication. *EMBO Journal,* 29**,** 3140-3155.

XUE, L.-Y., FRIEDMAN, L. R., OLEINICK, N. L. & CHIU, S.-M. 1994. Induction of DNA damage in γ-irradiated nuclei stripped of nuclear protein classes: differential modulation of double-strand break and DNA-protein crosslink formation. *International Journal of Radiation Biology,* 66**,** 11-21.

YAJIMA, H., FUJISAWA, H., NAKAJIMA, N. I., HIRAKAWA, H., JEGGO, P. A., OKAYASU, R. & FUJIMORI, A. 2013. The complexity of DNA double strand breaks is a critical factor enhancing end-resection. *DNA Repair,* 12**,** 936-946.

YU, X. & CHEN, J. 2004. DNA Damage-Induced Cell Cycle Checkpoint Control Requires CtIP, a Phosphorylation-Dependent Binding Partner of BRCA1 C-Terminal Domains. *Molecular and Cellular Biology,* 24**,** 9478-9486.

YUN, M. H. & HIOM, K. 2009. CtIP-BRCA1 modulates the choice of DNA double-strand-break repair pathway throughout the cell cycle. *Nature,* 459**,** 460-463.

ZIMMERMANN, M., LOTTERSBERGER, F., BUONOMO, S. B., SFEIR, A. & DE LANGE, T. 2013. 53BP1 Regulates DSB Repair Using Rif1 to Control 5′ End Resection. *Science,* 339**,** 700-704.

ZIV, Y., BIELOPOLSKI, D., GALANTY, Y., LUKAS, C., TAYA, Y., SCHULTZ, D. C., LUKAS, J., BEKKER-JENSEN, S., BARTEK, J. & SHILOH, Y. 2006. Chromatin relaxation in response to DNA double-strand breaks is modulated by a novel ATM- and KAP-1 dependent pathway. *Nature Cell Biology,* 8**,** 870-876.

8. Supplementary data

8.1 Variations of chromatin marker staining

To estimate the formation of IRIF in HC and EC regions we made a great effort to adhere to the same conditions and settings during antibody staining, microscopy scanning and image analysis in independent experiments. However, the chromatin architecture undergoes dynamic modification and remodeling processes to control transcription and we observed variations of the chromatin marker staining quantity.

In Fig. 44 the average proportion of HC in different samples in one set of experiment (n = 3-5) is shown. The proportion of HC volume varied between 4% and 21% and was in average 12%. Since we observed also in non-irradiated cells variations in the amount of HC we concluded that irradiation had no additional effect on HC proportion variations in our studies.

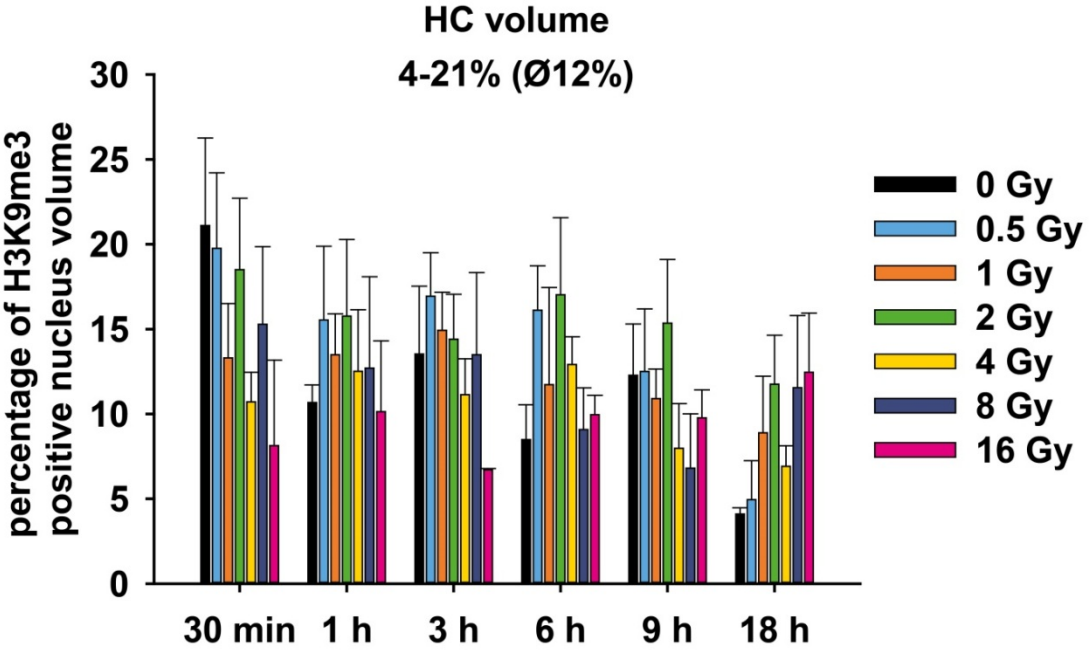

Figure 44: Percentage of HC volume after increasing irradiation dose at different time points post IR. Immunofluorescence microscopy of irradiated and non-irradiated A549 cells stained with the HC antibody against H3K9me3 and DAPI staining was performed. The image analysis with the Imaris software was used to calculate the nucleus volume (DAPI staining) and HC volume (H3K9me3 staining). Bars represent the mean percentage of HC volume of at least three independent experiments (n = 3-5) and error bars indicate the standard error of the mean values. In average, the percentage of HC was calculated in 20 (+/- 6) nuclei per time point and experiment. Analysis was restricted to late S and G_2 phase cells (positive cyclin B1 staining).

8.2 Supplementary tables

Table 12: Proportion of HC and EC areas in the analysis of γH2AX foci formation. We determined total chromatin volume by DAPI staining and HC volume was defined by H3K9me3 positive staining. The difference results in the EC volume. For every dose and time point the average proportion of HC and EC in the cells was calculated.

Dose (Gy)	time	HC (%) H3K9me3 positive regions	EC (%) H3K9me3 negative regions
0	30 min	12.13	87.87
	1 h	15.36	84.64
	3 h	12.28	87.72
	6 h	9.38	90.62
	9 h	7.33	92.67
0.5	30 min	11.03	88.97
	1 h	8.79	91.21
	3 h	9.83	90.17
	6 h	5.29	94.71
	9 h	7.66	92.34
1	30 min	11.98	88.02
	1 h	12.49	87.51
	3 h	10.87	89.13
	6 h	5.07	94.93
	9 h	27.29	72.71
2	30 min	10.57	89.43
	1 h	21.30	78.70
	3 h	13.36	86.64
	6 h	9.96	90.04
	9 h	10.49	89.51
Average		12%	88%

Table 13: Proportion of HC and EC areas in the analysis of Rad51 foci formation. We determined total chromatin volume by DAPI staining and HC volume was defined by H3K9me3 positive staining. The difference results in the EC volume. For every dose and time point the average proportion of HC and EC in the cells was calculated.

Dose (Gy)	time	HC (%) H3K9me3 positive regions	EC (%) H3K9me3 negative regions
0	30 min	21.11	78.89
	1 h	28.35	71.65
	3 h	13.54	86.46
	6 h	8.49	91.51
	9 h	12.28	87.72
	18 h	4.10	95.90
0.5	30 min	19.76	80.24
	1 h	15.54	84.46
	3 h	16.94	83.06
	6 h	16.11	83.89
	9 h	12.50	87.50
	18 h	4.95	95.05
1	30 min	13.30	86.70
	1 h	13.50	86.50
	3 h	14.93	85.07
	6 h	11.72	88.28
	9 h	10.90	89.10
	18 h	8.89	91.11
2	30 min	18.50	81.50
	1 h	15.77	84.23
	3 h	14.41	85.59
	6 h	17.03	82.97
	9 h	15.36	84.64
	18 h	11.75	88.25
4	30 min	10.71	89.29
	1 h	12.51	87.49
	3 h	11.13	88.87
	6 h	12.91	87.09
	9 h	7.97	92.03
	18 h	6.91	93.09
8	30 min	15.29	84.71
	1 h	12.70	87.30
	3 h	13.49	86.51
	6 h	9.08	90.92
	9 h	6.80	93.20
	18 h	11.55	88.45
16	30 min	8.13	91.87
	1 h	10.13	89.87
	3 h	4.50	95.50
	6 h	9.96	90.04
	9 h	9.77	90.23
	18 h	12.45	87.55
Average		13%	87%

Table 14: Proportion of HC and EC areas in the analysis of RPA foci formation. We determined total chromatin volume by DAPI staining and HC volume was defined by H3K9me3 positive staining. The difference results in the EC volume. For every dose and time point the average proportion of HC and EC in the cells was calculated.

Dose (Gy)	time	HC (%) H3K9me3 positive regions	EC (%) H3K9me3 negative regions
0	30 min	24.76	75.24
	1 h	31.24	68.76
	3 h	23.26	76.74
	6 h	36.72	63.28
	9 h	30.00	70.00
	18 h	26.36	73.64
0.5	30 min	34.13	65.87
	1 h	28.33	71.67
	3 h	37.72	62.28
	6 h	30.54	69.46
	9 h	28.27	71.73
	18 h	20.87	79.13
1	30 min	15.44	84.56
	1 h	27.35	72.65
	3 h	21.33	78.67
	6 h	29.73	70.27
	9 h	31.56	68.44
	18 h	18.82	81.18
2	30 min	21.33	78.67
	1 h	24.50	75.50
	3 h	25.40	74.60
	6 h	23.77	76.87
	9 h	26.25	73.75
	18 h	22.19	77.81
4	30 min	26.81	73.19
	1 h	20.54	79.46
	3 h	23.69	76.31
	6 h	27.03	72.97
	9 h	23.46	76.54
	18 h	30.37	69.63
8	30 min	21.56	78.44
	1 h	30.31	69.69
	3 h	26.83	73.17
	6 h	24.82	75.18
	9 h	15.73	84.27
	18 h	12.44	87.56
16	30 min	40.17	59.83
	1 h	20.83	79.17
	3 h	24.81	75.19
	6 h	29.95	70.05
	9 h	30.51	69.49
	18 h	21.02	78.98
	Average	26%	74%

Table 15: Proportion of HC and EC areas in the analysis of 53BP1 foci formation. We determined total chromatin volume by DAPI staining and HC volume was defined by H3K9me3 positive staining. The difference results in the EC volume. For every dose and time point the average proportion of HC and EC in the cells was calculated.

Dose (Gy)	time	HC (%) H3K9me3 positive regions	EC (%) H3K9me3 negative regions
0	30 min	41.91	58.09
	1 h	28.29	71.71
	3 h	31.84	68.16
	6 h	29.75	70.25
	9 h	28.23	71.77
	18 h	12.13	87.87
0.5	30 min	32.18	67.82
	1 h	22.79	77.21
	3 h	15.64	84.36
	6 h	27.40	72.60
	9 h	24.72	75.28
	18 h	22.49	77.51
1	30 min	23.86	76.14
	1 h	25.25	74.75
	3 h	35.62	64.38
	6 h	32.66	67.34
	9 h	31.21	68.79
	18 h	16.06	83.94
2	30 min	26.03	73.97
	1 h	28.66	71.34
	3 h	24.70	75.30
	6 h	28.73	71.27
	9 h	34.39	65.61
	18 h	14.60	85.40
4	30 min	38.57	61.43
	1 h	24.53	75.47
	3 h	37.28	62.72
	6 h	36.13	63.87
	9 h	28.68	71.32
	18 h	20.83	79.17
8	30 min	28.39	71.61
	1 h	31.33	68.67
	3 h	30.09	69.91
	6 h	29.68	70.32
	9 h	26.00	74.00
	18 h	16.69	83.31
16	30 min	19.35	80.65
	1 h	19.99	80.01
	3 h	32.49	67.51
	6 h	22.96	77.04
	9 h	22.49	77.51
	18 h	18.93	81.07
Average		27%	73%

Table 16: Numbers of Rad51 and γH2AX foci used to calculate the contribution of HRR in Fig. 22. The average numbers of total Rad51 foci and HC and EC Rad51 foci were determined by immunofluorescence data (Fig. 18). The average numbers of γH2AX foci were determined by immunofluorescence data for 0.5, 1 and 2 Gy (Fig. 16). Above irradiation doses of 2 Gy we used linear extrapolation to estimate foci numbers.

Dose (Gy)	All Rad51 foci	HC Rad51 foci	EC Rad51 foci	All γH2AX foci	HC γH2AX foci	EC γH2AX foci	All Rad51 foci/All γH2AX foci	HC Rad51 foci/HC γH2AX foci	EC Rad51 foci/EC γH2AX foci
0.5	11.46	2.67	8.79	20.18	2.79	17.39	0.57	0.96	0.51
1	12.17	2.08	10.10	50.94	10.47	40.48	0.24	0.20	0.25
2	21.65	5.74	14.54	87.39	26.20	61.19	0.25	0.22	0.24
4	23.62	5.71	17.91	179.68	48.96	130.72	0.13	0.12	0.14
8	25.71	4.75	21.54	359.36	97.92	261.44	0.07	0.05	0.08
16	17.07	3.80	15.10	718.72	195.84	522.88	0.02	0.02	0.03

Table 17: Numbers of 53BP1 and γH2AX foci used to calculate the contribution of 53BP1 in DSB repair in Fig. 27. The average numbers of total 53BP1 foci were determined by immunofluorescence data (Fig. 24). The average numbers of γH2AX foci were determined by immunofluorescence data for 0.5, 1 and 2 Gy (Fig. 16). Above irradiation doses of 2 Gy we used linear extrapolation to estimate foci numbers.

Dose (Gy)	All 53BP1 foci	All γH2AX foci	All 53BP1 foci/All γH2AX foci
0.5	**24.13**	**20.18**	**0.57**
1	**36.83**	**50.94**	**0.24**
2	**43.54**	**87.39**	**0.25**
4	**61.35**	**179.68**	**0.13**
8	**61.74**	**359.36**	**0.07**
16	**130.69**	**718.72**	**0.02**

Acknowledgements

I would like to thank my supervisor Prof. Dr. George Iliakis for giving me the opportunity to work on my PhD thesis at the Institute of Medical Radiation Biology. Thank you for your constant and outstanding support during my thesis work. I really enjoyed my time in your laboratory and it was a great pleasure for me to be part of your team.

I would like to thank the "Deutsche Forschungsgemeinschaft" for the financial support and for the opportunity to be part of the research training group 1739. In particular, I would like to thank Prof. Dr. Hemmo Meyer for being my mentor and supporting the development of my thesis with helpful discussions and suggestions during the annual retreats. I thank all other members of the research training group 1739 for the support and teachings as well as the great time during the retreats and social events.

A special thanks goes to Dr. Emil Mladenov who always gave me helpful suggestions and ideas and I thank you for your critical proofreading of my thesis.

I would like to thank Vladimir for his support during the life cell imaging experiments and for the great discussions and suggestions.

My thanks go to all colleagues in the laboratory, who were always very helpful and who are involved in creating a pleasant atmosphere in which I always enjoyed to work. Here I would particularly thank Tammy, Lisa and Katja for not just being great colleagues but also friends.

I am grateful for having a wonderful family and great friends who always support me.

Curriculum Vitae

Der Lebenslauf ist in der Online-Version aus Gründen des Datenschutzes nicht enthalten.

Der Lebenslauf ist in der Online-Version aus Gründen des Datenschutzes nicht enthalten.

Der Lebenslauf ist in der Online-Version aus Gründen des Datenschutzes nicht enthalten.

Declarations

Erklärung:

Hiermit erkläre ich, gem. § 6 Abs. (2) g) der Promotionsordnung der Fakultät für Biologie zur Erlangung der Dr. *rer. nat.*, dass ich das Arbeitsgebiet, dem das Thema „*The influence of chromatin structure on DNA double strand break repair pathway choice*“ zuzuordnen ist, in Forschung und Lehre vertrete und den Antrag von Frau Marilen Demond befürworte und die Betreuung auch im Falle eines Weggangs, wenn nicht wichtige Gründe dem entgegenstehen, weiterführen werde.

Essen, den _____ _____

Unterschrift eines Mitglieds der Universität Duisburg-Essen

Erklärung:

Hiermit erkläre ich, gem. § 7 Abs. (2) d) + f) der Promotionsordnung der Fakultät für Biologie zur Erlangung des Dr. rer. nat., dass ich die vorliegende Dissertation selbständig verfasst und mich keiner anderen als der angegebenen Hilfsmittel bedient, bei der Abfassung der Dissertation nur die angegeben Hilfsmittel benutzt und alle wörtlich oder inhaltlich übernommenen Stellen als solche gekennzeichnet habe.

Essen, den _____ _____

Unterschrift der Doktorandin

Erklärung:

Hiermit erkläre ich, gem. § 7 Abs. (2) e) + g) der Promotionsordnung der Fakultät für Biologie zur Erlangung des Dr. rer. nat., dass ich keine anderen Promotionen bzw. Promotionsversuche in der Vergangenheit durchgeführt habe und dass diese Arbeit von keiner anderen Fakultät/Fachbereich abgelehnt worden ist.

Essen, den _____ _____

Unterschrift der Doktorandin